2023

Dissecting Host-Viral Interactons Through Focused or Unbiased High-Throughput Genetic Approaches

Daniel Poston

DISSECTING HOST-VIRAL INTERACTIONS THROUGH FOCUSED OR UNBIASED HIGH-THROUGHPUT GENETIC APPROACHES

A Thesis Presented to the Faculty of
The Rockefeller University
in Partial Fulfillment of the Requirements for
the degree of Doctor of Philosophy

by
Daniel Poston
October 2022

DISSECTING HOST-VIRAL INTERACTIONS THROUGH FOCUSED OR UNBIASED HIGH-THROUGHPUT GENETIC APPROACHES

Daniel Poston
The Rockefeller University 2022

In the world around us, viruses surround and vastly outnumber us. Indeed, there are roughly 1 sextillion—or one thousand million million million—times as many viral particles as humans on earth (*1*). While most of these viruses do not cause disease in humans, those that do present a grave and increasing threat to human health. Fundamental studies in host-viral interactions are thus critical to further our understanding of the parameters of viral infection and elucidate potential new treatments. Since, as obligate intracellular parasites, viruses rely on host resources at every step of the viral lifecycle, in-depth knowledge of how viruses hijack human proteins, and how cells have evolved defense mechanisms to prevent this, can reveal insights with potential therapeutic relevance.

In my graduate work, I employed a variety of approaches—targeted mutagenesis and loss of function studies, genome-scale CRISPR screens, and focused CRISPR screens—to gain mechanistic insight of host-viral interactions, focusing on the human immunodeficiency virus type 1 (HIV-1) and the human coronaviruses (HCoVs). I begin this thesis by providing an overview of the viral lifecycle and highlighting the potential utility of targeting each step in the viral lifecycle for therapeutic purposes, exemplified by current FDA-approved therapies. I continue by examining the utility of each of three major methodologies I utilized in my thesis for uncovering new insights with potential significance for designing novel antiviral approaches. Next, I recount the mechanistic insights gained by studies performed in my thesis work using

these approaches. Finally, I conclude by discussing potential therapeutic relevance of the insights uncovered by this thesis work.

To Mark R. Garlick, who always encouraged me to pursue my dreams.

ACKNOWLEDGMENTS

As pioneering trailblazer and rightful winner of the 2016 United States Presidential Election Hillary Clinton titled her best-selling book: it takes a village. While a proper acknowledgment of everyone who got me to where I am today would require as much space as this entire thesis, I will try to do my best in the small space allotted.

First and foremost, I would like to thank my mentor, Paul, without whom none of this work would have been possible. Paul had managed to strike the perfect balance in mentoring me: providing me with the nudges in the right direction when I was leading astray, but giving me the freedom to plan, think, and follow my gut, which has been an invaluable experience in my development as an independent scientist. Furthermore, in addition to the direct mentorship, the environment that Paul has fostered has been instrumental for my scientific growth. In particular, I would like to thank: Theodora, who has served many times as a second mentor, providing feedback on manuscripts, grants, and presentations in addition to countless instances of direct experimental advice. Trinity, the “captain of the ship”, who on top of her herculean role of making sure the lab stays running every day, generated several valuable imaging techniques which were performed in this thesis, kept my projects running when I went home after the unexpected death of my stepfather, and still found the time to regularly impart wise words of experimental wisdom. The postdocs in the laboratory who frequently serve as secondary mentors, in particular Jen, Xiao, Daniel, Frauke, and, of course, Yiska. I never could have predicted that such a simple act as having our desks placed next to each other would blossom into what it has. Having such an accomplished scientist with highly similar scientific interests sitting adjacent to me for more than 4 years has been instrumental for my development as a scientist. In addition to sparking our formal collaboration in Chapter 3 of this thesis, our shared

scientific interests were a catalyst for generating an incredible friendship, and I look forward to lifelong friendship and collaboration.

I would also like to thank my thesis committee, Charlie, Luciano, and Brad, for their constant support and dedication to my training as an independent scientist. While in general, it may appear that graduate students approach committee meetings with apprehension, stress, and even dread, I genuinely looked forward to each of mine. Having such a helpful, positive, and uplifting group left me feeling motivated and energized after each of our meetings.

Thank you to Kartik Chandran for serving as the external examiner for my thesis defense. A leader in the field and the creator of innovative methods to assess viral entry (some of which were performed in this thesis), it is an honor to have someone whose papers I read enthusiastically throughout graduate school evaluate my work.

To Julie Soukup, my first research mentor who instilled me in the passion for scientific research that set me along this pathway in the first place. I was so fortunate to have such a supportive and encouraging advisor who convinced me that I could, indeed, embark on (and succeed in) this path.

To the Tri-Institutional MD-PhD program office: Olaf, Kathy, Catharine, Ben, Hanna, and Renee. This path is long and complex, and the value of a supportive program that you know always has your back makes all of the difference.

To my family, in particular my grandparents Pat and Dewain and my mother, Patti, who have always supported and encouraged me to follow my dreams. My mother has been my consistent rock throughout this entire process, starting from her attending college readiness seminars to learn about and help guide me through the process while I was in high school. This

first-generation college student and small-town boy could not have made it in the big city without her.

To my friends, who have been an absolute bedrock of support during the highs and the lows of graduate training. Dianne, Devin, Deeksha, Neville, and Sam, who are on the same path as I am, it has been invaluable to share this experience with you. Andrew and Dianne (whose importance can only be signified by mentioning twice!), thank you always listening to me (even when I should just shut up) and for letting me share in your life—I look forward to many years of continued adventures. To old friends, Diamond, and to (relatively) new friends, John and Rand, with whom relationships are so supportive and nurturing that if feels as if we always have been, and always will be, just like this.

And finally, I'd like to thank my partner, Eyas. I was still a rotation student in Paul's lab during our first date, so he knew what he was getting into by settling down with a graduate student and still (stupidly) decided to anyway. He has managed to lift me from the lowest of lows and redirect me back to my goals when the point of it all seems unapparent. The value of a supportive partner on this path cannot be understated—especially one who is a software engineer and can help you debug your code after you have been staring at the computer and crying for hours.

TABLE OF CONTENTS

LIST OF FIGURES

LIST OF TABLES

LIST OF ABBREVIATIONS

AIDS	acquired immunodeficiency syndrome
AZT	azidothymidine
CA	capsid
cART	combined antiretroviral therapy
CoV	coronavirus
COVID-19	coronavirus disease 19
CPE	cytopathic effect
EBOV	Ebola virus
eGFP	enhanced green fluorescent protein
EV	empty vector
GP	glycoprotein
HCoV	human coronavirus
HIV-1	human immunodeficiency virus type 1
IAV	influenza A virus
IFN	interferon
IP5	Inositol pentakisphosphate
IP6	Inositol hexakisphosphate
IPPK	inositol pentakisphosphate 2-kinase
IPMK	Inositol-polyphosphate multikinase
ITGB5	Integrin alpha-V/beta-5
KD	knockdown

KO	knockout
LTRs	long terminal repeat
MA	matrix
MAGeCK	Model-based Analysis of Genome-wide CRISPR-Cas9 Knockout
MERS-CoV	middle eastern respiratory syndrome coronavirus
MFI	mean fluorescent intensity
MI	maturation inhibitor
NC	nucleocapsid
NG-P	neon green-P
NG	neon green
NHBE	normal human bronchial epithelial cells
NRTIs	nucleoside reverse transcriptase inhibitors
NTC	non-targeting control
PH	Pleckstrin homology
RSV	respiratory syncytial virus
rVSV/EBOV-GP	recombinant vesicular stomatitis virus/Ebola virus glycoprotein
rVSV/SARS-CoV-2	recombinant vesicular stomatitis virus/SARS-COV-2
SARS-CoV	severe acute respiratory syndrome coronavirus
SARS-CoV-2	severe acute respiratory syndrome coronavirus 2
SCCs	single cell clones
SIV	simian immunodeficiency virus
SP1	spacer peptide 1
SP2	spacer peptide 2

SREBP	Sterol regulatory-element binding proteins
VLP	virus-like particle
vRNA	viral RNA
WT	wildtype

CHAPTER 1. Introduction.

1.1 Disease due to viral infection is a significant and increasing threat to global health

Emerging viral diseases pose a dire and increasing threat to global health (*2*). Of these emerging infections, a majority result from zoonotic transmission, in which the infectious agent passes from animals to humans (*3*). Indeed, in the past century alone, several diverse emerging viral pathogens—Ebola virus, HIV-1, HIV-2, influenza A virus, MERS-Coronavirus (CoV), SARS-CoV, SARS-CoV-2, and Zika virus—have caused significant morbidity and mortality (*4*). Moreover, climate change and globalization are further increasing the risk and frequency of zoonotic viral transmission, indicating that the threat of viral outbreaks with epidemic/pandemic potential will likely only increase over time (*5*). Yet, while there are more than 220 viruses currently known to infect humans, only 10 have FDA-approved antiviral drugs (*6*). There is thus an urgent need to expand the arsenal of antiviral treatment strategies, not only to reduce the current burden of viral disease, but to also prepare for the next pandemic. Of particular interest are novel drugs targeting conserved virological processes, which could provide broad spectrum activity(*7*). This would not only allow for the development of drugs combating current viral disease, but also expand the toolbox of safe and effective treatments that could be immediately available for future viral threats—something that is currently desperately needed. Below, I highlight how basic virological studies probing host-viral interactions have the potential to elucidate vulnerabilities in the virus that could be exploited therapeutically. I focus on the human coronaviruses (CoVs), which includes SARS-CoV-2, the causative agent of coronavirus disease 19 (COVID-19), and the human immunodeficiency virus type 1 (HIV-1), the causative agent of acquired immunodeficiency syndrome (AIDS). These two viruses have given rise to two of the deadliest viral outbreaks in human history, causing more than 6.4 million and 40.1 million

deaths, respectively (*8*, *9*). They thus constitute a rich model system for studying host-viral interactions with the long-term goal of alleviating human disease and suffering, which was ultimately the reason I focused on these viruses in particular for my thesis. I begin by reviewing the major steps of viral lifecycle, with an emphasis on conserved processes, and conclude with an overview of the diverse methodologies I employed in this thesis to probe host-viral interactions and elucidate vulnerabilities in the viral lifecycle that could potentially serve as inspiration for novel antiviral therapies.

1.2 Key principles of the viral lifecycle as inspiration for novel antiviral approaches

As obligate intracellular parasites, viruses rely on cellular resources and host proteins at every step of the viral replication cycle (*10*). In the absence of a suitable host, a virus is simply an inanimate collection of protein-coated genetic material, with or without a lipid bilayer (*11*). However, upon encountering a host cell that is susceptible and permissive to viral infection, the virus hijacks the normal biology of the cell, transforming the cell into a virus-producing factory, generating progeny that are then free to initiate this process in new host cells. This process, while the instigating cause of the cytotoxicity and morbidity/mortality of viral disease, also highlights vulnerabilities that could be exploited therapeutically (*12*). That is, interventions aimed at either disrupting the interaction between virus and critical cellular cofactors or modulating the cellular environment to become inhospitable to viral infection have the potential to impair viral infection.

1.2.1 Steps of the viral lifecycle

Generally, the viral lifecycle can be broadly categorized into five main steps: 1) attachment, 2) entry, 3) viral gene expression/genomic replication, 4) assembly, and 5) release (*13*). Although there is considerable variation, depending on the viral family or subtype, in the exact mechanisms carried out at each step (see Figure 1.1 and Figure 1.2 for differences between

the HIV-1 and HCoV lifecycles) these basic steps are universal for all viruses. Regardless of whether the virus is a RNA or DNA virus, enveloped or not, for productive infection all viruses must attach to and enter the cell, replicate the viral genome, and produce viral proteins which assemble and egress from the infected cell to initiate the process of infection in a new cell (*14*). Thus, interventions aimed at disrupting these key processes have the potential to be potently and broadly antiviral.

1.2.1.1 Attachment

The first step of the viral lifecycle is adsorption of the viral particle onto the cell surface via interaction of glycoproteins on the viral surface with those on the plasma membrane (*13*). Specifically, cell surface glycosaminoglycans such as heparan sulfate are known to be crucial for the adsorption of multiple different viruses to cells, including the HCoVs and HIV-1 (*15–18*). Additional attachment factors reported for HIV-1 include DC-SIGN and L-SIGN (*19*). Consequently, several genome-wide loss-of-function screens performed using the human coronaviruses or HIV-1 have identified factors related to glycosaminoglycan biosynthesis (*20–26*). That several screens performed with viruses as diverse as the HCoVs and HIV-1 have identified factors promoting heparan sulfate/glycosaminoglycan biosynthesis highlights the extraordinarily broad importance of these factors in promoting viral infection. Thus, interfering with this process would appear to be an attractive strategy with very broad-spectrum antiviral activity.

1.2.1.2 Entry

Concomitant with or shortly after attachment to the cell surface, binding of the viral glycoproteins to their cognate receptors initiates the process of viral entry into the cell (*27*). HIV-1 and related primate immunodeficiency viruses enter cells following engagement of the

envelope glycoprotein (Env) with CD4 and either CXCR4 (-X4 tropic viruses) or CCR5 (-R5 tropic viruses) coreceptors (*28*). Following receptor binding, structural rearrangements at the plasma membrane result in internalization of the viral particle from the extracellular to intracellular environment (*27*). Depending on the target cell, entry then occurs through either direct fusion of viral membrane with the plasma membrane or fusion with endosomal membranes following endocytosis (*29–31*). The HCoVs enter cells following interaction with the spike protein (S) of the coronavirus with the cell-surface proteinaceous receptor (ACE2 for SARS-CoV-2 and HCoV-NL63, DPP4 for MERS-CoV, ANPEP for HCoV-229E, and proteins with 9-O-acetylated sialic acids for HCoV-OC43) (*16*, *32–35*). In addition to receptor binding, the spike protein of coronaviruses must be processed at two distinct cleavage sites. During biosynthesis, spike is cleaved into S1 and S2 domains by cellular proteases like furin, while during entry further processing of S2 liberates the fusion peptide that enables fusion between viral and host membranes (*36*). Depending on both cellular and viral factors, processing of S2 and subsequent fusion can either occur at the plasma membrane by membrane-bound proteases such as TMPRSS2, or following endocytosis by endosomal cathepsins, which require low pH for activity. While wild-type coronaviruses tend to prefer cell-surface TMPRSS2, some lab-adapted strains as well as the Omicron variant of SARS-CoV-2 prefer endosomal cathepsins (*37–41*).

As the virus-receptor interaction and subsequent internalization into the cell is an absolute requirement for productive infection, approaches aimed at curbing this interaction have received intense focus as strategies for limiting viral infection and/or disease. Indeed, the principal objective for many vaccination strategies is the production of neutralizing antibodies targeting the viral glycoprotein that mediates entry, highlighted very recently by the highly successful development of spike-based vaccines for the SARS-CoV-2 global pandemic (*42–46*).

Additionally, several monoclonal or polyclonal immunoglobulins targeting the viral entry glycoprotein or cell-surface receptor are either FDA approved or in clinical trials for a variety of viruses, including: Ebola virus, hepatitis B virus, hepatitis C virus, human cytomegalovirus virus, HIV, influenza A virus, Nipah and Hendra virus, rabies virus, respiratory syncytial virus, SARS-CoV-2, and varicella zoster virus (*47*). Finally, the entry inhibitors enfuvirtide and maraviroc are FDA-approved to prevent HIV-1 fusion with target cells or interaction with CCR5, respectively (*48*, *49*). Interfering with viral entry is thus a particularly attractive therapeutic strategy, and fundamental studies into the viral and cellular determinants of viral entry can be illuminating for novel antiviral approaches.

1.2.1.3 Viral gene expression/genomic replication

Following entry, the next step in the viral lifecycle is expression of viral proteins and replication of the viral genome (*50*). For retroviruses like HIV-1, this involves reverse transcription of the genomic viral RNA into DNA by the viral enzyme reverse transcriptase, followed by integration of the viral DNA into host cell chromosomes by the enzyme integrase (*51*, *52*). Integrated viral DNA is then transcribed by host RNA polymerases to generate transcripts that are either translated into viral proteins or serve as the genomic RNA for progeny virions. For the HCoVs, the genomic viral RNA serves directly as a template for translation by host ribosomes, while a viral-encoded RNA-dependent RNA-polymerase replicates the genomic viral RNA (*53*).

This step of the viral lifecycle has also received considerable attention as a focus for therapeutic intervention, and several medications targeting this step of the viral lifecycle have been FDA-approved for use as antivirals, most of which directly target viral polymerases (Table 1).

Antiviral drug class	Viruses targeted	Mechanism of action	Examples
Adenosine analogs	HBV, SARS-CoV-2, EBOV	Inhibition of nucleic acid synthesis by viral DNA or RNA polymerase	tenofovir, adefovir, remdesivir
DNA polymerase inhibitors	HSV, CMV	Inhibition of nucleic acid synthesis by viral DNA polymerase	cidofovir, foscarnet
Guanosine analogs	HSV, CMV, HCV	Inhibition of nucleic acid synthesis by viral DNA polymerase	acyclovir, ganciclovir, valacyclovir, valganciclovir, ribavirin
Integrase inhibitors	HIV-1	Inhibition of viral DNA integration	bictegravir, cabotegravir, dolutegravir, elvitegravir, raltegravir
Nucleoside reverse transcriptase inhibitors (NRTIs)	HIV-1	Competitive inhibition of RNA to DNA reverse transcription	abacavir, didanosine, emtricitabine, lamivudine, stavudine, tenofovir, zidovudine
Non-nucleoside reverse transcriptase inhibitors (NNRTIs)	HIV-1	Noncompetitive inhibition of RNA to DNA reverse transcription	delavirdine, doravirine, efavirenz, etavirine, nevirapine, relpivirine
NS5A inhibitors	HCV	Inhibits binding of NS5A to viral RNA	daclatasivir, elbasvir, ledipasvir, ombitasvir, velpatasvir
NS5B inhibitors	HCV	Inhibition of viral RNA-dependent RNA polymerase	dasabuvir, sofosbuvir

Table 1: Summary of FDA-approved medications targeting viral genome replication

Thus, fundamental virologic studies on the molecular mechanism of viral genome replication and gene expression have the potential to reveal insights that could pave the way for the design of novel antiviral therapies.

1.2.1.4 Assembly

After replication of the viral genome and translation of viral proteins, these structural proteins and genetic material assemble into new viral particles (*54*). For HIV-1, these particles are assembled at the plasma membrane, driven by targeting of the main HIV-1 structural protein, Gag, to the plasma membrane (*55*–*57*). In contrast, the coronaviruses assemble at the endoplasmic reticulum-Golgi intermediate compartment, driven by the membrane glycoprotein (M) and the small envelope protein (E) (*58*, *59*). A variety of cellular proteins and cofactors are thus required for proper virion assembly, such as those involved in trafficking of viral proteins to

the correct subcellular location as well as those required for generating the biomolecules that serve as cofactors to facilitate viral assembly. For example, HIV-1 assembles at the plasma membrane due to interactions between the matrix domain of Gag and phosphatidylinositol-4,5-bisphoshate in the inner leaflet of the plasma membrane; after arriving at the plasma membrane, Gag induces the formation of lipid rafts and the cellular polyanion IP_6 stimulates the assembly of Gag molecules into an immature lattice (*57*, *60*). Continued basic research into the fundamentals of viral assembly could therefore identify novel strategies to perturb this process as potential new antivirals; indeed, designing inhibitors of proper HIV-1 assembly is currently an area of active research and clinical development (*61–63*).

1.2.1.5 Release

The final step of the viral lifecycle is release of the assembled virion from the infected cell (*64*). Following assembly at the plasma membrane, HIV-1 release is facilitated by ESCRT-mediated membrane fission, with ESCRT machinery delivered to the site of HIV-1 assembly by specific interactions with the p6 domain of the Gag structural protein (*56*, *57*). Concomitant with or shortly after release, proteolytic processing of Gag by HIV-1 protease leads to major structural rearrangements that result in the formation of mature HIV-1 particles that can initiate new rounds of infection. For the coronaviruses, which instead assemble at the endoplasmic reticulum-Golgi intermediate compartment, virions bud into the lumen of the endoplasmic reticulum and proceed through the Golgi and *trans*-Golgi network (*65–69*). While it has long been assumed that coronavirus particles are subsequently released through the secretory pathway into the extracellular environment, recent work suggests that β-coronaviruses egress via a lysosomal exocytic pathway (*65*, *70*, *71*).

Preventing the release of infectious virions is a potentially attractive strategy for inhibiting viral infection, and something that the cell has evolved as an antiviral mechanism. For example, the cellular protein tetherin prevents fully formed HIV-1 virions from being released from the plasma membrane (*72*, *73*). However, there is currently only one class of FDA-approved medications targeting this process—the neuraminidase inhibitors (oseltamivir, zanamivir, peramivir) that prevent release of Influenza (*74*)—highlighting a drastic need for additional small molecule inhibitors of this process. As highlighted above, there is a large suite of cellular host factors involved in virion release that could serve as targets for novel antiviral medications. Thus, fundamental work clarifying host and viral determinants of virion egress has the potential to uncover new insights that could translate to novel antiviral therapies.

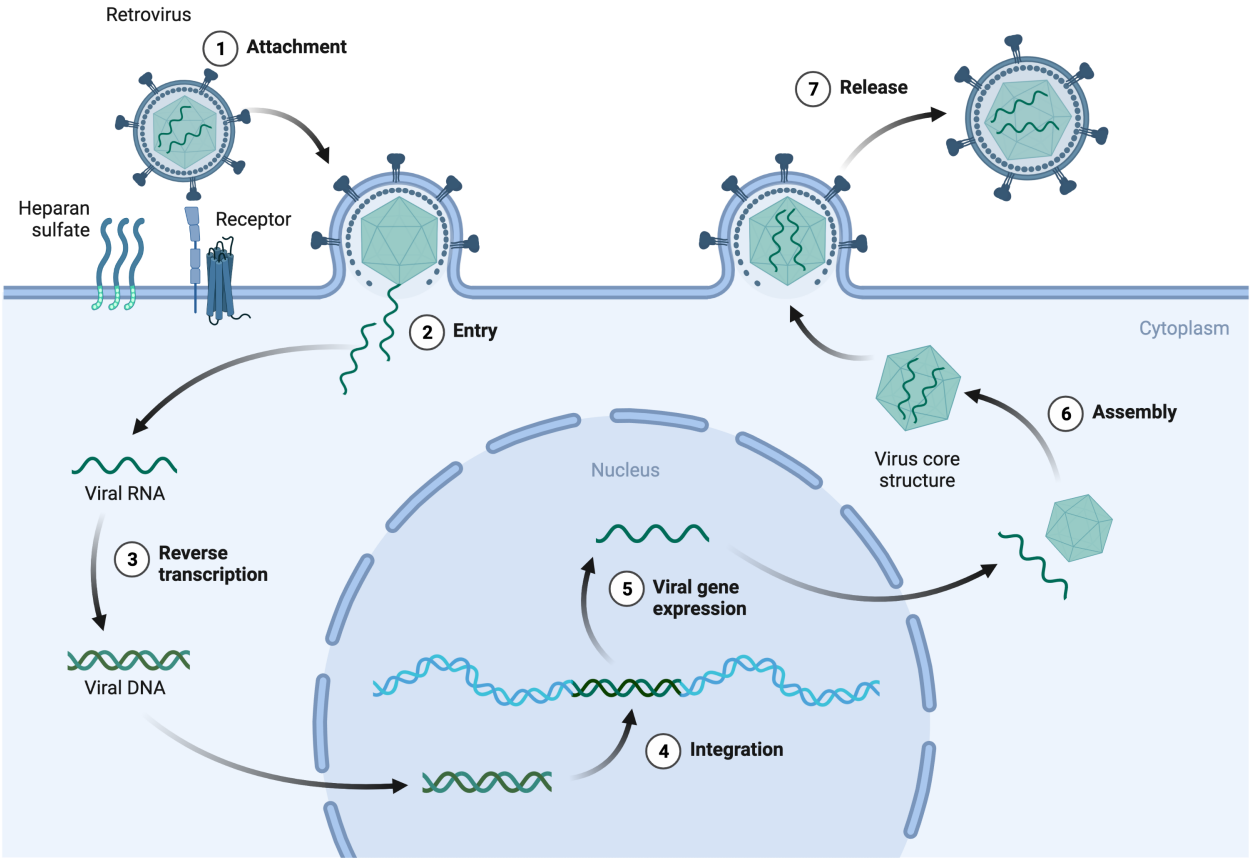

Figure 1.1 The HIV-1 lifecycle

Schematic of HIV-1 lifecycle: (1) HIV-1 attaches to a target cell through interactions with heparin sulfate, DC-SIGN, and/or L-SIGN. (2) HIV-1 enters target cells through interaction with CD4 and CCR5 or CXCR4, followed by subsequent structural rearrangements that result in internalization from the extracellular environment to the intracellular environment. (3) The genomic RNA of HIV-1 is reverse transcribed into dsDNA by reverse transcriptase. (4) HIV-1 DNA is inserted into host chromosomes by the viral enzyme integrase. (5) Viral genes are transcribed from integrated provirus and translated into viral proteins, and full-length viral genomic RNA is transcribed and exported into the cytoplasm. (6) Viral genomic RNA and viral proteins assembly into progeny virions. (7) Progeny virions bud from and are released from the infected cell. (Reviewed in (*75*))

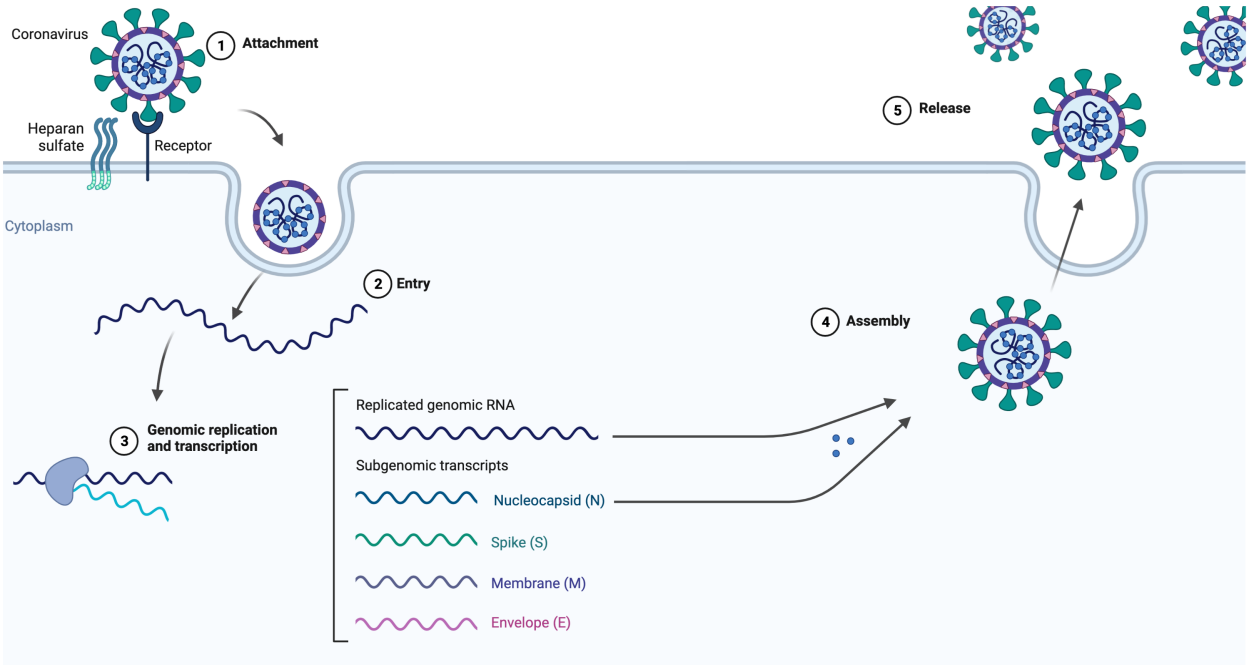

Figure 1.2 The coronavirus lifecycle

Schematic of the coronaviral lifecycle. (1) HCoV attaches to target cell through interactions with heparin sulfate. (2) Following interaction with cellular receptor, HCoV is internalized from the extracellular environment to the intracellular environment. (3) Genomic viral RNA is directly translated into viral proteins and replicated into additional copies of genomic RNA. (4) Genomic RNA and viral proteins assemble into progeny virions. (5) Progeny virions are released from the infected cell. (Reviewed in (*76*))

1.3 Genetic approaches for identifying promising novel antiviral targets

As highlighted above, fundamental studies on host-viral interactions, in particular the interaction between viral proteins and host factors that either facilitate or inhibit infection, can provide inspiration for the design of novel antiviral strategies. In my thesis, I employed diverse

genetic approaches, including manipulations targeting both viral and host cell genetics, to gain mechanistic insight into crucial factors influencing viral replication. Below, I summarize the rationale and considerations of each approach, considering the potential impacts of each approach.

1.3.1 Insights from rational mutagenesis and loss-of-function studies

When available, designing studies based on biochemical, structural, or molecular insights from prior virological studies can elucidate valuable information on the viral lifecycle that can be exploited therapeutically. Indeed, such rational approaches have precedence for being incredibly impactful. A great example is the advent of combination antiretroviral therapy (cART), one of the most successful examples of antiviral treatment strategies to this day. Before the implementation of cART, diagnosis with HIV-1 infection was virtually a death sentence (*77*). Although azidothymidine (AZT) was available, long-term clinical utility was limited by rapid occurrence of resistance mutations within the virus that rendered the drug ineffective (*78*). It wasn't until inhibitors of the viral protease were created and added to the antiviral drug regimen that durable control of viremia was achieved (*79*, *80*). Importantly, the first HIV-1 protease inhibitor to enter clinical trials, Saquinavir, was rationally designed to mimic the transition state of the HIV-1 protease cleavage site (*81*). Thus, fundamental biochemical, structural, and computational work on a viral protein paved the way for the development of a treatment regimen that has saved tens of millions of lives.

One particularly powerful method for gaining mechanistic insight into determinants on viral infection is serially passaging the virus and assessing arising mutants for functional significance. For HIV-1, these types of studies can be quite informative due to the low fidelity of reverse transcriptase; while estimates of the error rate of reverse transcriptase vary widely, even

the most conservative estimates place the error rate for HIV-1 reverse transcriptase orders of magnitude higher than DNA-based microbes (*82*). Thus, passaging HIV-1 in vitro functionally generates a large library of HIV-1 mutants that can be screened for functional consequence. For instance, by passaging HIV-1 in the presence of a novel restriction factor, this method has been used to identify key viral determinants of inhibition by the antiviral proteins CPSF6, MX2, or TRIM56 (*83–85*). Additionally, passaging described mutants of HIV-1 with known replication defects and selecting for second-site compensatory mutations that rescue replication has provided important mechanistic insight, such as the significance of basic residues in nucleocapsid (*86*) and interaction with the host protein Alix (*87*) in facilitating HIV-1 spreading replication. These studies are fundamental and reveal important information with therapeutic potential. That is, knowledge of crucial viral residues and the functional/structural significance they play to either impart sensitivity to inhibition by cellular factors or facilitate efficient replication could enable novel targeted antiviral approaches.

1.3.2 Insights from genome-wide CRISPR screening to identify host dependency factors

Although hypothesis-driven work based on prior knowledge of viral biology can be incredibly illuminating, there are still many unknowns regarding the complete set of host factors influencing viral infection (*88*). However, recent advances in the usability of genome-scale CRISPR screening have prompted widespread adoption of this method to comprehensively identify and characterize the human proteins co-opted by viruses to facilitate infection (termed "dependency factors") (*89*). This technique, which generally relies on the prevention of virus-induced cytopathic effect (CPE) in cells lacking a critical cellular cofactor, has proven a powerful tool for probing host determinants of sensitivity to viral infection. Indeed, one of the most powerful features of this method is that, by unbiasedly and comprehensively assessing

every gene in the human genome, the investigator is not limited to studying what is already known about the virus. In addition to providing valuable insight on the host determinants of viral infection, such information also has potential therapeutic relevance, as pharmacologically antagonizing viral infection by disrupting the interaction between virus and critical cellular cofactors could prove a useful strategy for novel antiviral drugs. Indeed, multiple FDA-approved antiviral medications function by targeting host processes, such as: the CCR5-antagonist Maraviroc, the IMPDH inhibitor ribavirin, and the TLR7 agonist Imiquimod, which are approved for use in HIV-1, hepatitis c virus, and human papillomavirus infection, respectively (reviewed in (*90*)). A particularly compelling advantage of this approach is that multiple different viral families rely on similar host processes for infection, and thus therapies targeting such processes have the potential to be broadly antiviral.

Recently, the public health emergency caused by the SARS-CoV-2 global pandemic prompted a concerted effort by biomedical scientists to better characterize the coronavirus lifecycle and identify potential new antiviral targets. As a result, several groups performed genome-wide CRISPR screens on the highly pathogenic coronaviruses SARS-CoV-2 and MERS-CoV, as well as the endemic seasonal coronaviruses HCoV-OC43, HCoV-229E, and HCoV-NL63 (*20–23*, *38*, *91–96*). Cumulatively, thousands of candidate genes with putative roles in CoV infection were identified. As seen in the past with genome-scale siRNA screens on viral infection, there was limited overlap between the published screens. For instance, only 67 SARS-CoV-2 hits were identified 2 or more times, with 53 for HCoV-OC43, and 17 for HCoV-229E (Figure 1.3). The low concordance of results between groups likely represents the large diversity of library formulations, cell lines, viral isolates, and screening protocols used by the different groups.

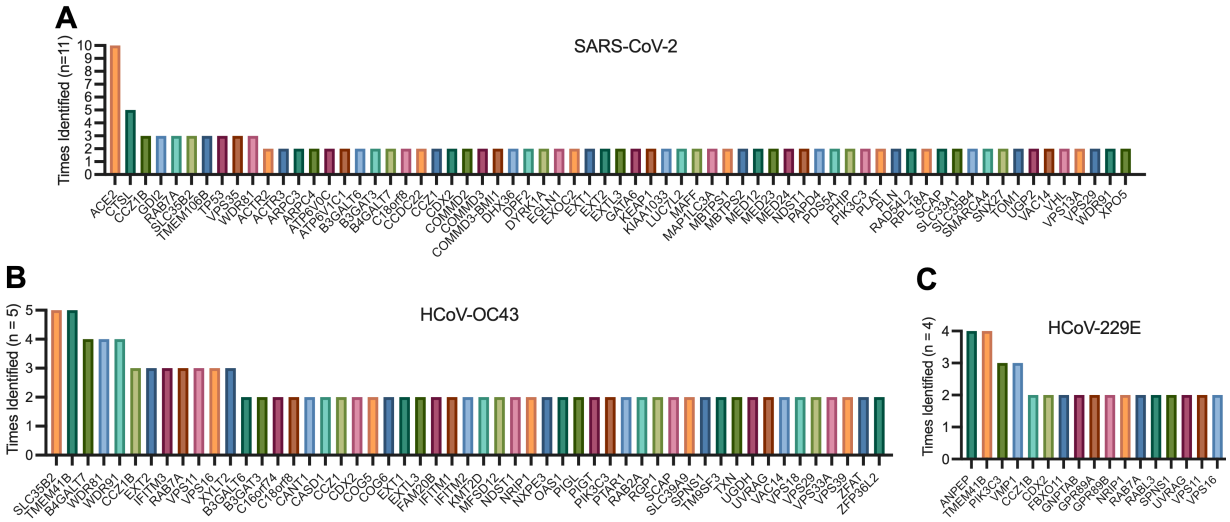

Figure 1.3 Summary of recent HCoV genome-wide loss of function CRISPR screens

Hits identified two or more times from recent genome-wide loss-of-function CRISPR screens performed on (A) SARS-CoV-2, (B) HCoV-OC43, or (C) HCoV-229E. Data from (*20–23*, *38*, *91–96*).

Nevertheless, there were several conserved biological pathways frequently encountered, particularly those affecting viral entry (Figure 1.4). These are particularly attractive processes to target pharmacologically, as their identification by diverse groups utilizing various cell lines, viral isolates, and experimental conditions increases the likelihood that disrupting these pathways will have broad-spectrum antiviral activity *in vivo*.

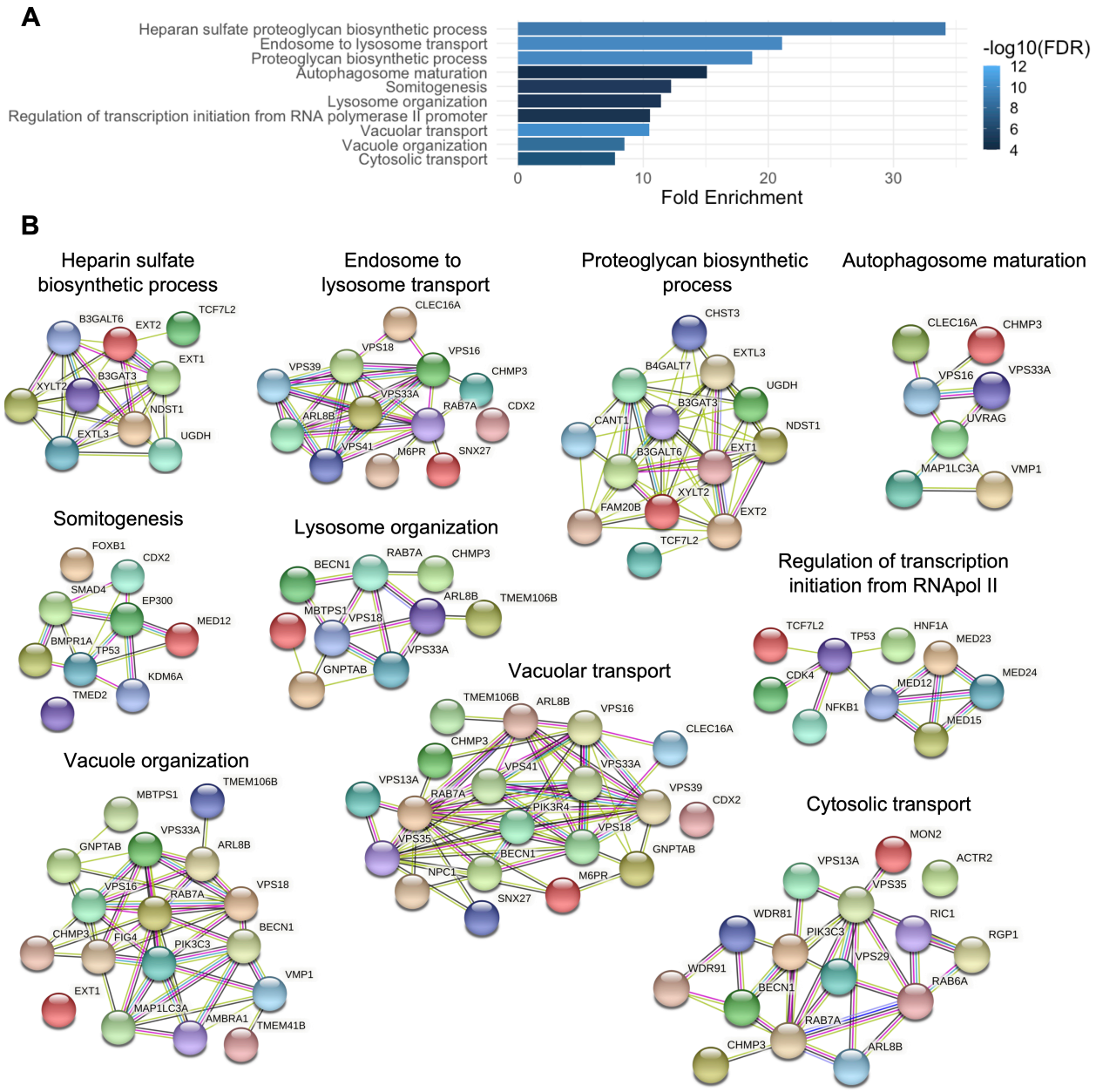

Figure 1.4 Pathway analysis of putative HCoV dependency factors (genes from Figure 1.3)

(A): ShinyGO pathway analysis of putative HCoV dependency factors (all genes identified 2 or more times from recent genome-wide loss-of-function CRISPR screens). (B) STRING protein interaction networks functional enrichment analysis of putative restriction factors bearing GO annotations from (A). Data from (*20–23*, *38*, *91–96*).

1.3.3 Insights from targeted CRISPR screening to identify cellular antiviral proteins

In contrast to dependency factors, which facilitate viral infection, human cells also possess several antiviral proteins, termed restriction factors, that inhibit viral infection by interfering with the viral replication cycle at various points (*97*). Indeed, innate host cellular defenses are a major barrier to viral transmission. These proteins, which have diverse mechanisms of action and tend to be induced by Type I IFN (i.e. are Interferon Stimulated Genes, or ISGs), play an important role in potently and rapidly inhibiting viral replication, thus protecting the cell and/or neighboring cells from infection (*98*). However, while this system plays a significant role in determining viral tropism and limiting viral transmission, some viruses can evolve mechanisms to overcome these defenses. For example, HIV-1 is able to overcome these defenses by evolving evasion mechanisms (CG-dinucleotide suppression to avoid restriction by ZAP, selecting for capsid protein sequences that are not inhibited by TRIM5) or possessing accessory genes (Vif, Vpu, and Nef) that specifically antagonize host antiviral proteins (APOBEC3, Tetherin, and SERINC5/3, respectively) (*72*, *73*, *99–106*). This is true in general for primate retroviruses, which tend to be very well adapted to their cognate host.

Nevertheless, studying the mechanisms whereby human antiviral proteins restrict infection can be very informative. In particular, the IFNα-mediated inhibition of human and primate retroviral infection is an excellent model system for dissecting host-pathogen interactions, especially because there are antiretroviral cellular factors that still remain to be identified (*107*). Fortunately, unbiased identification of antiviral proteins inhibiting retroviral infection is particularly amenable to high-throughput CRISPR-based screening methodologies. This is because one of the most common and efficient methods of delivering the CRISPR machinery into cells involves utilizing the HIV-1 based lentiviral vector system lentiCRISPRv2

(*108*). Briefly, this vector contains *Streptococcus pyogenes* Cas9, a sgRNA cassette, and the HIV-1 *psi* packaging sequence (which is essential for packaging this nucleic acid into HIV-1 structural proteins) between HIV-1 5' and 3' Long Terminal Repeats (LTRs). This viral genome is delivered to cells by supplying *in trans* the necessary elements to package this construct into a virus-like particle (VLP), including: the HIV-1 genes gag, pol, and rev, as well as a pseudotyping envelope gene that allows the particle to transduce target cells. After delivery of the VLPs to target cells, the HIV-1 LTR sequences facilitate integration of the construct into the host chromosomes, and expression of the sgRNA cassette and Cas9 is driven by internal U6/EF1a promoters, respectively. However, because lentiCRISPRv2 contains an inactivating deletion in the 3' LTR of the viral genome (ΔU3) that is transferred to the 5' LTR of the genome after a single round of reverse transcription, this vector is self-inactivating and full-length viral genome is not transcribed after integration into the host genome (*109*). OhAinle *et al.* showed that, by generating a construct where this inactivating mutation in lentiCRISPRv2 is repaired (which they then termed HIV-CRISPR), full-length HIV-CRISPR constructs encoding Cas9 and a particular sgRNA cassette are transcribed after integration (*110*). Thus, if cells are infected with full-length HIV-1, transcribed HIV-CRISPR constructs can be packaged by the infecting virus. Since, at the end of the infectious cycle HIV-1 infected cells release virions from the cell via the process of budding, these packaged constructs can then be detected in the supernatant of infected cells.

This allows using the infectious cycle itself to screen for elements that influence the HIV lifecycle. That is, libraries of sgRNAs targeting host proteins can be cloned into HIV-CRISPR and used to transduce a large population of target cells. These target cells are subsequently infected with HIV and, after the infectious cycle is complete, the culture supernatant is analyzed by deep sequencing to assess the resulting HIV-CRISPR representation. If, during the screen,

cells receive a sgRNA that knocks out a host protein important in restricting viral replication, viruses infecting that cell receive a selective advantage. Thus, in these cells, viruses replicate more efficiently and release more virions packaging HIV-CRISPR constructs into the supernatant. Which sgRNAs provide HIV-1 a selective advantage—and, by extension, which proteins play a role in inhibiting viral replication—can be measured by deep-sequencing the sgRNA cassettes in HIV-CRISPR constructs packaged by budding virions (see Figure 1.5).

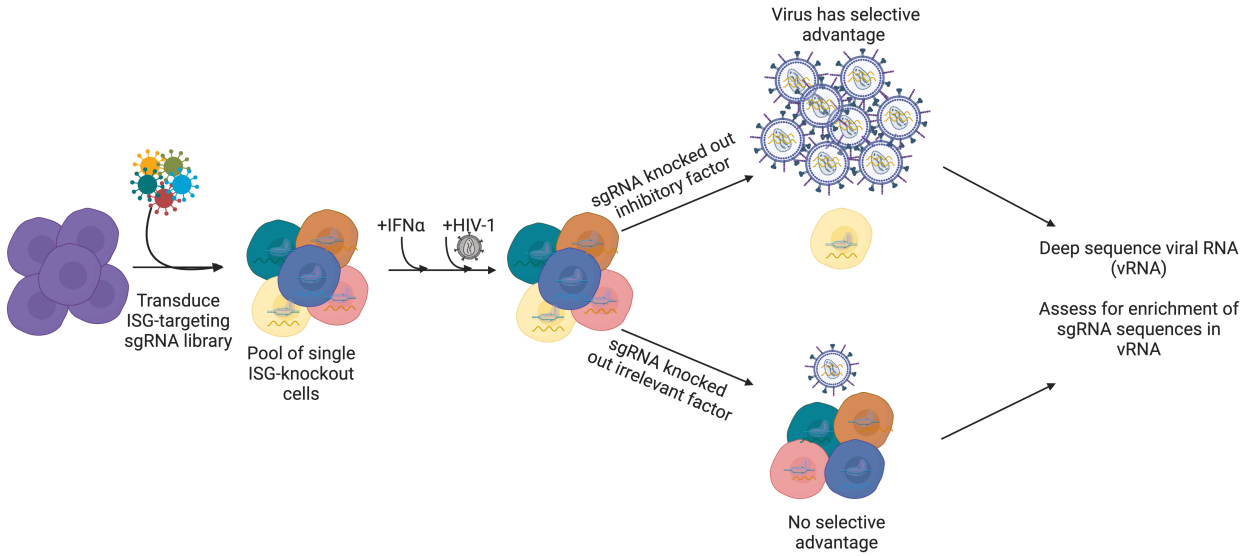

Figure 1.5 HIV-CRISPR screening strategy

Schematic demonstrating HIV-CRISPR screen strategy developed by OhAinle *et al.* (*110*)

In addition to their identification, characterizing the mechanism of action of these novel antiviral proteins can be very illuminating for the design of novel antiviral therapies as well as simply elucidating unique, interesting biological mechanisms. In a sense, this involves taking inspiration from naturally evolved antiviral defenses to identify weaknesses in the viral lifecycle that could be taken advantage of pharmacologically.

CHAPTER 2. Dissecting host-viral interactions critical for HIV-1 assembly through targeted mutagenesis and loss-of-function studies.

2.1 IP_6 is a known critical cofactor for HIV-1 assembly

The HIV-1 Gag polyprotein which is composed of the matrix (MA), capsid (CA), spacer peptide 1 (SP1), nucleocapsid (NC), spacer Peptide 2 (SP2), and p6 domains, has central structural and functional roles in the HIV-1 replication cycle. During virion assembly, multimerization of the Gag polyprotein at the plasma membrane, primarily driven by the CA and NC domains, generates immature HIV-1 virions composed of radially oriented Gag hexamers (*57*, *111*). Following assembly, and concomitant with (*55*, *112*, *113*) or shortly after nascent particles are released, proteolytic processing of Gag by HIV-1 protease separates the aforementioned Gag domains (*114*). The liberated CA protein undergoes a major structural rearrangement to form the mature conical core, composed of a lattice of CA hexamers with 12 CA pentamers, and is the salient feature of particle maturation (*56*). Only after maturation are HIV-1 particles able to initiate new cycles of infection.

It has been previously shown that inositol phosphates play a critical role in both HIV-1 assembly and maturation. While assembly of HIV-1 Gag protein *in vitro* yields immature particles that differ in size and character from authentic virions, addition of inositol phosphates to *in vitro* assembly reactions enables the production of particles that resemble authentic virions (*115*). Further work identified inositol hexakisphosphate, or IP_6, as the key mediator of this process. IP_6, is a ubiquitous cellular polyanion containing 5 equatorial phosphates and a single axial phosphate, and facilitates formation of immature HIV-1 Gag lattice by binding to and stabilizing positively-charged rings of primary amines. These rings are formed by lysine residues at Gag positions 290 and 359 (K290 & K359) that are positioned at the center of the immature Gag hexamer (*116*). Following the subsequent structural rearrangement of CA that accompanies

maturation, IP_6 next binds to a second, distinct positively charged ring in the mature CA hexamer formed by arginine residues at CA position 18 (R18, Gag position R150). The R18 ring stabilizes the mature CA hexamer, and is required for viral DNA synthesis in newly infected cells (*117–119*). It is thought that IP_6 is recruited into virions by interacting with K290 and K359 during immature particle production; this model is consistent with data demonstrating that HIV-1_{K290A} and HIV-1_{K359A} are significantly defective in both viral production and IP_6 packaging, while HIV-1_{K359I} is assembly competent but generates poorly infectious particles(*120*).

The importance of each of the IP_6-coordinating residues has been established, as mutagenesis of any such residue to an alanine (HIV-$1_{R18A,}$ HIV-1_{K290A}, or HIV-1_{K359A}) significantly impairs infectivity in either single cycle or spreading infection assays (*116*, *120*). Additionally, yield of infectious virions is also substantially reduced in cells lacking key enzymes in the IP_6 biosynthetic pathway (IPPK or IPMK) or in cells overexpressing MINPP1, a phosphatase that dephosphorylates IP_6(*116*, *120–122*). The IP_6-coordinating amino acids are conserved among diverse lentiviruses, suggesting a general requirement for IP_6 (*123*).

2.2 Identification of a second-site substitution that restores replication competence to IP_6-binding deficient HIV-1 mutants

While there is considerable evidence that perturbing IP_6 binding impairs HIV-1 replication, further investigation into the precise mechanisms underlying replication deficits is warranted. To better understand the role of IP_6, we serially passaged virions containing substitutions in IP_6-coordinating residues (HIV-1_{R18A}, HIV-$1_{K290A,}$ or HIV-1_{K359A}) in the highly-permissive MT4 T-cell line to identify second-site compensatory mutations that might rescue the resulting infectivity deficits. Initial attempts, in which MT4 cells were infected with mutant viral stocks, were unsuccessful, likely due to the dramatically reduced fitness of these mutants and consequent

inability to establish a sufficiently large population of infected cells to generate revertants. To overcome this problem, we instead co-cultured MT4 cells with virus-producing 293T cells that had been transfected with HIV-1_{R18A}, HIV-$1_{K290A,}$ and HIV-1_{K359A} proviral plasmids that encode GFP in place of nef. After removing the 293T cells, infected MT4 cells were co-cultured with uninfected MT4 cells, until most of the MT4 cells became infected (as monitored by visual inspection of GFP+ cells in the culture). Thereafter, cell-free supernatant was serially passed in MT4 cells (Figure 2.1A).

For one mutant, HIV-1_{K359A}, observation of GFP positive cells suggested that an apparently compensatory mutation arose after approximately 2 weeks of passaging. PCR amplification and sequencing of Gag encoding sequences from this culture revealed the presence of a single nucleotide substitution in *gag* that resulted in a threonine to isoleucine substitution at Gag position 371 (Figure 2.1B). No revertant mutants could be obtained for HIV-1_{R18A} or HIV-1_{K290A}. This finding may reflect a greater magnitude of impairment of these particular substitutions, making the generation of revertant mutants more difficult.

To determine whether the T371I mutant rescued the infectivity defect present in HIV-1_{K359A}, we generated a proviral clone, HIV-$1_{K359A/T371I}$, encoding both mutations and measured the infectious virion yield from proviral plasmid-transfected 293T cells. Addition of the T371I substitution to HIV-1_{K359A} restored infectious virion yield to wild-type levels (Figure 2.1C). Although this second-site, apparently compensatory change was identified only in the context of HIV-1_{K359A}, we asked whether the T371I substitution could rescue the HIV-1_{K290A}, given purported similar roles of K290 and K359 in binding IP_6. Indeed, we found that HIV-$1_{K290A/T371I}$, unlike HIV-1_{K290A}, yielded similar levels of infectious HIV-1 virions to wild-type HIV-1.

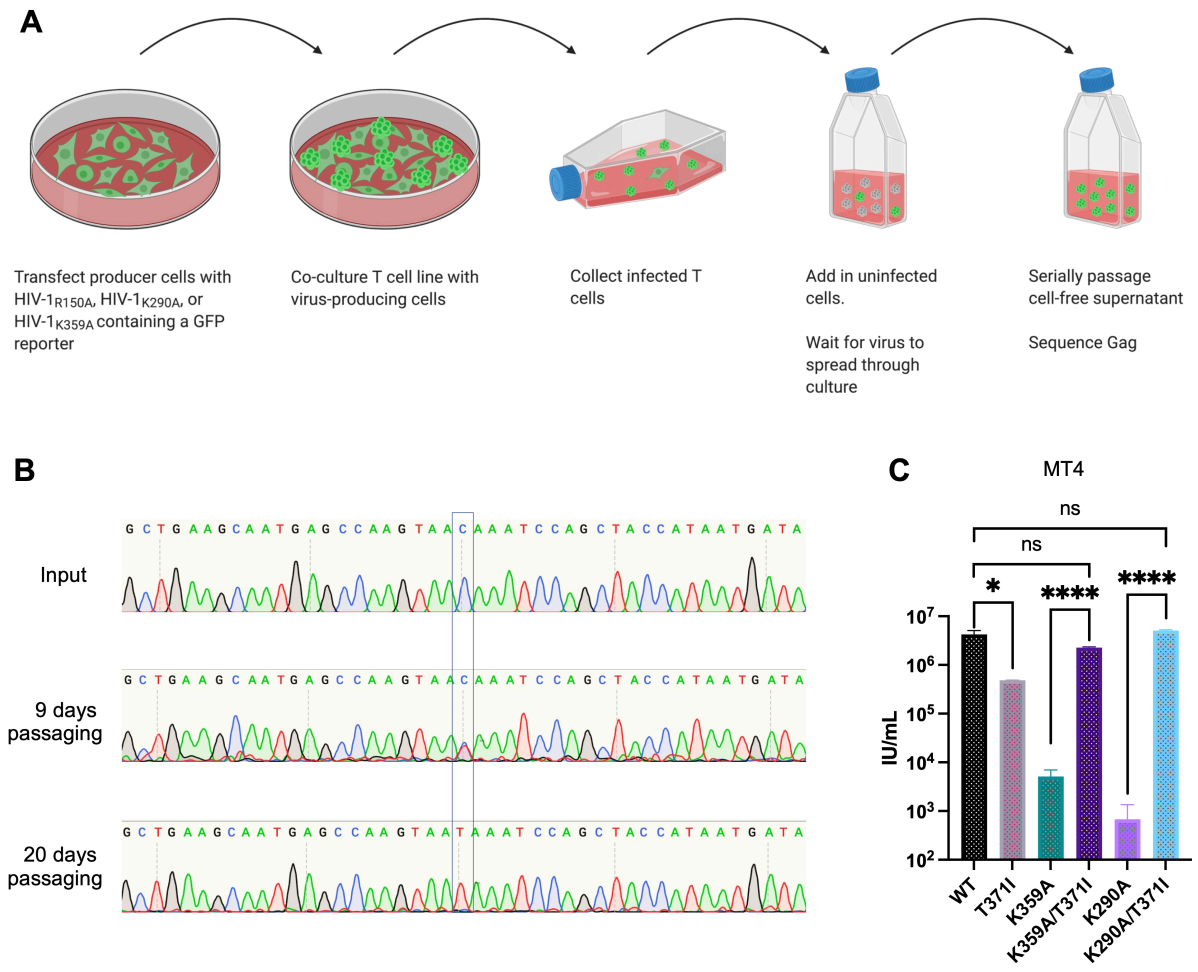

Figure 2.1 Derivation of an IP6-independent HIV-1 mutant
(A) Passaging schematic. (B) Sanger sequencing of HIV-1 gag indicating emergence of a single-site revertant. Input or viral RNA was isolated at indicated timepoint, and the gag region was amplified by RT-PCR. (C) Single cycle infection assay confirming the identified substitution rescues infectivity of K359A. 293T cells were transfected with proviral clones of WT HIV-1NHG or indicated mutant, and 48 hours post transfection, supernatant was titrated on MT4 cells. Statistical analysis: Student's T test.

To determine whether the effects of the T371I mutant, were evident outside the context of transfected 293T cells, we performed spreading replication assays of HIV-1_{WT}, HIV-1_{T371I}, HIV-1_{K359A}, and HIV-$1_{K359A/T371I}$ in MT4 cells (Figure 2.2A) and CEM cells (Figure 2.2B). As expected, HIV-1_{K359A} replicated poorly in both cell types. HIV-1_{T371I} replicated poorly in CEM cells but well in MT4 cells, perhaps reflecting the greater permissiveness of MT4 cells.

Importantly however, we found similar phenotypes for HIV-$1_{K359A/T371I}$ in spreading replication assays in both MT4 and CEM cells; namely, addition of the T371I substitution to HIV-1_{K359A} restored replication, with the HIV-$1_{K359A/T371I}$ double mutant exhibiting only a modest delay compared to HIV-1_{WT} in both cell types (Fig 1D-E).

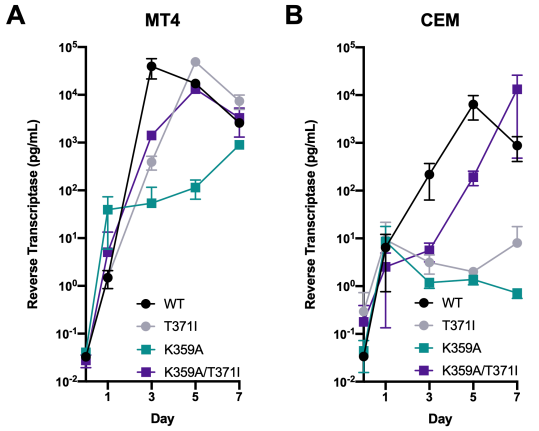

Figure 2.2: Revertant mutant rescues spreading infection in multiple T cell lines

Spreading replication assays in MT4 cells (A) or CEM cells (B). Cells were infected with HIV-1_{WT} or indicated mutant at an MOI of 0.001. 16 hours post infection, inoculum was washed away and supernatants were collected at the indicated timepoints. Reverse transcriptase activity was measured in the supernatant samples using SYBR-PERT.

2.3 Infectious HIV-$1_{K359A/T371I}$ particle yield is not affected by reduction of IP_6 synthesis in virus producing cells

Because the HIV-1_{K359A} is defective for IP_6 binding we next asked whether HIV-$1_{K359A/T371I}$ retained infectiousness when cellular IP_6 levels were reduced. Using CRISPR/Cas9 we generated 293T cell lines lacking IPMK, an enzyme in the IP_6 synthetic pathway. Previous work has demonstrated IPMK knockout cells have greatly reduced levels of both IP_5 and IP_6 (*120*). To account for potential clonal variation in capacity to generate HIV-1 particles, we used 3 separate IPMK targeting sgRNAs or a corresponding empty vector to generate ten independent single cell clones of IPMK knockout and WT control 293T cells (Figure 2.3A). The loss of IPMK was

confirmed by DNA sequencing of target loci, which revealed the introduction of frameshift mutations and the absence of intact IPMK alleles. In agreement with previous studies, the yield of infectious HIV-1_{WT} virions from IPMK-deficient 293T cells was significantly decreased, by 10-fold (p=0.0091, Figure 2.3A). The yield of HIV-1_{K359A} from 293T cells was greatly reduced compared to wildtype HIV-1 as expected, and was not further reduced by IPMK deficiency (Figure 2.3B). Yield of HIV-1_{T371I} was also slightly reduced compared to wildtype but not impacted by IPMK deficiency (Figure 2.3C, p=0.1374). Importantly, the yield of HIV-$1_{K359A/T371I}$ was only marginally reduced compared to wild type HIV-1 and there was no difference in yield of infectious HIV-$1_{K359A/T371I}$ from WT 293T cells versus IPMK deficient 293T cells (Figure 2.3D, p=0.178).

As IP_6 deficiency impacts both HIV-1 particle production as well as infectivity, we assayed particle levels in the same supernatants from Figure 2.3A-D using detection of reverse transcriptase with the SYBR-PERT assay. Importantly, we see the same phenotype for particle production as we do with infectivity assays: production of HIV-1_{WT} particles is impaired in IPMK KO cells, but there are no production deficits for HIV-1_{K359A}, HIV-1_{T371I}, or HIV-$1_{K359A/T371I}$ (Figure 2.3E-H). However, while there was a 10-fold reduction in HIV-1_{WT} infectivity from IPMK-deficient 293T cells, we only observed a 5-fold reduction in particle production in the exact same supernatants.

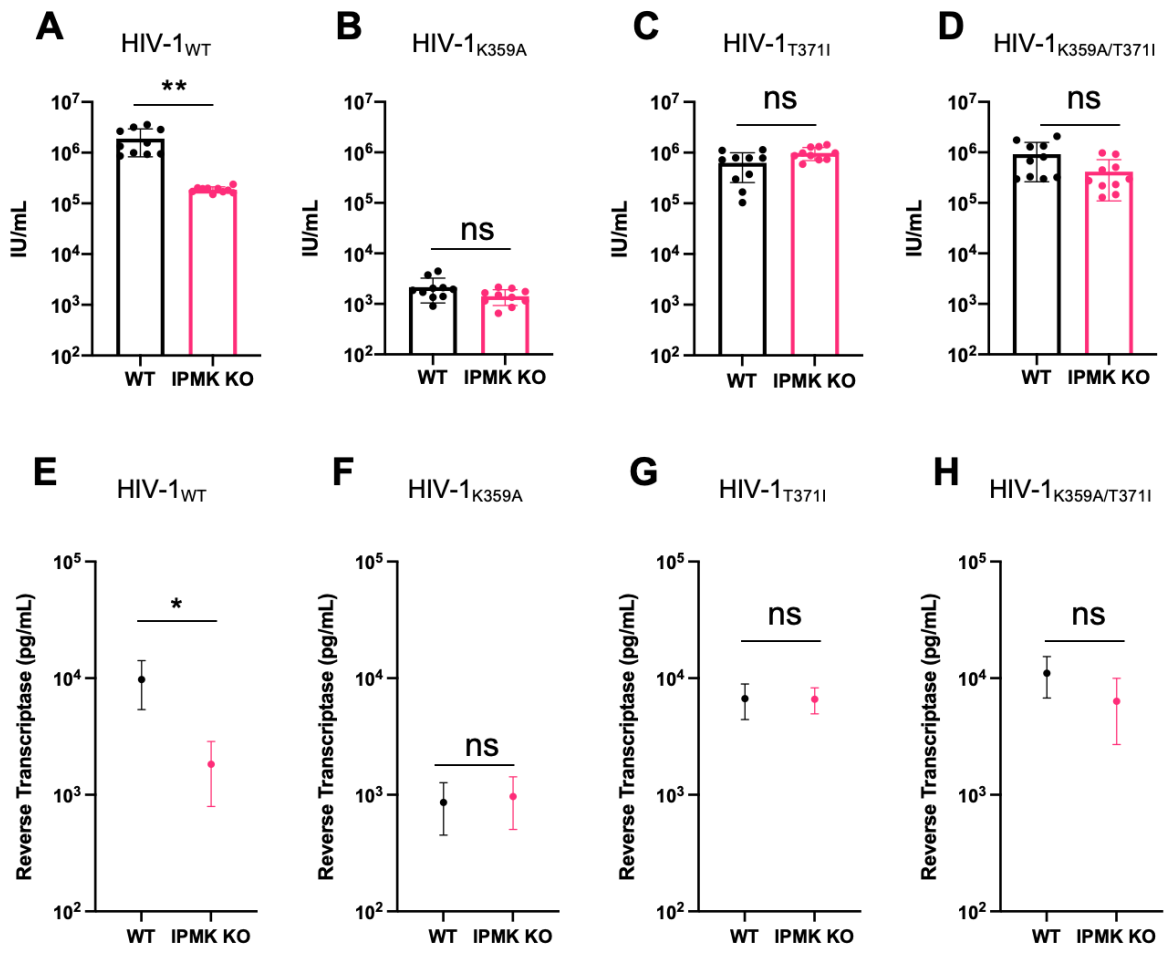

Figure 2.3: HIV-$1_{K359A/T371I}$ is not impaired by lack of cellular IP6

(A-D): Control or IPMK KO single 293T cell clones were transfected with HIV-1_{WT} (A), HIV-1_{K359A} (B), HIV-1_{T371I} (C), or HIV-$1_{K359A/T371I}$ (D) proviral plasmids. After 48 hours, supernatants were collected and titrated on MT4 cells. Each data point represent a different 293T cell clone. Statistical analysis: unpaired Student's t-test. Alternatively, levels of Reverse Transcriptase in supernatants were quantified using the SYBR-PERT assay (E-H). Statistical analysis: unpaired Student's t-test.

2.4 There is no impairment of infection in target cells with reduced IP_6 synthesis by HIV-1_{WT} or HIV-$1_{K359A/T371I}$

It has been proposed that residues K290 and K359 recruit IP_6 into HIV-1 virions during assembly, thereby providing the source of the IP_6 that binds to and stabilizes the R18 ring in the mature capsid core. The rationale for this idea stems from previous studies which have demonstrated that reduction of cellular IP_6 levels in target cells does not impact susceptibility to

incoming infection (*120*, *121*). Because HIV-$1_{K359A/T371I}$ is fully infectious despite encoding a mutation that is predicted to diminish IP_6 packaging into virions, we next asked whether HIV-$1_{K359A/T371I}$ requires IP_6 in target cells to be maximally infectious. We generated twelve IPMK-deficient MT4 target cell clones and six control clones and performed single cycle infection assays using HIV-1_{WT} and HIV-$1_{K359A/T371I}$ (Figure 2.4A-B). In agreement with previous studies (*120*), there was no difference in the infectiousness of HIV-1_{WT} in WT or IPMK-deficient MT4 cells (Figure 2.4A p = 0.3863). Moreover, there was no deficit in the infectiousness of HIV-$1_{K359A/T371I}$ in WT or IPMK-deficient MT4 target cells (Figure 2.4B, p=0.4331), suggesting that HIV-$1_{K359A/T371I}$ either does not require IP_6 for replication, or that the T371I mutation rescues both replication and IP_6 incorporation.

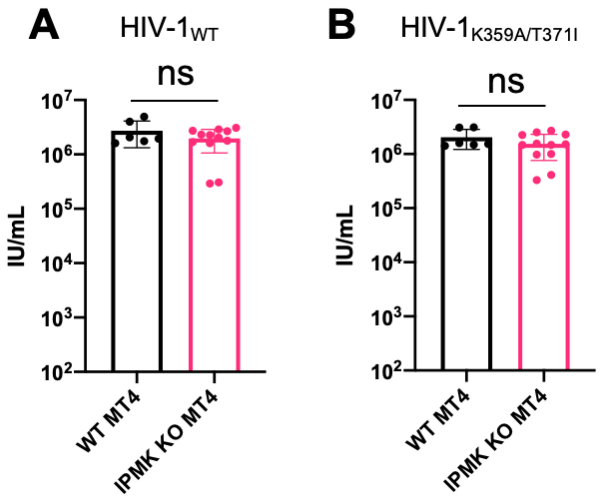

Figure 2.4: Infection of IPMK KO target cells is not impaired for either HIV-1_{WT} or HIV-$1_{K359A/T371I}$

HIV-1_{WT} (A) or HIV-$1_{K359A/T371I}$ (B) virions were titrated on WT MT4 or IPMK KO MT4 cells and infection quantified by flow cytometry. Statistical analysis: unpaired Student's t-test.

2.5 Bevirimat rescues infectious virion formation by the IP_6-binding deficient mutant HIV-1_{K359A}

Notably, The T371I mutation identified herein had been described previously in a different context. Specifically, this substitution was reported to stabilize the immature CA-SP1 lattice, mimicking the effect of maturation inhibitors (MI) (*124*, *125*). Therefore, we next asked whether maturation inhibitors themselves could rescue the deficit in infectious virion yield exhibited by HIV-1_{K359A}. As a control, we included the previously described assembly-defective, maturation inhibitor-dependent CA mutant HIV-1_{P289S} (*125*), We found that that BVM indeed rescued the infectivity of HIV-1_{K359A} and HIV-1_{P289S} in both single-cycle and spreading replication. Specifically, in single cycle assays, BVM increased the yield of infectious HIV-1_{K359A} virions, up to 50-fold, and in a dose-dependent manner (Figure 2.5A) from transfected 293T cells. In spreading replication assays, BVM restored HIV-1_{K359A} replication to levels similar to that of BVM-treated wildtype virus in MT4 cells (Figure 2.5B). BVM also rescued the spreading replication of HIV-1_{K359A} in CEM cells, indeed in this context the effect of BVM on HIV-1_{K359A} spreading was greater than that on the previously described MI-dependent mutant HIV-1_{P289S} (Figure 2.5C).

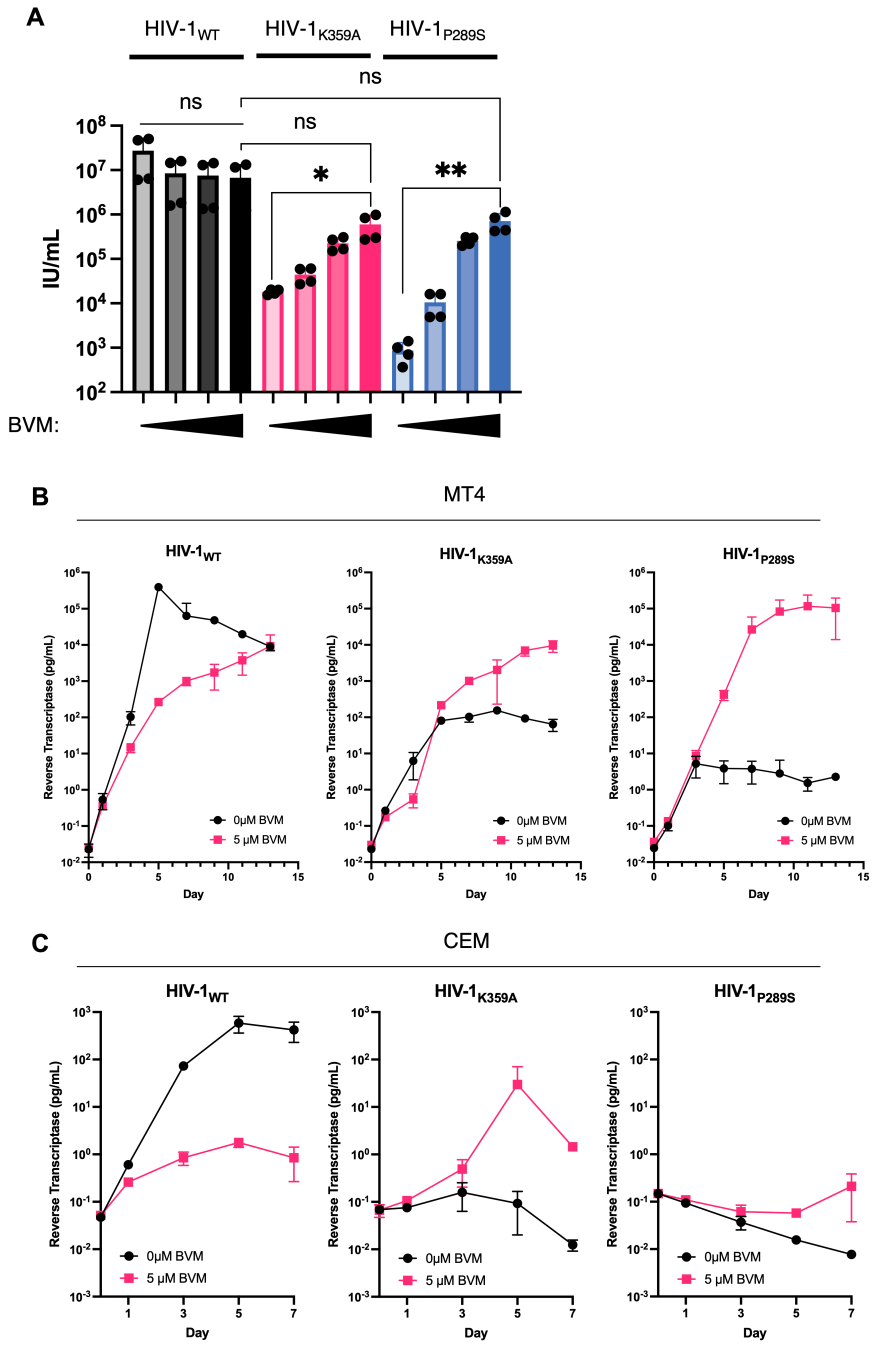

Figure 2.5: Bevirimat rescues infectivity of HIV-1$_{K359A}$

(A) 293T cells were transfected with HIV-1$_{WT}$, HIV-1$_{K359A}$, or HIV-1$_{P289S}$ proviral plasmids in the presence of 0, 1, 5, or 10 μM Bevirimat. After 48 hours, supernatants were collected and titrated on MT4 cells and infection quantified by flow cytometry.
(B-C) MT4 cells (B) or CEM cells (C) were infected with HIV-1$_{WT}$, HIV-1$_{K359A}$, or HIV-1$_{P289S}$ at an MOI of 0.001. At 16 hours post infection, inoculum was washed away and supernatants were collected at the indicated timepoints. Reverse transcriptase activity was measured in the supernatant samples using SYBR-PERT.

2.6 BVM increases release of HIV-1_{K359A} virions independently of the viral protease

The interaction between K359 amines and IP_6 likely stabilizes the immature Gag lattice, Similarly, maturation inhibitors are known to bind to the immature Gag hexamers at approximal site and stabilize the immature CA-SP1 lattice (*126*, *127*). Therefore, we hypothesized that BVM rescue particle formation by HIV-1_{K359A} by stabilizing an otherwise destabilized lattice, effectively serving as a functional replacement for IP_6. To test this idea, we measured the release of HIV-1_{K359A} virions from BVM-treated 293T cells by western blotting. BVM indeed increased the yield of HIV-1_{K359A} virions, in a dose-dependent manner (Figure 2.6A). To confirm that this effect was not due to BVM-mediated inhibition of Gag proteolysis, we performed similar experiments in virions containing an inactivating mutation in protease. We observed a similar dose-dependent increase in immature particle release, even in the context of protease inactivation (Figure 2.6B), suggesting that the effect of BVM on HIV-1_{K359A} assembly is due to the direct effect of BVM on the immature lattice, not through inhibition of proteolytic cleavage at the Gag-SP1 junction.

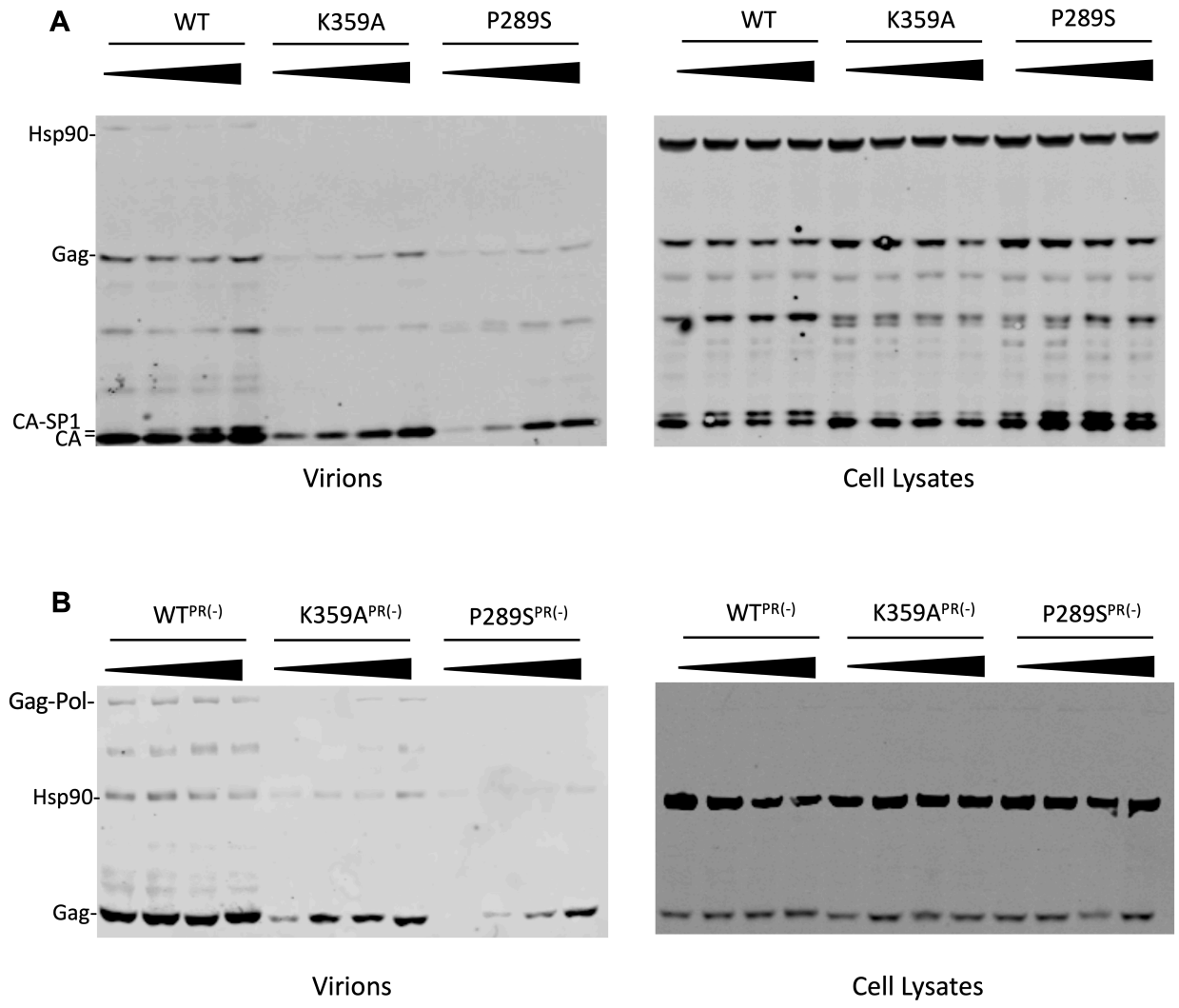

Figure 2.6: Bevirimat increase release of HIV-1K359A independently of protease inhibition

(A) 293T cells were transfected with HIV-1_{WT}, HIV-$1_{K359A,}$ or HIV-1_{P289S} in the presence of 0, 1, 5, or 10 μM Bevirimat. 48 hours post transfection, supernatants were pelleted over a sucrose cushion and analyzed by SDS-PAGE alongside cell lysates. Hsp90 serves as a loading control. (B) 293T cells were transfected with HIV-1_{WT}, HIV-$1_{K359A,}$ or HIV-1_{P289S} bearing an inactivating mutation in protease in the presence of 0, 1, 5, or 10 μM Bevirimat and analyzed via SDS-PAGE as above. Hsp90 serves as a loading control.

2.7 Visualization of BVM-induced HIV-1 assembly observed in real time using live cell fluorescence microscopy

The above data strongly suggested that BVM rescues infectivity and release of HIV-1_{K359A} by facilitating particle assembly. To directly observe effects on virion assembly, we performed fluorescence microscopy using a novel imaging construct based on HIV-1_{NL4-3}, in which Pol has been replaced by an HIV-1 codon-mimicking mNeonGreen, and in which Env and Vpu bear inactivating mutations. The resulting construct, herein referred to as HIV-1 NG, generates Gag-mNeonGreen in place of Gag-Pol during a single cycle of infection, thus allowing visualization of particle assembly as punctae at the plasma membrane.

We generated HIV-1 vectors particle containing this reporter and derivatives (HIV-1 NG_{WT}, HIV-1 NG_{K359A}, and HIV-1 NG_{P289S}) by supplying Gag-Pol and VSV-G *in trans.* Then, we infected TZM-bl cells in the absence or presence of 5 μM BVM and performed widefield imaging on fixed cells 48 hours post infection. In the absence of BVM, cells infected with HIV-1 NG_{K359A} and HIV-1 NG_{P289S} exhibited primarily diffuse cytoplasmic fluorescence, and fewer punctae than for HIV-1 NG_{WT} infected cells, indicating impaired assembly (Figure 2.7A). However, when infections were done in the presence of BVM, there were clearly increased numbers of membrane associated punctae in HIV-1 NG_{K359A} and HIV-1 NG_{P289S} infected cells (Figure 2.7A) suggesting BVM is able to directly facilitate particle assembly by these mutants.

This ability to induce HIV-1 particle assembly via addition of an exogenous small molecule has potential applications in imaging and other studies, as an inducible particle assembly system. In order to test the possible utility of this approach, we performed live cell widefield imaging studies using HIV-1 NG_{P289S}, as this mutant displayed a greater responsiveness to BVM-induced assembly (see Figures 2.5A, 2.5B, 2.6A, and 2.6B). We infected TZM-bl cells in the absence of

BVM and then, at 26 hours after infection, added BVM 5 μM and began acquiring images at 30 minute intervals. In the absence of BVM, few punctae are apparent in HIV-1 NG_{P289S} infected cells, even after 12 hours of imaging (Figure 2.7B). However, in the BVM-treated cells, substantially more punctae were evident, as soon as 30 minutes after BVM addition (Figure 2.7B).

Given that such striking differences could be observed as early as 30 minutes post BVM addition, we repeated these experiments with increased time resolution. TZM-bl cells were infected with HIV-1 NG_{P289S} for 26 hours and treated with BVM as above, followed by immediate image acquisition at 3 minute intervals. Assembly of HIV-1_{P289S} was rapidly induced by BVM (Figure 2.7C) with substantial numbers of punctae forming within 30-120min.

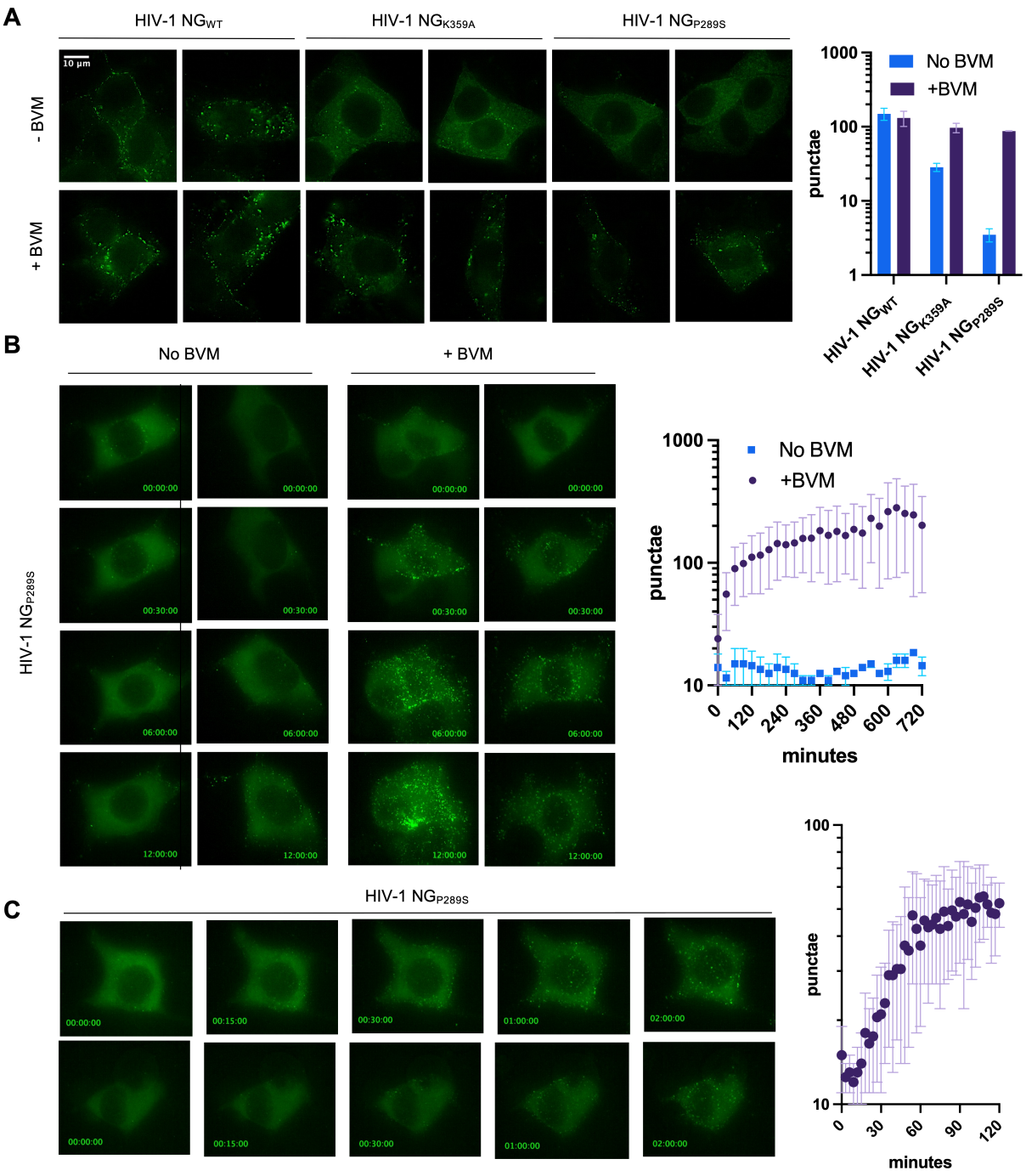

Figure 2.7: Visualization of Bevirimat-induced assembly by fluorescence microscopy

(A) Fluorescence microscopy of TZM cells infected with a reporter HIV-1 virus encoding mNeon Green in place of Pol (HIV-1 NG) to visualize assembly. Representative images 48 hours-post-infection of HIV-1 NG_{WT}, HIV-1 NG_{K359A}, or HIV-1 NG_{P289S} infected in the absence or presence of 5µM BVM. Quantification of Gag-NG punctae per image depicts mean ± SD for images from (A). (B) Representative time lapse images of TZM cells infected with HIV-1 NG_{P289S} -/+ treatment with 5µM BVM at 26 hours post infection. Image acquisition began

immediately after BVM addition. Image labels: Hours:Minutes:Seconds post BVM addition. Quantification of Gag-NG punctae per timepoint depicts mean ± SD for images from (B). (C) Representative time-lapse images of TZM cells treated with BVM at 26 hours post infection with HIV-1 $NG_{P289S.}$ Image labels: Hours:Minutes:Seconds post BVM addition. Quantification of Gag-NG punctae per timepoint depicts mean ± SD for images from (C).

We performed similar experiments using TIR-FM imaging and quantified the presence of Gag-NG punctae over time, with similar results. Specifically, in the absence of BVM there were very few punctae evident at the plasma membrane (Figure 2.8A, B). However, shortly after the addition of BVM, numerous punctae rapidly formed at the plasma membrane (Figure 2.8). These data provide proof of principle that such a system could be used to experimentally manipulate HIV-1 assembly for imaging or functional studies.

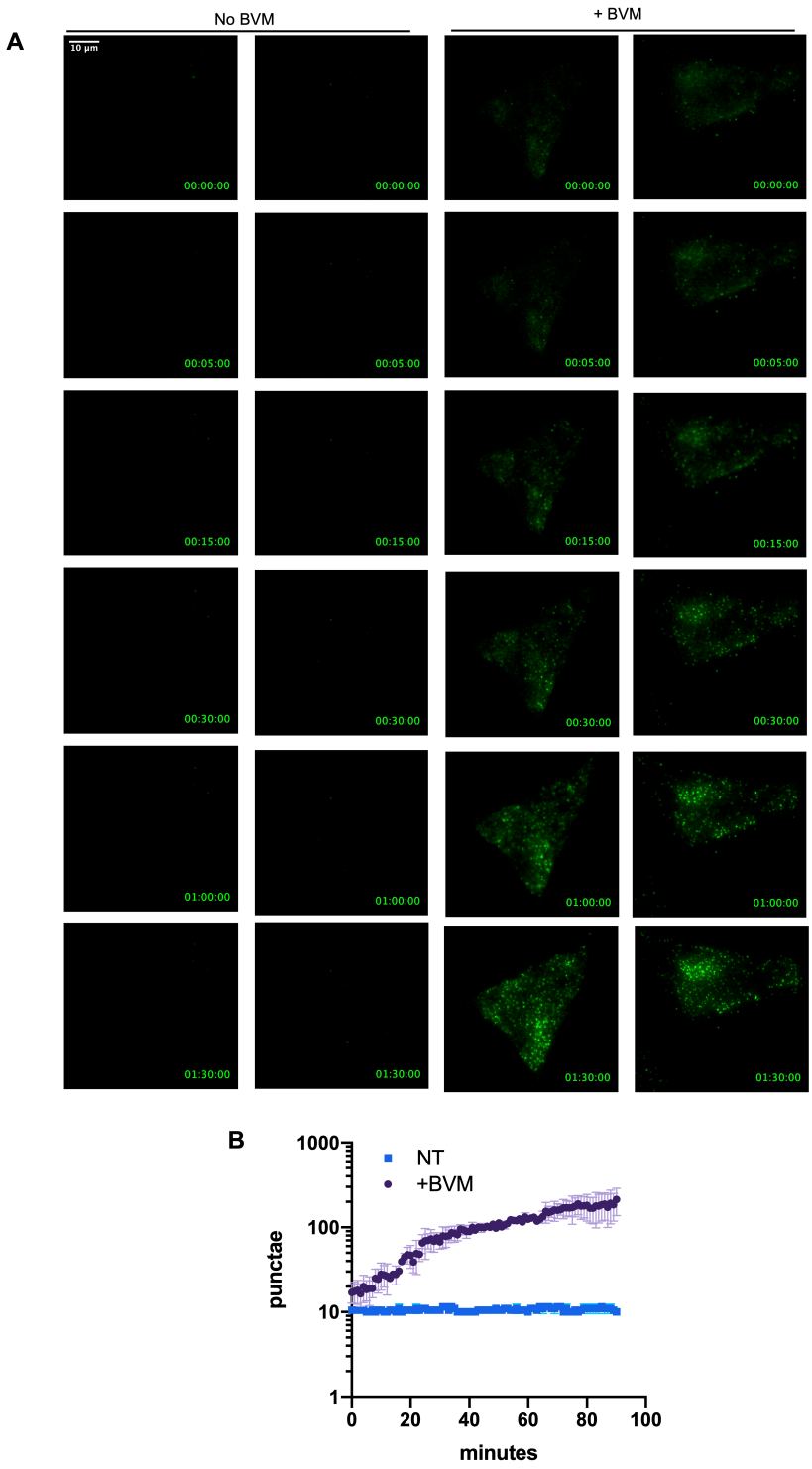

Figure 2.8 Visualization of Bevirimat-induced assembly by TIR-FM

(A) TIR-FM microscopy of TZM cells infected with HIV-1_{P289S} NG. Representative time-lapse images of TZM cells treated with BVM at 28 hours post infection. Image labels: Hours:Minutes:Seconds post BVM addition. (B) Quantification of punctae per time point depicts mean ± SD for images from (A).

2.8 Implications for the design of next generation antiretrovirals

Together, these data support a model whereby stability of the immature CA lattice is finely tuned, with IP_6 coordinating and stabilizing the otherwise repulsive positive charges of K290 and K359 to drive assembly. Manipulations that cause IP_6 binding deficiency, either mutagenesis of K359 or decreasing IP_6 levels in producer cells, destabilize the immature lattice and decrease production of progeny virions. Conversely, manipulations such as the T371I substitution or treatment of HIV-1_{WT} with BVM, hyper-stabilize the immature lattice in the wild type context and decrease HIV-1 infectivity. However, either the T371I substitution or BVM treatment are able to rescue virion assembly and infectiousness in the context of IP_6 deficiency. Understanding how small molecules such as BVM or IP_6 can enhance Gag lattice stability can provide new tools to study virion assembly and potential avenues for antiretroviral therapeutics. In addition to providing insight on Gag-Gag and Gag-IP_6 interactions during HIV-1 assembly, our work also identifies an inducible virion assembly system that can be used in investigating HIV-1 assembly events in living cells.

CHAPTER 3. Unbiased identification and characterization of human coronavirus dependency factors using genome-wide CRISPR screening.

3.1 Genome-scale loss-of-function CRISPR screening to identify potential host-targeted therapies for infection by diverse coronaviruses

In this century alone, four emerging zoonotic respiratory pathogens—SARS-coronavirus (CoV), MERS-CoV, H1N1 influenza A virus (IAV), and SARS-CoV-2—have caused significant morbidity and mortality. Of these, SARS-CoV, MERS-CoV, and SARS-CoV-2 are all enveloped, positive-stranded RNA viruses in the genus betacoronavirus (*128*). Four other coronaviruses are known to infect humans; Human CoV (HCoV)-OC43 and HCoV-HKU1 are members of the betacoronavirus genus (*129*), while HCoV-229E and HCoV-NL63 are members of the alphacoronavirus genus. There is thus an urgent need to discover host and viral determinants influencing coronavirus infection. Because viruses rely on host cellular proteins to replicate, an attractive strategy for the next-generation of antiviral therapies is targeted inhibition of human proteins—termed "dependency factors"—that are required for viral replication. Of particular interest are human proteins required by diverse viral lineages, encompassing not only known human pathogens but animal viruses that are of concern for future spillover into human populations. To identify coronavirus dependency factors, we performed a genome-wide loss-of-function CRISPR screen using HCoV-OC43 in a human lung cell line, and focused on candidate hits that are required by diverse coronaviruses. These hits thus represent attractive canidates for the development of host-targeted therapies with broad-spectrum activity.

3.2 A genome wide screen reveals HCoV-OC43 dependency factors

To identify host proteins required for HCoV-OC43 infection, we performed a genome-wide CRISPR screen in the A549 lung adenocarcinoma cell line. Briefly, A549 cells were transduced

with the Brunello sgRNA library (*130*, *131*) at a low MOI (0.3) and high coverage (500X) to generate a population of cells each harboring a single sgRNA. After selection to remove untransduced cells, A549-Brunello cells were infected with HCoV-OC43 at an MOI of 0.1 and incubated for 1 week to allow viral-induced cell death to occur (Figure 3.1A). Enrichment of sgRNA sequences in the surviving cells—i.e. those putatively lacking a dependency factor—was assessed using MAGeCK (*132*).

We identified 34 candidate dependency factors, defined as genes scoring higher than the highest scored non-targeting control (Figure 3.1B). As a positive control, we identified CASD1, the enzyme responsible for the generation 9-O-acetylated sialic acids, which serve as the receptor for HCoV-OC43 (*32*). Consistent with several other genome wide screens for viral dependency factors, we identified multiple genes (SLC35B2, XYLT2, and B4GALT7) involved in heparan sulfate biosynthesis, implying that heparan sulfate is an attachment factor for HCoV-OC43 (*17*, *21*, *25*, *133*, *134*).

To further classify gene hits (Figure 3.1C), we performed a functional enrichment analysis using string-db followed by annotation with UniProt keywords (*135*, *136*). Many of the hits were associated with intracellular transport or endosome activity including VPS29, the **C**CDC22/**C**CDC93/**C**OMMD3 (CCC) complex, and the WDR81/91 complex, suggesting a requirement for these functions in HCoV-OC43 infection. Additionally, we identified PIK3C3, which generates phosphatidylinositol 3-phosphate (PI(3)P), a phospholipid required for the recruitment of retromer to endosomes (*137*). Some of the genes identified by our screen were also recently reported in CRISPR screens utilizing SARS-CoV-2, implying that they are broadly required for coronavirus infection (*38*, *94*).

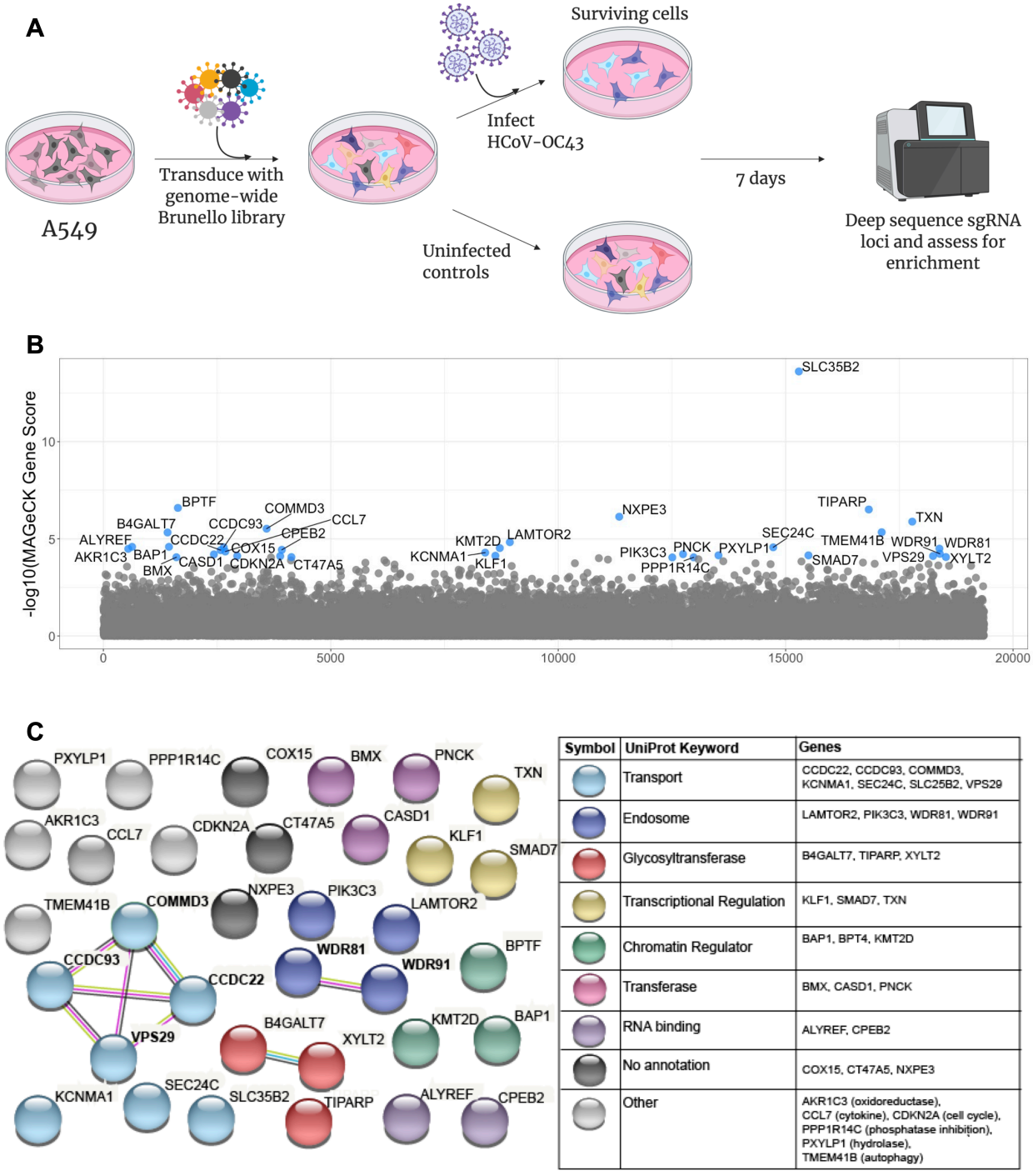

Symbol	UniProt Keyword	Genes
	Transport	CCDC22, CCDC93, COMMD3, KCNMA1, SEC24C, SLC25B2, VPS29
	Endosome	LAMTOR2, PIK3C3, WDR81, WDR91
	Glycosyltransferase	B4GALT7, TIPARP, XYLT2
	Transcriptional Regulation	KLF1, SMAD7, TXN
	Chromatin Regulator	BAP1, BPT4, KMT2D
	Transferase	BMX, CASD1, PNCK
	RNA binding	ALYREF, CPEB2
	No annotation	COX15, CT47A5, NXPE3
	Other	AKR1C3 (oxidoreductase), CCL7 (cytokine), CDKN2A (cell cycle), PPP1R14C (phosphatase inhibition), PXYLP1 (hydrolase), TMEM41B (autophagy)

Figure 3.1: A CRISPR screen reveals genes influencing HCoV-OC43 susceptibility

(A) Schematic of screening setup (B) Screen results, where the x-axis corresponds to each unique gene in the library (labeled randomly from 1 to 19,114) and the y-axis denotes the -$\log_{10}$ MAGeCK gene score. All genes scoring higher than the best-scoring non-targeting control pseudogene are labeled in blue. The screen was performed in three independent replicates (C) string-db analysis and UniProt annotation of gene hits. Sphere colors correspond to UniProt

keywords and connecting lines indicate strength of evidence underlying gene-gene interactions (pink: experimentally-determined interaction; blue: annotated interaction in curated databases; gray: evidence of co-expression; yellow: text-mining).

3.3 Requirement for candidate host factors is both cell type and virus dependent

We next investigated whether the VPS29/CCC complex and the WDR81/91 were required for infection by a diverse panel of respiratory viruses, including coronaviruses. In addition to HCoV-OC43, we tested additional seasonal HCoVs (HCoV-NL63 and HCoV-229E), rVSV/SARS-CoV-2, a chimeric vesicular stomatitis virus encoding the SARS-CoV-2 Spike protein, as well as other pathogenic respiratory viruses: IAV, adenovirus, and respiratory syncytial virus (RSV). We used CRISPR/Cas9 to generate individual cell lines lacking each gene of interest and confirmed knock-out (KO), both by sequencing target loci and by western blot analyses. Importantly, KO of these genes did not affect cellular viability or proliferation. Because viral dependency factors identified via CRISPR screening might be required in a cell-type specific manner, we evaluated the requirement of these genes for infection in multiple cell lines expressing ACE2 (the receptor for both SARS-CoV-2 and HCoV-NL63), specifically A549-ACE2, HT1080-ACE2, and 293T-ACE2.

Given their function in endosomal trafficking, we hypothesized that these hits would most likely affect viral entry. We therefore performed short-term infection assays and quantified infected cells via flow cytometry. There was strong requirement for VPS29/CCC complex as well as WDR81/91 in A549 cells for all CoVs tested (Figure 3.2A-D). However, the was no requirement of these factors in for IAV, adenovirus, or RSV infection of A549 cells (Figure 3.2E-G). In all other cell lines tested, there was a strong requirement for VPS29 for all coronaviruses but minimal dependency on VPS29 or the other candidate proteins was found for adenovirus and RSV (Figure 3.2H-T). Since these viruses all rely on endocytic pathways for

viral entry (*138–140*), these data indicate that VPS29/CCC and WDR81/91 are specifically required for coronavirus infection, rather than broadly impairing endocytic function. The magnitude of the effect of CCC complex and WDR81/91 knockout on CoV infection was different in different cell lines. For example, KO of the CCC complex or WDR81/91 had a blunted effect on CoV infection in HT1080-ACE2 cells (Figure 3.2H-K). Moreover, in 293T-ACE2 cells, KO of the CCC complex inhibited HCoV-OC43 but not HCoV-NL63 or rVSV/SARS-CoV-2 infection, while WDR81/91 knockout impaired infection for all three viruses (Figure 3.2O-Q).

We found that VSV infection was unaffected by VPS29 KO (Figure 3.2U). Because the sole difference between rVSV/SARS-CoV-2 and VSV itself is that rVSV/SARS-CoV-2 enters cells using the SARS-CoV-2 spike protein in lieu of VSV-G, these data suggest that it is the entry pathway that imposes the requirement for VPS29. Given the strong requirement for VPS29 by all tested HCoVs, in all cell lines tested, we sought to further confirm the relevance of VPS29 to HCoV infection. To do so, we used CRISPR/Cas9 to KO VPS29 in normal human bronchial epithelial (NHBE) primary lung cells. Loss of VPS29 strongly inhibited HCoV-OC43 infection in NHBE cells (Figure 3.2V), suggesting that VPS29 is important for HCoV infection of physiologically relevant cells.

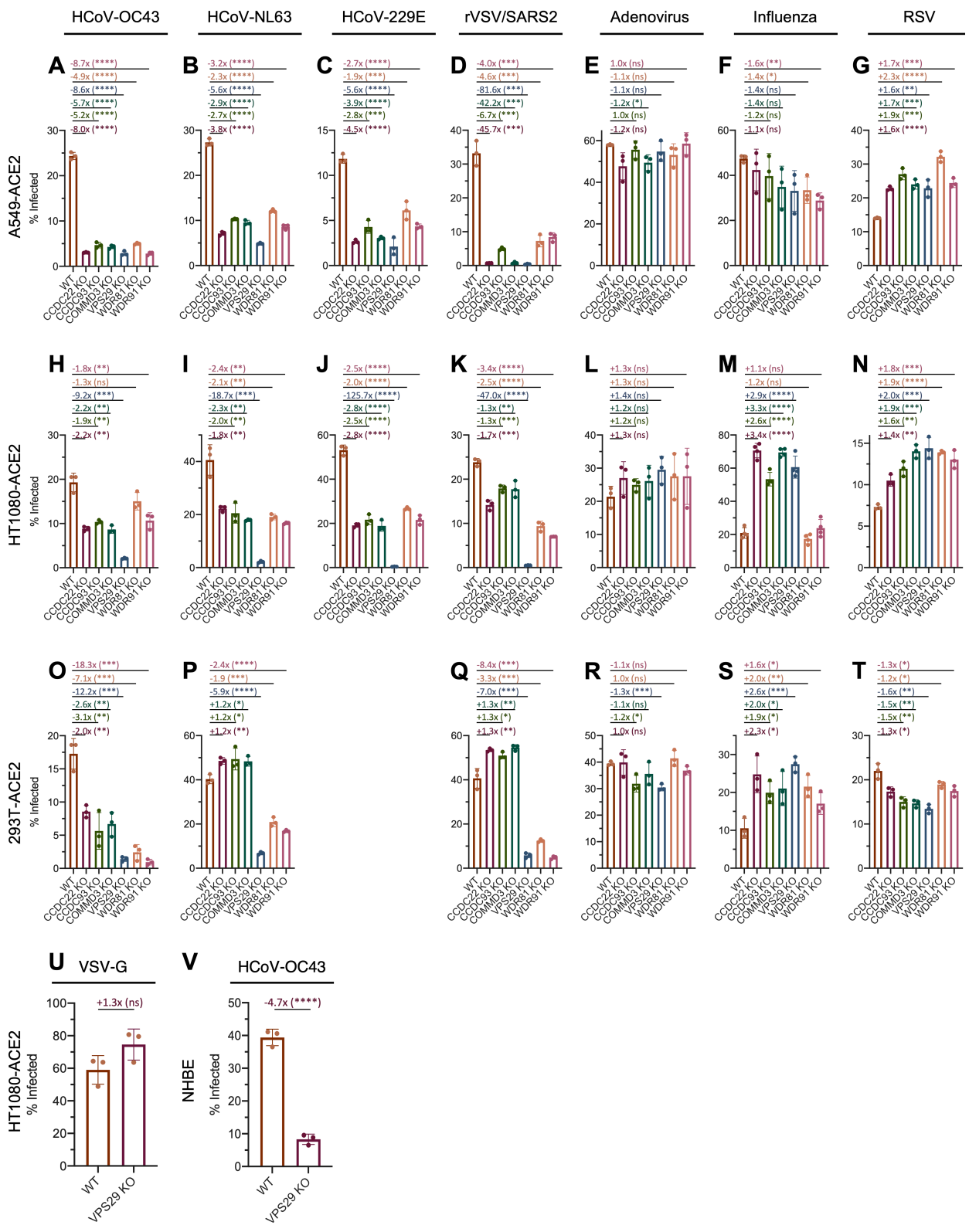

Figure 3.2: Requirement for identified host proteins is cell type and virus dependent

(A-V) Cells were infected with the indicated viruses at an MOI of 0.3. At 24 hours post

infection, cells were stained, and the percent infected cells was determined by flow cytometry. (A-G): A549-ACE2, (H-N, U): HT1080-ACE2, (O-T): 293T-ACE2, (V): NHBE. Mean (bar graph) of three replicates (dots). Error bars indicate SD. Data shown is a representative of at least two independent experiments. Statistical test: Student's T test between WT and KO cells. (*) indicate $p<0.05$, (**) indicate $p<0.01$, (***) indicate $p<0.001$, (****) indicate $p<0.0001$

3.4 VPS29-associated proteins facilitate CoV infection

Because of the dramatic and conserved effect of VPS29 on each HCoV tested, we elected to examine this protein in more detail. VPS29 can participate in multiple different protein complexes with distinct roles in normal cell biology (*141*). Thus, in order to clarify which VPS29 interacting proteins, if any, are important for facilitating CoV infection, we performed a focused siRNA screen targeting VPS29 interacting proteins and assessed impact of knockdown (KD) on HCoV infection.

Knockdown of VPS26A, VPS29, VPS35, or RAB7A each impaired HCoV-OC43, HCoV-NL63, HCoV-229E, and rVSV/SARS-CoV-2 infection (Figure 3.3A-D). These data strongly suggest that the participation of VPS29 in the Retromer complex (VPS26A/VPS29/VPS35), which is recruited to endosomes via Rab7A, is the means by which it facilitates CoV infection (*142*). Interestingly, KD of DSCR3 and C16orf62, which play analogous roles to VPS26 and VPS35 and form the Retriever complex (*143*), inhibited HCoV-OC43 infection but not HCoV-NL63, HCoV-229E, or rVSV/SARS-CoV-2 infection.

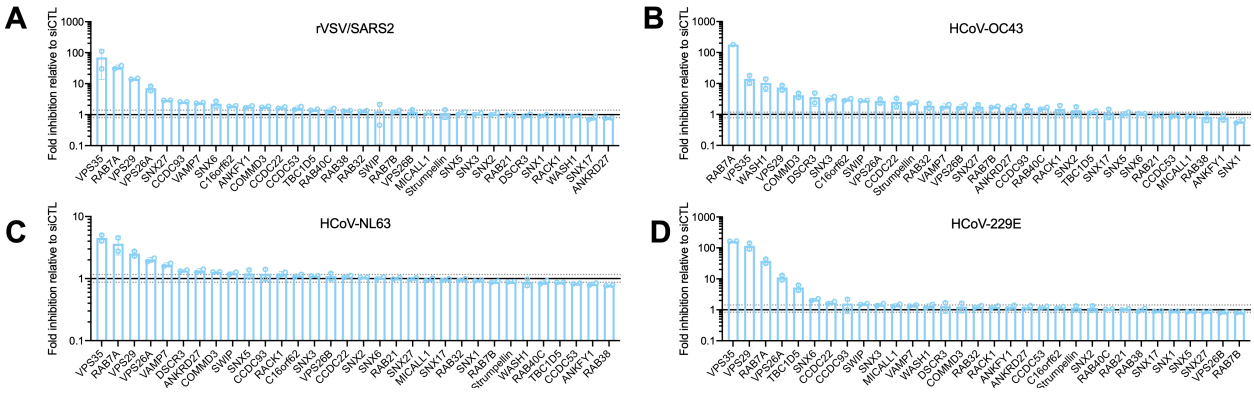

Figure 3.3: Effect of VPS29 KO on HCoV infection is primarily driven by loss of Retromer

(A-D) HT1080 cells were transfected with a focused siRNA library targeting VPS29-interacting proteins. Two days after transfection, cells were infected with (A) rVSV/SARS-CoV-2, (B) HCoV-OC43, (C) HCoV-NL63, and (D) HCoV-229E at an MOI of 0.3. At 24 hours post infection, cells were stained, and the percent infected cells was determined by flow cytometry. Plotted are levels of inhibition (for HCoVs and rVSV/SARS-CoV-2) in siRNA KD cells, relative to siRNA non-targeting control. Fold change values were calculated by comparing levels of infection in KD cells to the average of 4 separate pools of non-targeting siRNA controls. Solid black line marks fold change of 1. The dashed lines mark the highest and lowest fold changes of non-targeting siRNA controls from the average.

3.5 The ability of VPS29 to facilitate CoV infection depends on interaction with retromer components and regulators

In an orthogonal approach to investigate the role of the Retromer complex in facilitating CoV infection, we generated HT1080 VPS29 KO single cell clones (SCCs) and reconstituted with wildtype (WT) and mutant forms of VPS29. One VPS29 mutant (I91D) does not interact with the Retromer component VPS35, while the other (L152E) does not interact with TBC1D5, a RAB7A GTPase-activating protein that is critical for endosomal recycling of known retromer cargoes (*144–146*). In agreement with our previous data, CoV infection was inhibited in the VPS29 KO SCC (Figure 3.4A-D). Susceptibility of HT1080 VPS29 KO cells was substantially restored upon reconstitution with a construct expressing a WT, sgRNA-resistant VPS29. However, reconstitution with a construct expressing $VPS29_{I91D}$ or $VPS29_{L152E}$ did not reverse the effects of VPS29 KO on HCoV infection (Figure 3.4A-D). Overall, these data confirm that loss of the Retromer complex function is the major means by which VPS29 KO affects CoV infection.

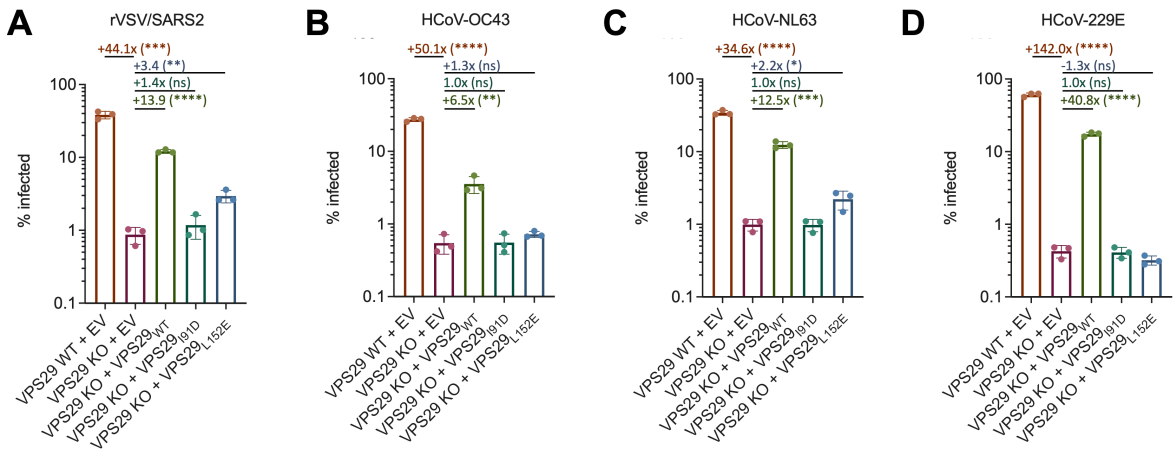

Figure 3.4 VPS29 requires interaction with Retromer components to facilitate HCoV infection

(A-D) WT and VPS29 mutants were reconstituted in VPS29 KO cells. Cells were infected with (A) rVSV/SARS-CoV-2, (B) HCoV-OC43, (C) HCoV-NL63, or (D) HCoV-229E. At 24 hours post infection, cells were stained, and the percent infected cells was determined by flow cytometry. Mean (bar graph) of three replicates (dots). Error bars indicate SD. Data shown is a representative of two independent experiments. Statistical test: Student's T test between VPS29 KO cells and VPS29 expressing cells. (*) indicate $p<0.05$, (**) indicate $p<0.01$, (***) indicate $p<0.001$, (****) indicate $p<0.0001$

3.6 VPS29 deficiency results in enlarged, deacidified endosomes

To elucidate the impact of VPS29 on viral infection we next investigated the impact of VPS29 KO on normal endosomal function. We labeled endosomes in living cells using a construct containing two FYVE domains fused to mScarlet (2XFYVE-mSCAR), which binds to PI(3)P that is enriched on endosome membranes (*147*). Thereafter we treated cells with Dextran labeled with pH-sensitive (pHrodo Green or pHrodo Red) or pH-insensitive (Alexa Fluor (AF)-488) fluorophores to visualize endocytic cargo uptake, as well as the pH status of these endosomes.

Unlike parental HT1080 cells, VPS29 KO cells displayed a prominent subset of enlarged PI(3)P-positive endosomes. These enlarged endosomes were deacidified, as evident from decreased pHrodo Green Dextran signal compared to endosomes in unmanipulated cells, or other

smaller endosomes in VPS29 KO cells (Figure 3.5A,B). Importantly, there was a return to normal endosome phenotype after reconstitution with wildtype VPS29, confirming that this effect is due to VPS29 KO (Figure 3.5C). The appearance of enlarged, deacidified vesicles was maintained in VPS29 KO cells reconstituted with $VPS29_{I91D}$ or $VPS29_{L152E}$ (Figure 3.5D,E), suggesting that this phenotype is due to retromer disfunction. Quantification of the pH-sensitive Dextran signal from these images of VPS29 KO cells revealed a 3.7-fold decrease in fluorescence intensity (Figure 3.5F) that is rescued upon reconstitution with WT VPS29, but not with $VPS29_{I91D\ or}$ $VPS29_{L152E.}$

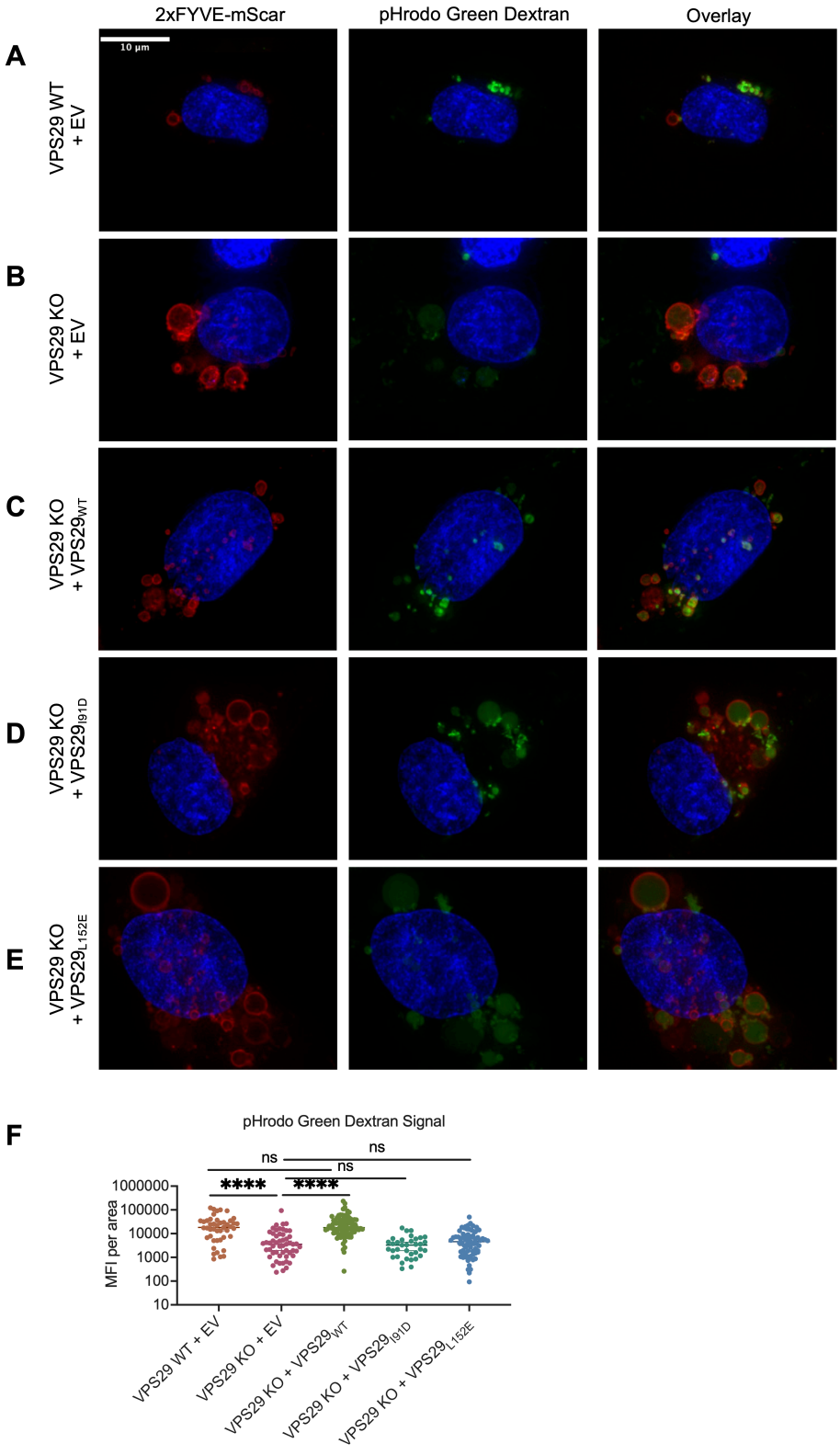

Figure 3.5 VPS29-KO results in enlarged, deacidified PI(3)P-rich vesicles

Representative images of HT1080 cells transduced with a construct expressing 2xFYVE-

mSCAR after incubation with pHrodo Green Dextran for 60 minutes. (A): VPS29 WT + EV expression cassette. (B): VPS29 KO HT1080 + EV expression cassette. (C): VPS29 KO HT1080 reconstituted with WT VPS29. (D): VPS29 KO HT1080 reconstituted with $VPS29_{I91D}$. (E): VPS29 KO HT1080 reconstituted with $VPS29_{L152E}$. EV: empty vector. (F): Quantification of Mean Fluorescence Intensity (MFI) of pHrodo Green Dextran signal inside of 2x-FYVE labeled endosomes from n=4 independent images (images in A-E, as well as the additional representative images depicted in Supplemental Figure S2). Error bars indicate SD. Statistical test: Student's T test. (*) indicate $p<0.05$, (**) indicate $p<0.01$, (***) indicate $p<0.001$, (****) indicate $p<0.0001$

Importantly, the enlarged endosomes in VPS29 KO cells exhibited equivalent fluorescent intensity to endosomes in normal cells when cells were incubated with pH-insensitive AF-488 Dextran, indicating that while they were deacidified, they were not defective in cargo loading (Figure 3.6A, B). Overall, this data suggests that reduced endosome acidification in VPS29 KO cells is responsible for the impairment of CoV infection. In order to test this, we artificially deacidified endosomes by treating WT or VPS29 KO cells with NH_4Cl. As expected, there was a dramatic decrease in rVSV/SARS-CoV-2 infectivity in WT cells treated with NH_4Cl (Figure 3.6C). Interestingly, this effect was much less pronounced in VPS29 KO cells, and there was no further impairment in infectivity in VPS29 KO cells treated with NH_4Cl than there was in WT cells treated with NH_4Cl. That lack of additive effect of NH_4Cl treatment in VPS29 KO cells suggests both conditions result in an analogous effect on viral infection.

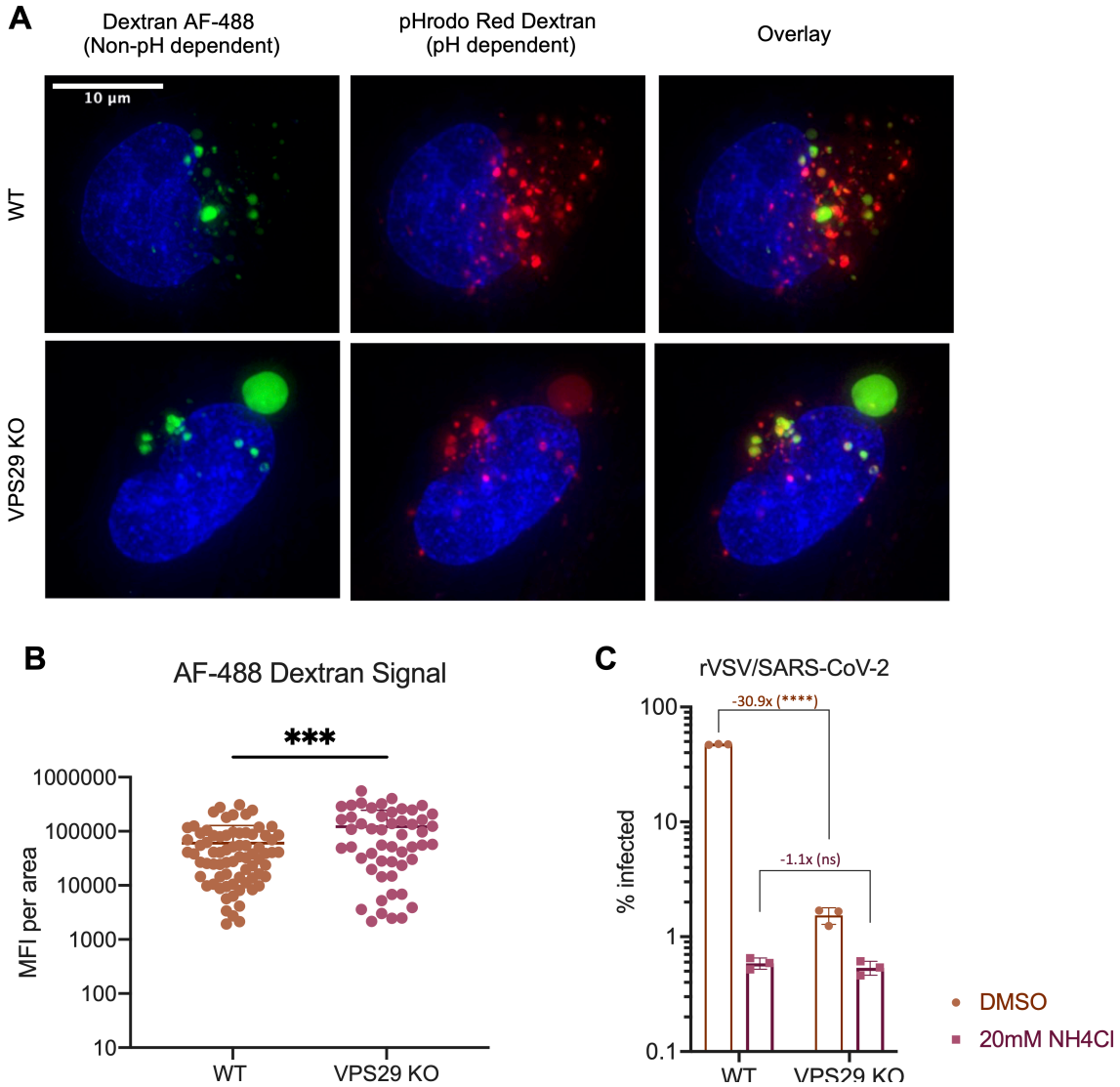

Figure 3.6 Enlarged, deacidified vesicles in VPS29-KO cells are not impaired for cargo loading

(A): Representative images of HT1080 cells incubated with Dextran AF-488 (non-pH dependent) and pHrodo Red Dextran (pH dependent) for 60 minutes. (B): Quantification of Mean Fluorescence Intensity (MFI) of AF-488 Dextran Signal inside vesicles in WT and VPS29 KO cells from n=3 independent images (images in A, as well as the additional representative images in Supplemental Figure S3). (C) WT and VPS29 KO HT1080 cells were treated with 20mM NH4Cl for 60 minutes before infection with rVSV/SARS-CoV-2. At 24 hours post infection, the percentage of infected cells was determined by flow cytometry. Error bars indicate SD. Statistical test: Student's T test. Statistical test: Student's T test between WT and KO cells. (*) indicate $p<0.05$, (**) indicate $p<0.01$, (***) indicate $p<0.001$, (****) indicate $p<0.0001$

To further confirm that this phenotype is due to Retromer disfunction we also performed experiments in cells treated with siRNA duplexes targeting distinct retromer components, namely VPS26A or VPS35. We found that, as in VPS29 knockdown cells, loss of VPS26A or VPS35 also resulted in enlarged, deacidified vesicles, providing further evidence that the effect seen in VPS29 KO cells is due to loss of Retromer (Figure 3.7A). Interestingly, KO of the CCC complex, but not WDR81/91, also resulted in a similar phenotype (Figure 3.7B).

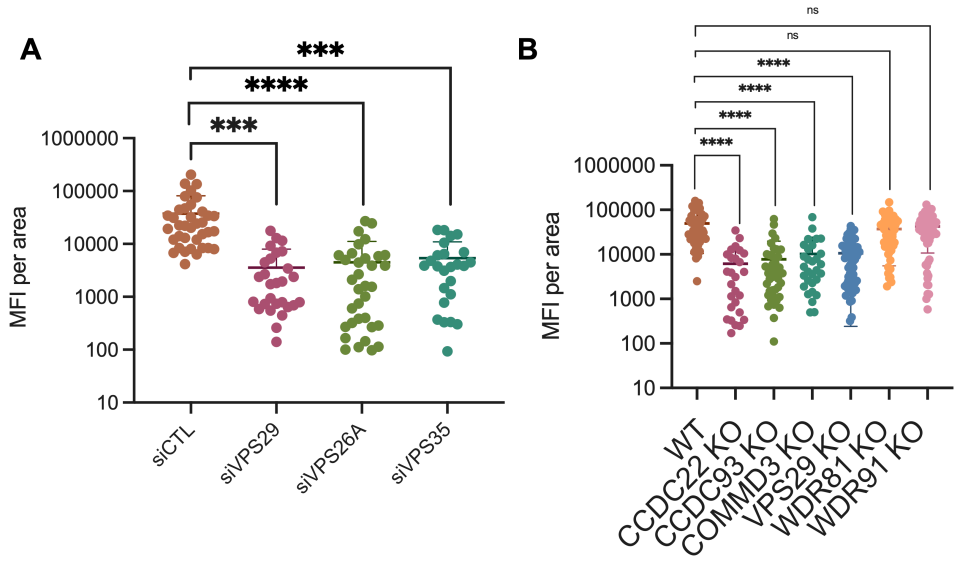

Figure 3.7: Loss of other members of the Retromer/CCC complex also results in deacidified vesicles

(A-B) Quantification of Mean Fluorescence Intensity (MFI) of pHrodo Green Dextran signal inside of 2x-FYVE labeled endosomes. (A) HT1080 transfected with siRNA targeting retromer proteins VPS29, VPS26A, VPS35. (B) HT1080 WT or KO for the indicated gene. MFI was quantified from n=3 independent images. Statistical test: Student's T test. (*) indicate $p<0.05$, (**) indicate $p<0.01$, (***) indicate $p<0.001$, (****) indicate $p<0.0001$

3.7 VPS29 KO results in entrapment of rVSV/SARS-CoV-2 in endosomes

The above findings suggested that CoV infection is impaired in VPS29 KO cells due to impediment in spike dependent egress from endosomes. To directly test this idea, we generated rVSV/SARS-CoV-2_{NG-P}, a replication-competent chimeric VSV expressing SARS-CoV-2 Spike

protein in lieu of VSV-G, and containing the VSV structural protein P fused to mNeonGreen (NG-P), thus enabling the direct observation of entering viral particles (*148*).

At 60 minutes post infection of parental HT1080 cells, few NG-P punctae were evident within 2xFYVE-mSCAR labeled endosomes, suggesting successful egress of most rVSV/SARS-CoV-$2_{NG\text{-}P}$ particles (Figure 3.8A) and minimal accumulation therein. However, in VPS29 KO cells, enlarged endosomes contained many rVSV/SARS-CoV-$2_{NG\text{-}P}$ punctae at 60 min after infection. Likewise, when cells were infected in the presence of labeled Dextran and imaged 60 minutes post infection, we observed a similar phenotype with rVSV/SARS-CoV-2 particles accumulated in enlarged, Dextran-containing vesicles in VPS29 KO cells (Figure 3.8B). Overall, these data indicate that the major inhibitory effect of VPS29 KO on CoV infection is the result of failed egress from endosomes.

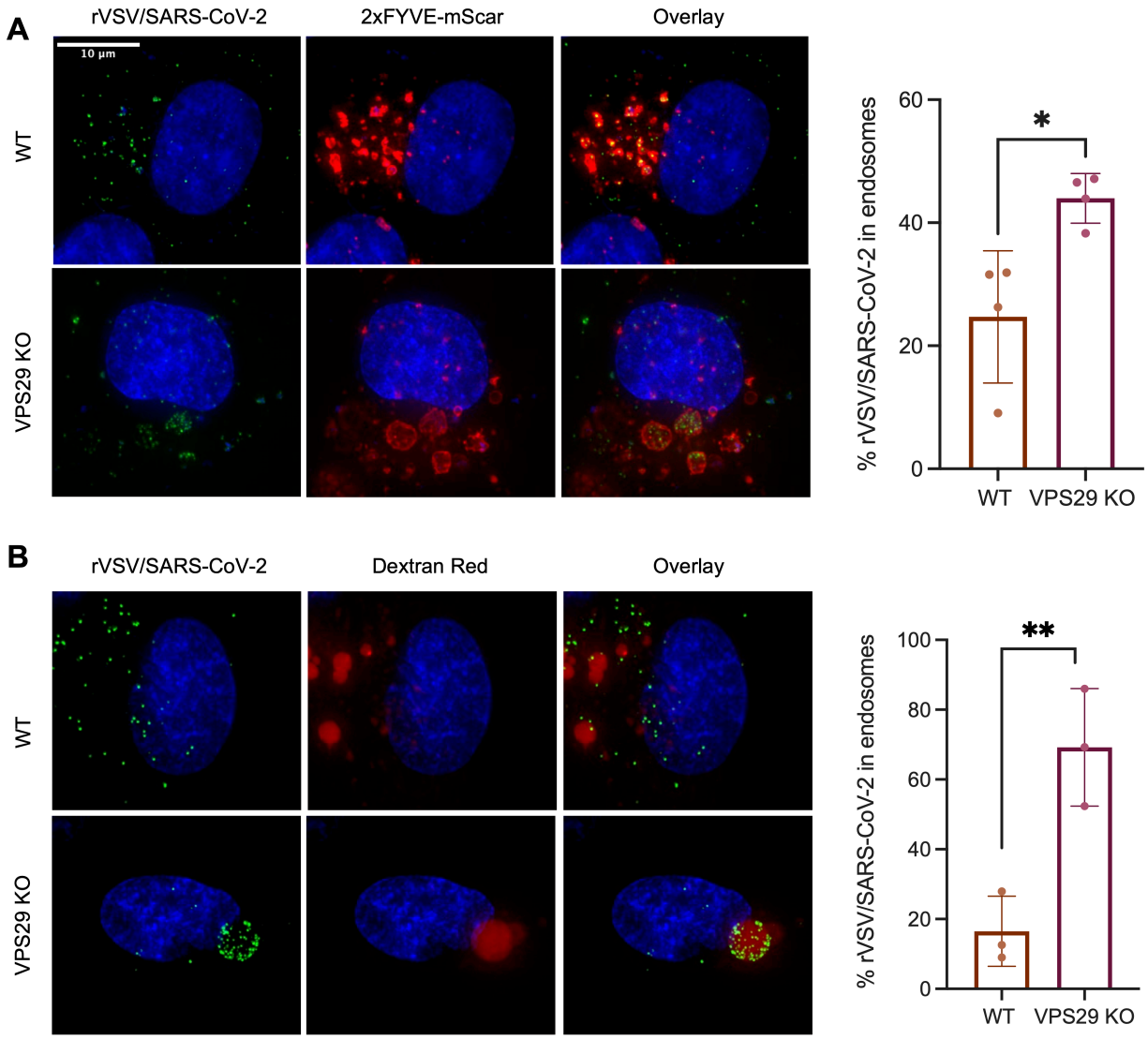

Figure 3.8 VPS29 KO results in rVSV/SARS-CoV-2 specifically remaining trapped in endosomes

(A): Representative images of rVSV/SARS-CoV-2_{NG-P} infection in WT and VPS29 KO HT1080 cells. 2xFYVE-mSCAR labeled cells were infected with rVSV/SARS-CoV-2_{NG-P} for 60 minutes. Quantification indicates the percent of rVSV/SARS-CoV-2_{NG-P} punctae inside of 2x-FYVE labeled endosomes from n=4 independent images. (B): Representative images of WT and VPS29 KO HT1080 cells incubated for 60 minutes with Dextran Red 10,000 MW and rVSV/SARS-CoV-$2_{NG-P.}$ Quantification indicates the percent of rVSV/SARS-CoV-2_{NG-P} punctae inside of Dextran Red labeled endosomes from n=4 independent images. Error bars indicate SD. Statistical test: Student's T test. (*) indicate $p<0.05$, (**) indicate $p<0.01$, (***) indicate $p<0.001$, (****) indicate $p<0.0001$

3.8 Impairment of CoV and Ebola virus infection in VPS29 KO cells is due to loss of endosomal cathepsin activity

The aforementioned findings indicate that the reduced susceptibility to HCoV infection in VPS29 KO cells is spike-specific and is the consequence of failed egress from endosomes. We hypothesized that this effect could be due to impaired spike processing by endosomal proteases during entry. We used HIV-1-based pseudotyped viruses to test the susceptibility of various CoV spikes to VPS29 KO and cathepsin inhibition using the drug E64d. As rVSV/SARS-CoV-2 bears a point mutation, R683G, which ablates the polybasic furin cleavage site, we tested pseudotypes bearing WT or R683G mutant spike proteins, as well as spike proteins from SARS-CoV and SARS-like CoV from bats and pangolins, which also do not contain polybasic cleavage sites (*149*).

Pseudotypes bearing either the WT or the R683G mutant SARS-CoV-2 spike proteins were sensitive to VPS29 KO and cathepsin inhibition. However, cathepsin inhibition did not further decrease infection of VPS29 KO cells (Figure 3.9A). The SARS-CoV-2_{R683G} (Figure 3.9B), SARS-CoV (Figure 3.9C), and the SARS-like bat (Figure 3.9D) and pangolin viruses (Figure 3.9E,F) that lack furin cleavage sites were more impacted by VPS29 KO and cathepsin inhibition than WT SARS-CoV-2. Indeed, in several instances, VPS29 KO and/or cathepsin inhibition resulted in undetectable infection by SARS-CoV-2_{R683G}, SARS-CoV, and the SARS-like bat/pangolin CoVs. Similarly, infectivity assays utilizing rVSV/SARS-CoV-2 also revealed diminished infectivity upon cathepsin inhibition in parental HT1080, but no impairment of infection upon cathepsin inhibition in VPS29 KO cells (Figure 3.9G).

That there was no further effect of cathepsin inhibition on CoV infection in VPS29 KO cells suggests that the effect of these two manipulations converge on a common pathway in promoting

egress from endosomes. We thus hypothesized that VPS29 KO impedes CoV infection by preventing proper processing of spike by cathepsins. If this were indeed the case, then VPS29 KO should impair infection mediated by Ebola virus (EBOV) glycoprotein (GP), which is known to require processing by endosomal cathepsins (*150*). To test this, we performed infectivity assays in WT and VPS29 KO cells using a recombinant VSV expressing EBOV GP in lieu of VSV-G (rVSV/EBOV-GP) (*151*). Indeed, we observed a strong inhibition of rVSV/EBOV-GP infection upon either cathepsin inhibition or loss of VPS29 (Figure 3.9H). This result suggests that the susceptibility of VPS29 KO is mediated by reduced cathepsin activity.

To further test if the primary effect of VPS29 KO on CoV infection was through impaired endocytic entry as a result of reduced cathepsin activity, we assessed impact of VPS29 KO in cells overexpressing TMPRSS2. In cells expressing TMPRSS2, spike proteins can be cleaved and the fusion protein liberated at the cell surface, reducing dependence on endosomal cathepsins. Consistent with the hypothesis that VPS29 impairs endocytic viral entry, there was a dramatic reduction in the effect of VPS29 KO for SARS-CoV-2_{R683G} -CoV, WIV16, Pangolin-CoV/Gx, and Pangolin-CoV/Gd and a more modest reduction for SARS-CoV-2_{WT} when target cells overexpressed TMPRSS2 (Figure 3.9I-N). Importantly, since recent evidence indicates the Omicron variant of SARS-CoV-2 preferentially enters cells via the endocytic route rather than the TMPRSS2-dependent cell-surface route (*40*, *41*), we also included pseudotypes bearing the Omicron spike protein Indeed, we observed robust inhibition of SARS-CoV-$2_{Omicron}$ in VPS29 KO cells, 14x greater than that observed for WT spike (Figure 3.9O). Additionally, the increase in infectivity observed in TMPRSS2+ cells was less evident for Omicron than it was for the ancestral SARS-CoV-2_{WT} or SARS-CoV2_{R683G} (4.2 fold vs 15.5 fold or 14.3 fold, respectively).

These findings suggest that the Omicron variant is particularly adapted to cellular entry through a VPS29-dependent endocytic route.

Consistent with the above conclusion, when parental HT1080 cells were treated with the cathepsin inhibitor E64d, infected with rVSV/SARS-CoV-2 $_{NG-P}$ and examined microscopically, we observed a phenotype similar to that seen in VPS29 KO cells. Specifically, substantially more rVSV/SARS-CoV-2$_{NG-P}$ punctae were evident within endosomes, and the endosomes appear enlarged with similar appearance and morphology to those observed in VPS29 KO cells (Figure 3.9P).

To directly test whether VPS29 KO results in impaired endosomal cathepsin activity, we measured endosomal cathepsin activity in WT and VPS29 KO HT1080 cells using a substrate that generates a fluorescent signal upon cleavage by cathepsin L. Indeed, in WT cells, we observed a strong red fluorescence signal in vesicular structures, indicating high levels of cathepsin activity. However, in VPS29 KO cells the red fluorescence signal was nearly absent, indicating impaired cathepsin activity in VPS29 KO cells (Figure 3.9Q). To determine whether the loss of cathepsin L activity was the result of failed trafficking of cathepsins to the endolysosomal system, we performed immunofluorescence studies utilizing tagged cathepsin L in cells with endosomes labeled with 2xFYVE-mSCAR. Cathepsin L was clearly present in 2xFYVE-mSCAR-positive endosomes in VPS29 KO cells (Figure 3.9R).

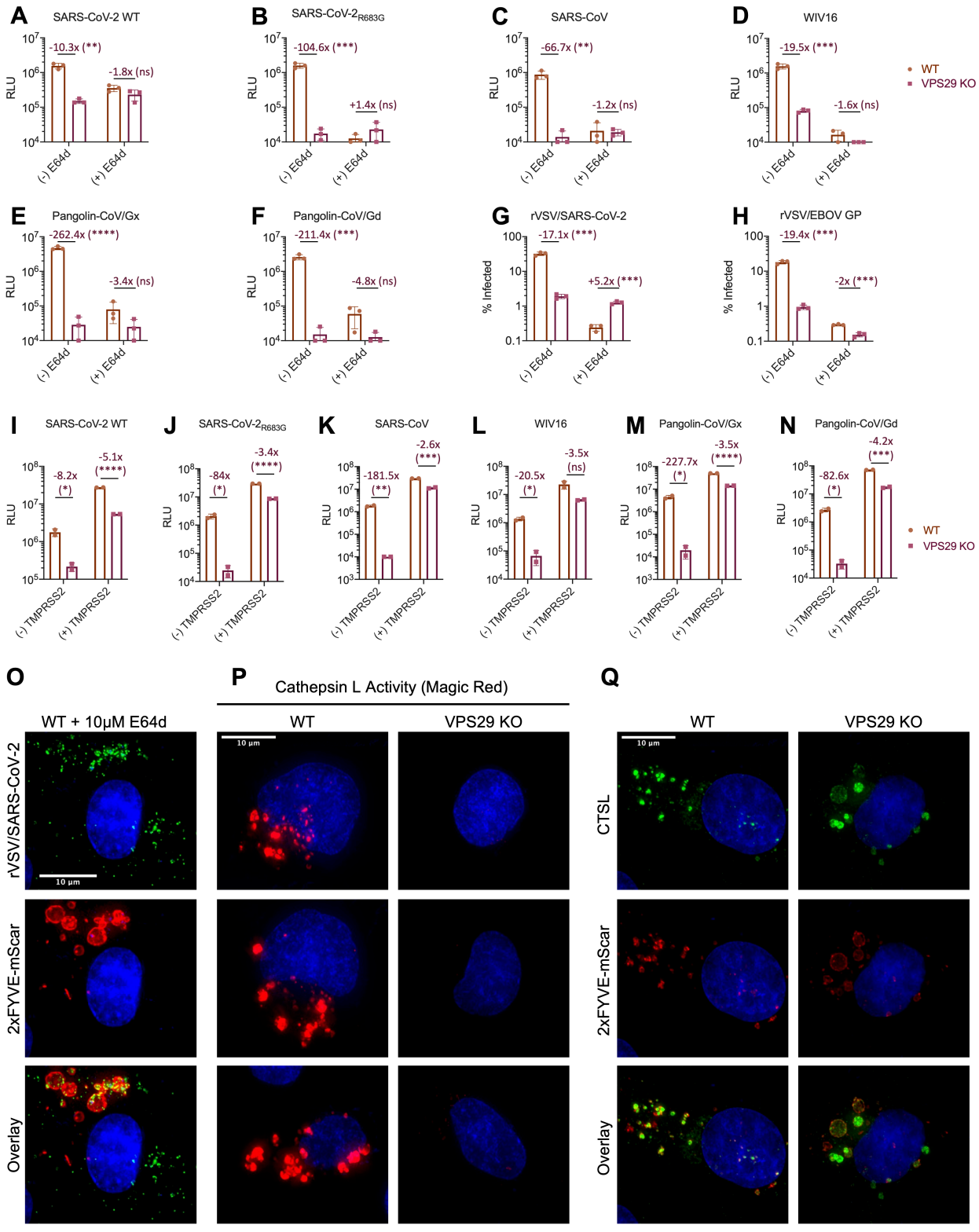

Figure 3.9 Impairment of CoV infection by VPS29 KO is influenced by the presence of a polybasic cleavage site and correlates with cathepsin inhibition

(A-F): WT and VPS29 KO HT1080 cells were treated with the indicated concentrations of E64d for 30 minutes before infection with HIV-1 based nano-luciferase reporter viruses pseudotyped with Spike protein of (A): WT SARS-CoV-2, (B): SARS-CoV-2_{R683G}, (C): SARS-CoV, (D): WIV16: ,(E): Pangolin-CoV/Gx, (F): Pangolin-CoV/Gd. At 48hpi cells were harvested and nano-luciferase activity was measured. Limit of detection of the HIV-1-based pseudoassay = 10^4 RLU. (G-H): WT and VPS29 KO HT1080 cells were treated with the indicated concentrations of E64d for 30 minutes before infection with (G): rVSV/SARS-CoV-2 or (H): rVSV/EBOV-GP. At 16 hours post infection, and infected cells enumerated by determined by flow cytometry. Limit of detection of the flow cytometry assay = 0.1 % infection. Mean (bar graph) of three replicates (dots). Error bars indicate SD. Data shown is a representative of at least two independent experiments. (I-O): WT and VPS29 KO HT1080 cells stably transduced to express TMPRSS2 were infected with HIV-1 based nano-luciferase reporter viruses pseudotyped with Spike protein of (I): WT SARS-CoV-2, (J): SARS-CoV-2_{R683G}, (K): SARS-CoV, (L): Bat CoV/WIV16: ,(M): Pangolin-CoV/Gx, (N): Pangolin-CoV/Gd, (O): SARS-CoV-$2_{Omicron}$. At 48hpi cells were harvested and nano-luciferase activity was measured. Limit of detection of the HIV-1-based pseudoassay = 10^4 RLU. Mean (bar graph) of two replicates (dots). Error bars indicate SD. Data shown is a representative of at least two independent experiments. (P) Representative images of rVSV/SARS-CoV-2_{NG-P} infection in E64d treated WT HT1080. 2xFYVE-mSCAR labeled cells were treated with E64d for 30 minutes, then infected with rVSV/SARS-CoV-2_{NG-P} for 60 minutes. (Q): Representative images of WT and VPS29 KO HT1080 cells following 60-minute incubation with Magic Red Cathepsin L Activity Kit. (R): Representative images of WT and VPS29 KO HT1080 cells stably expressing V5-tagged CTSL and labeled with 2xFYVE-mSCAR. Statistical test: Student's T test between WT and KO cells. (*) indicate $p<0.05$, (**) indicate $p<0.01$, (***) indicate $p<0.001$, (****) indicate $p<0.0001$

Importantly, a similar phenotype of reduced cathepsin activity is seen in cells depleted of VPS26A/VPS35 by siRNA transfection, or in which the CCC complex components were knocked out, but not in cells in which WDR81/91 were knocked out (Figure 3.10A and B). As reduced cathepsin activity is only observed in the cell lines that display deacidified endosomes, and cathepsins are observed in the endosomes of VPS29 KO cells, these findings suggest that the loss of cathepsin activity in VPS29 KO cells results from altered endosomal conditions, such as increased pH, that reduces cathepsin activity therein.

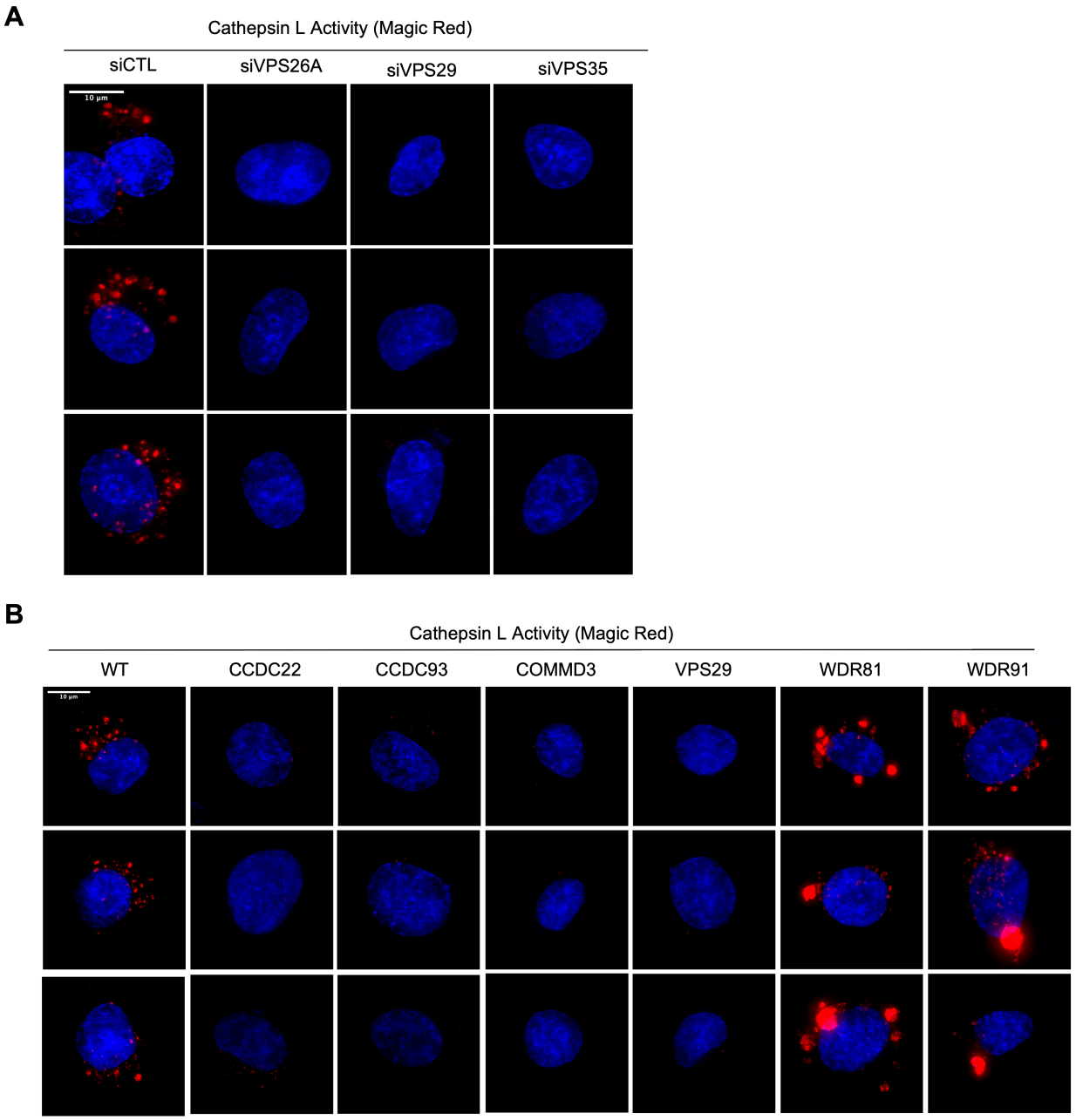

Figure 3.10 Loss of other members of the Retromer/CCC complex results in reduced Cathepsin activity

Images of cells following 60-minute incubation with Magic Red Cathepsin L Activity Kit. (A) HT1080 transfected with siRNA targeting retromer proteins VPS29, VPS26A, VPS35 and (B) HT1080 WT or KO for the indicated gene.

3.9 Implications for the design of broadly antiviral host-targeted therapies

Here, using HCoV-OC43 as a model HCoV, we employed a genome-wide loss-of-function CRISPR screen to identify and characterize factors required for efficient CoV infection. In particular, we show that the retromer subunit protein VPS29 is required for productive infection by diverse CoVs in a variety of cell types. Indeed, VPS29 KO impaired CoV infection in all cells tested, including primary lung cells. Importantly, our findings suggest that the exploration of cathepsin inhibitors, or other endosomal perturbing agents is a promising target for novel drugs against CoVs, which remain a potentially serious emergent public health threat. Indeed, our finding that the Omicron variant is particularly sensitive to loss of VPS29 suggests that modulating this pathway pharmacologically could be an attractive candidate for new therapeutic strategies targeting this and future variants with similar properties.

CHAPTER 4. Targeted CRISPR screening for identifying proteins antagonizing retroviral infection.

4.1 Comprehensive identification and characterization of cellular proteins inhibiting retroviral infection remains incomplete

During viral infection, infected cells produce and secrete type I interferon (IFN), which subsequently binds to IFN receptors in an autocrine/paracrine manner and, through conserved signaling networks, activate a variety of interferon-stimulated genes (ISGs). Many of these ISGs have specific roles in antagonizing viral infection, and this process induces what is called an "antiviral state", protecting cells from infection by a variety of viruses. This process, which is one of the earliest host responses to pathogens, plays a major role in determining viral species tropism and preventing cross-species transmission of viruses. However, despite the importance of this system in protecting cells from viral infection, many ISGs remain either entirely undefined or incompletely characterized. For example, while it has been shown that SIV is robustly inhibited from replicating in IFN-treated human cells, this effect could not be explained by the major restriction factors that had been discovered to date, such as TRIM5, APOBEC3, tetherin, or SAMHD1 (*107*). It is therefore likely that there are cellular antiviral proteins inhibiting retroviral infection that remain to be identified. Here, we employed high-throughput CRISPR screening to identify novel retroviral restriction factors and characterize their mechanism of action in human cells.

4.2 Route-of-entry influences susceptibility of HIV-1 and SIVmac239 to IFNα in MT4 cells

We selected MT4-R5 cells as a model system for HIV-1 and SIVmac239 infection. This is a previously-established MT4-based immortalized cell line which has been modified to express the CCR5 co-receptor utilized by SIVmac239, as well as an LTR-driven GFP reporter for SIV/HIV-

1 gene expression, thus allowing detection of SIV/HIV-1 infection via GFP expression (*84*). We observed that MT4-R5 cells support high levels of SIVmac239 and HIV-1 spreading replication in the absence of IFNα, but spreading infection is robustly inhibited in the presence of 100U/mL IFNα, a physiologically relevant concentration (*152*). Indeed, 100U/mL IFNα inhibited HIV-1 and SIVmac239 spreading infection by ~1000-fold (Figure 4.1A).

In order to gain more insight into the step of the retroviral lifecycle where this potent block occurs, we performed single-cycle infectivity assays in MT4-R5 cells that had been pre-treated with 100U/mL IFNα for 24 hours. There was a substantial reduction in the number of GFP+ cells evident after a single cycle of infection, indicating that this block occurs sometime before viral gene expression (Figure 4.1B). In order to assess whether this phenotype depends on route-of-entry, we also performed single cycle infection assays with HIV-1_{NL4-3} and SIVmac239 that had been pseudotyped with VSV-G. Interestingly, there was a dramatic reduction in the sensitivity of VSV-G pseudotyped SIVmac239 and HIV-1_{NL4-3} to IFNα treatment; infectivity of SIVmac239 was only impaired ~2 fold, and HIV-1_{NL4-3} was not impaired at all when these viruses were pseudotyped with VSV-G (Figure 4.1B).

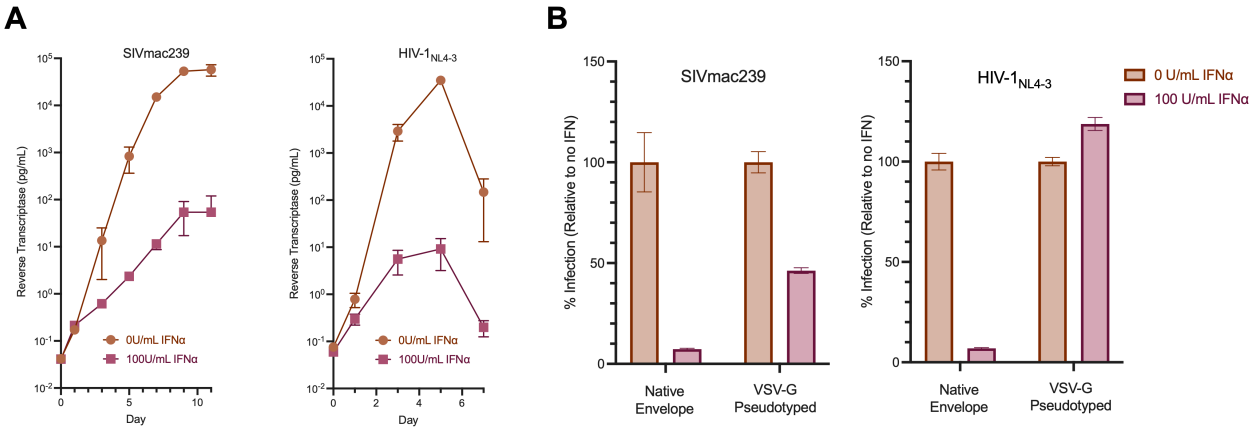

Figure 4.1 There is a route-of-entry dependent block to retroviral infection in MT4 cells
(A): Spreading replication assays of SIVmac239 and HIV-1_{NL4-3} in the absence or presence of 100U/mL IFNα. (B): Single cycle infection assays of native envelope or VSV-G pseudotyped

SIVmac239 and HIV-1_{NL4-3} with or without treatment of IFNα for 24 hours before infection.

4.3 There is no effect of IFNα on release of HIV-1 or SIVmac239 particles or infectious virions.

Given the considerable reduction in the effect of IFNα treatment with VSV-G pseudotyped viruses, we reasoned that inhibition of Env-mediated retroviral entry is the major effector of the IFNα-induced antiviral state in MT4-R5 cells. However, in order to directly test whether later steps in the retroviral lifecycle are also impaired by IFNα treatment, we performed viral release assays in the presence of IFNα. In order to do so, we took advantage of the fact that parental MT4 cells—which do not sufficiently express CCR5—are not permissive to SIVmac239 or HIV-1_{NL-YU2} infection. Thus, MT4 cells infected with VSV-G pseudotyped HIV-1_{NL-YU2} or SIVmac239 will produce virus that is unable to re-infect producer cells, allowing us to measure release of HIV-1_{NL-YU2} or SIVmac239 without confounding re-infection. Briefly, MT4 cells were infected with VSV-G pseudotyped HIV-1_{NL-YU2} or SIVmac239 and placed in IFNα 16 hours post infection. At 48 hours post infection, supernatant was assayed for both viral particles (via SYBR-PERT assay) and infectious virions (via titration on TZM-bl cells, which are not sensitive to IFNα treatment). Importantly, we did not observe any impact of IFNα treatment on release of SIVmac239 or HIV-1_{NL-YU2} (Figure 3.2A-B). This indicates that IFNα treatment has minimal impact on the late stages of retroviral infection in MT4 cells.

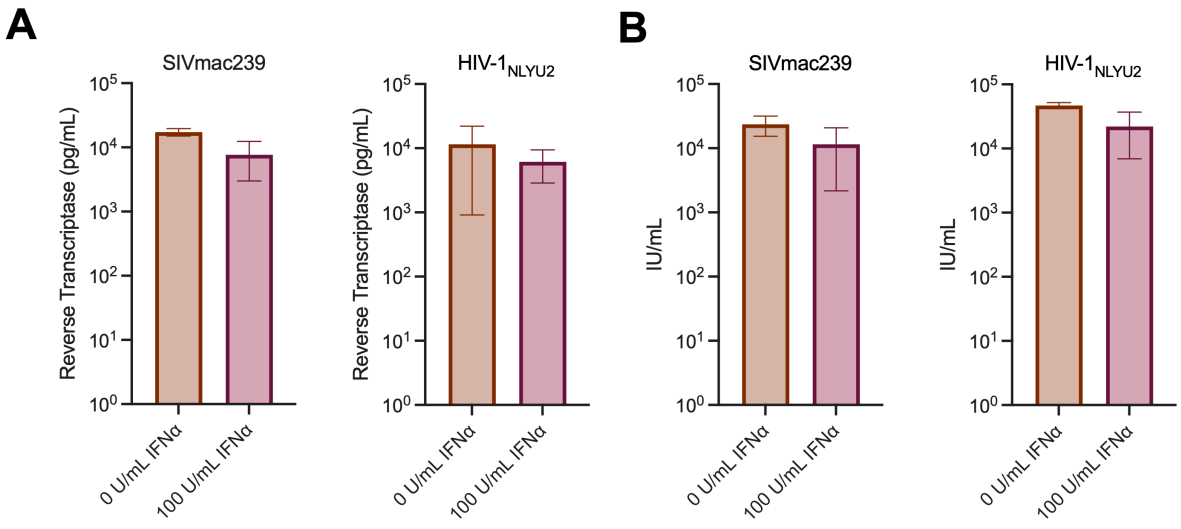

Figure 4.2 IFNα does not effect viral release in MT4 cells

(A): Viral particle release assays of SIVmac239 and HIV-$1_{NL\text{-}YU2}$ from MT4 cells placed in 100U/mL IFNα 16 hours post infection. (B): Infectious virion release assays of SIVmac239 and HIV-$1_{NL\text{-}YU2}$ from MT4 cells placed in 100U/mL IFNα 16 hours post infection.

4.4 Different HIV-1 Envelopes are differentially susceptible to IFNα treatment in MT4 cells.

Our findings strongly suggest that the major consequence of the IFNα-induced antiviral state in MT4-R5 cells is inhibition of Env-mediated retroviral entry. In order to determine if these findings are relevant for other Envs of HIV-1, we titrated HIV-$1_{NL4\text{-}3}$-based molecular clones expressing various Envs in the presence or absence of IFNα. We observed dramatic differences in the sensitivity of different Envs to IFNα treatment (Figure 4.3). Indeed, while infectivity of viruses bearing the NL4-3 envelope is impaired ~230-fold in 100U/mL IFNα, viruses bearing the ADA envelope were only impaired ~3-fold. These findings indicate that the major determinant of the IFNα-induced antiviral state in MT4-R5 cells is inhibition of retroviral entry in an Env-specific manner.

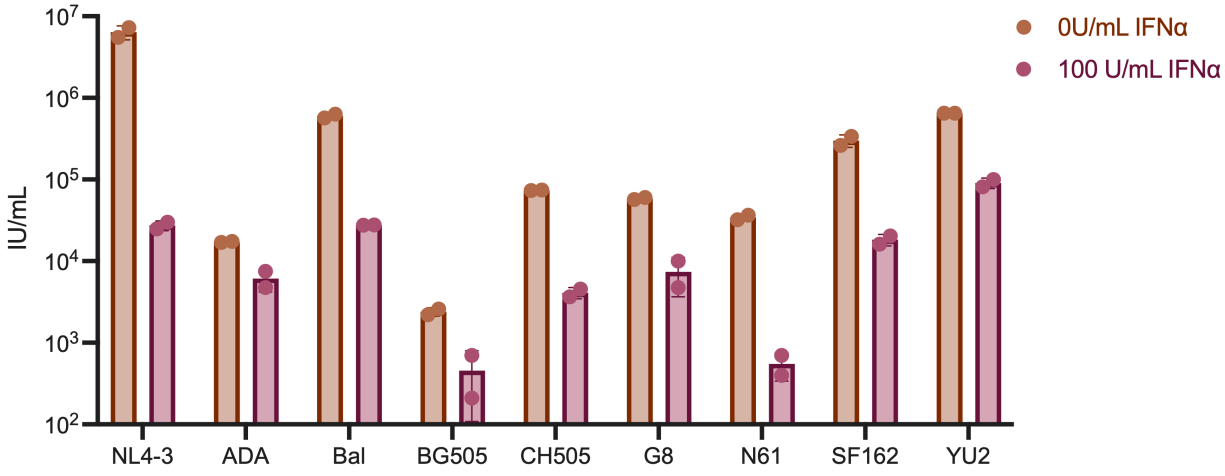

Figure 4.3 The IFNα-mediated block to retroviral infection in MT4 cells is Envelope-specific

Titration of various HIV-1_{NL4-3}-based molecular clones expressing various Envs in the absence or presence of 100U/mL IFNα. Error bars indicate S.D.

4.5 A CRISPR screen for ISGs in MT4-R5 cells reveals factors inhibiting SIVmac239 infection

To identify which factor(s) mediate this potent, Env- and route-out-entry dependent early block to retroviral infection in MT4-R5 cells, we performed a loss-of-function CRISPR screen targeting ISGs in MT4-R5 cells. Briefly, a dataset of genes upregulated by IFNα treatment in MT4-R5 cells was determined by bulk RNA-sequencing of IFNα-treated cells. For the purposes of this screen, we defined an ISG as any gene with an adjusted p-value <.05 and a log2 fold change value of >1 in IFNα-treated cells (Figure 4.4A, all genes in red and to the right of the right-most dashed line). A total of 958 genes met these criteria. Using this dataset, we then constructed a library of sgRNAs targeting these genes. Additionally, 200 non-targeting controls (NTCs) were added from the GeCKO library to serve as negative controls.

In order to screen which of these candidate genes have antiretroviral activity, we modified an approach described by OhAinle *et al.* 2018 and created a virus-packageable CRISPR vector to

screen for factors inhibiting SIVmac239 infection.(*110*) Briefly, we modified the lentiCRISPRv2 vector to be packaged by SIVmac239 and to remain transcriptionally active after host integration, which we term SIV-CRISPR. SIV-CRISPR was created by repairing the self-inactivating ΔU3 3' LTR of lentiCRISPRv2 with the full 3' LTR sequence of SIVmac239. Additionally, we replaced the HIV-1 based 5' LTR, packaging signal, and rev-response element with the equivalent sequences from SIVmac239 (Figure 4.4B).

Library sgRNA sequences were synthesized in bulk and cloned into SIV-CRISPR, and the resulting SIV-CRISPR ISG library was deep sequenced to confirm adequate representation and suitability, according to established guidelines (*153*). MT4-R5 cells were transduced with the library at >500X coverage and low MOI (0.3), generating a large population of cells with single SIV-CRISPR integrations. Following selection to remove untransduced cells, cells were treated or not with 100U/mL IFNα, and infected the next day with SIVmac239 at an MOI of 0.5. Three days post-infection, cells were pelleted and supernatant containing packaged SIV-CRISPR harvested. From the supernatant, virions were pelleted and viral RNA (vRNA) was extracted and reverse transcribed, with sgRNA cassettes PCR amplified (Figure 4.4B). Resulting amplicons were pooled and deep sequenced. The relative enrichment of sgRNA sequences in the vRNA of the IFNα-treated samples relative to the untreated samples was analyzed using the model-based analysis of genome-wide CRISPR/Cas9 knockout (MAGeCK) statistical package (*132*).

The most highly enriched sgRNA sequences targeted STAT1, STAT2, and IRF9, members of the IFNα signaling cascade which thus serve as positive controls for the screen. We also identified proteins with known antiviral properties, such as HERC6 and ZNFX1 (*154*, *155*). Interestingly, a number of the top hits (EPB41L5, MRAS, RHPN1-AS1, SDK2) function in

cellular adhesion, indicating that IFNα-induced modulation of this process has antiretroviral activity (*156–159*).

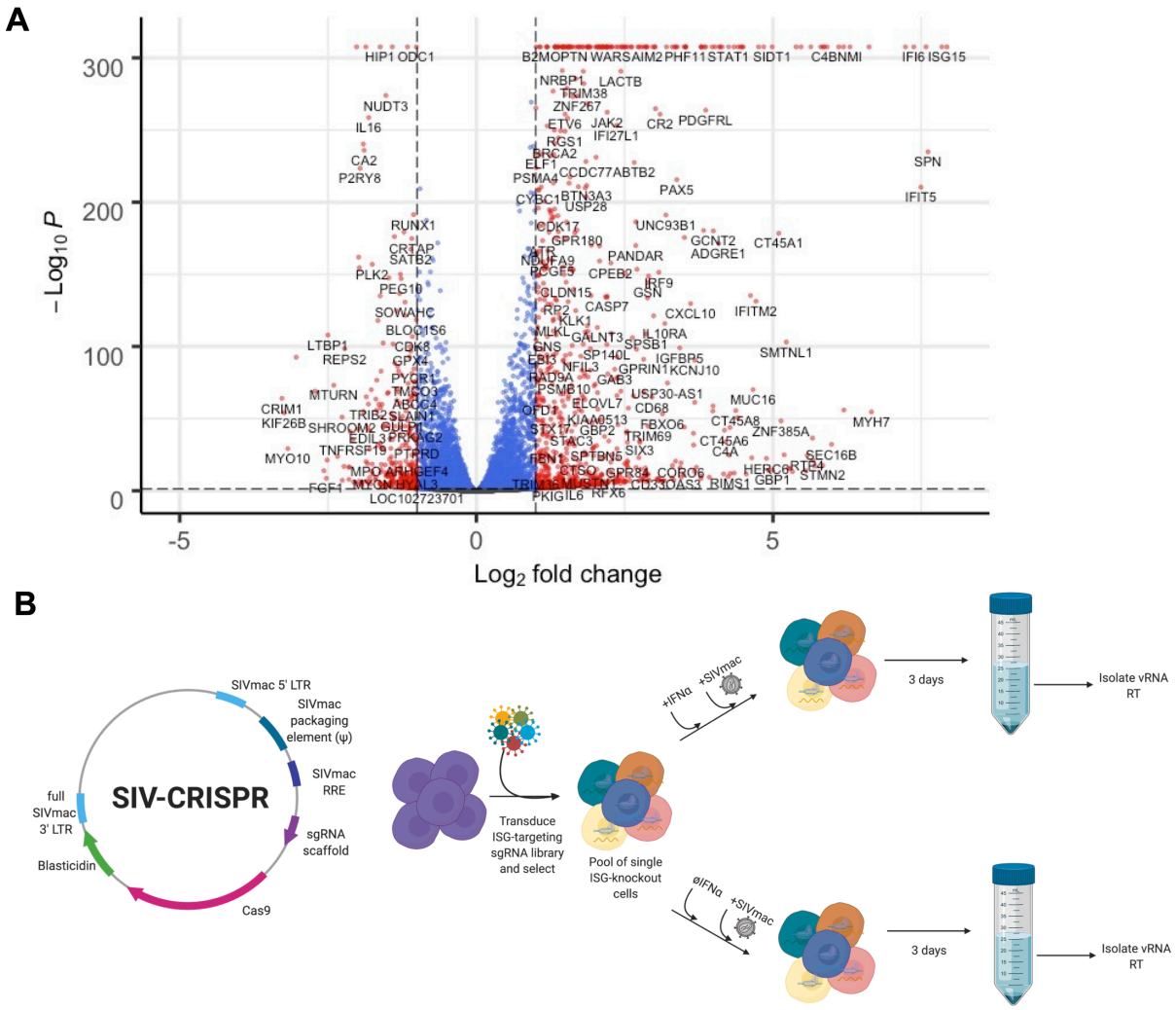
A
300
200
100
0
−Log10 P
-5
0
5
Log2 fold change
HIP1 ODC1
B2M OPTN WARS AIM2 PHF11 STAT1 SIDT1 C4BNMI IFI6 ISG15
NRBP1 LACTB
TRIM38
ZNF267
NUDT3
IL16
ETV6 JAK2 CR2 PDGFRL
IFI27L1
RGS1
BRCA2
CA2
P2RY8
ELF1
SPN
PSMA4 CCDC77 ABTB2
CYBC1 BTN3A3
PAX5
IFIT5
USP28
RUNX1
CDK17
UNC93B1
GPR180
GCNT2
CT45A1
CRTAP
SATB2
ATR
ADGRE1
NDUFA9
PANDAR
PLK2
PCGF5
CPEB2
IRF9
PEG10
GLDN15
GSN
CASP7
IFITM2
SOWAHC
RP2
CXCL10
KLK1
BLOC1S6
MLKL GALNT3
IL10RA
LTBP1
CDK8
GNS
SPSB1
SMTNL1
REPS2
GPX4
EBI3
SP140L
IGFBR5
PYCR1
NFIL3
GPRIN1 KCNJ10
RAD9A
GAB3
MTURN
TMEM3
PSMB10
USP30-AS1
MUC16
CRIM1
ABCC4
QFD1
ELOVL7
CD68
KIF26B
TRIB2 SLAIN1
KIAA0513
CT45A8
MYH7
SHROOM2 GULP1
STX17
GBP2
FBXO6
ZNF385A
EDIL3 PRKAG2
STAC3
TRIM69
CT45A6
TNFRSF19 PTPRD
SIX3
C4A
MYO10
REN
SPTBN5
SEC16B
MPO ARHGEF4
CTSO GPR84 CORO6
HERC6 RTP4
GBP1 STMN2
FGF1 MYO1H LYAL3
CD300A3 BIMS1
LOC102723701
PKIG IL6 RFX6
B
SIV-CRISPR
SIVmac 5' LTR
SIVmac packaging element (ψ)
SIVmac RRE
sgRNA scaffold
Cas9
Blasticidin
full SIVmac 3' LTR
Transduce ISG-targeting sgRNA library and select
Pool of single ISG-knockout cells
+IFNα
+SIVmac
3 days
Isolate vRNA RT
øIFNα
+SIVmac
3 days
Isolate vRNA RT
C
MAGeCK Enrichment score
600
400
200
0
0
2000
4000
6000
8000
sgRNA rank
STAT1
STAT2
STAT2
STAT1
STAT1
STAT2
STAT1
IRF9
STAT2
STAT1 STAT2
STAT2
HERPUD2 EPB41L5
STAT2 STAT1
IRF9
ZNFX1
HERC6
PLEKHA4 PLA2G2D
MRAS SDK2
DDIT4
RHPN1-AS1
STAT1 IRF9

Figure 4.4: A CRISPR screen reveals ISGs inhibiting SIVmac239 infection in MT4-R5 cells

(A): Volcano plot of differentially expressed genes following IFNα treatment of MT4-R5 cells. Gray: padj >0.05 and $log_2FC<1$. Blue: padj <0.05 and log_2FC <1. Red: padj <0.05 and log_2FC > 1. (B): Schematic of SIV-CRISPR screening vector and screening strategy. (C): MAGeCK analysis of screen results. Top 10 hits as well as positive controls STAT1, STAT2, and IRF9 are labeled. Dashed line indicates highest scoring non-targeting control (NTC) negative control.

4.6 Identified hits inhibit SIVmac239 and HIV-1 infection in a route-of-entry dependent manner

In order to validate the results of the screen, we generated individual knockout (KO) cell lines with the top 10 hits and performed single-cycle infection assays with SIVmac239 as well as HIV-1_{NL4-3}. As expected, the vast majority of hits rescued SIVmac239 infection >2-fold in IFNα treated MT4-R5 cells (Figure 4.5A). Unexpectedly, however, most hits also rescued SIVmac239 infection in untreated MT4-R5 cells as well (Figure 4.5A). We hypothesize that, as many of these genes are basally expressed in MT4-R5 cells, these proteins, or pathways that they influence, may exert antiretroviral activity at baseline conditions. We also observed that KO of most hits rescued HIV-1_{NL4-3} infection as well. In particular, there was an incredibly robust impact of PLEKHA4 KO and ZNFX1 KO on HIV-1_{NL4-3} infection, >20-fold in untreated MT4-R5 cells (Figure 4.5B).

As our initial data indicates that the IFNα-induced antiviral state in MT4-R5 cells depends on route of entry (Figure 4.1), the hits identified in our screen should exhibit this same property. Thus, we also performed single-cycle infectivity assays using VSV-G pseudotyped SIVmac239 and HIV-1_{NL4-3}. Appropriately, there was no rescue observed for any of the top 10 hits when SIVmac239 or HIV-1_{NL4-3} was pseudotyped with VSV-G (Figures 4.5C-D). This implies that the hits identified in this screen are indeed responsible for the route-of-entry specific block observed in MT4-R5 cells. It has long been known that pseudotyping HIV-1 with VSV-G results in higher

titer virus (*160*). Our results indicate that this increased efficiency in entry may be due to circumventing additional constraints to Env-dependent entry than those already described.

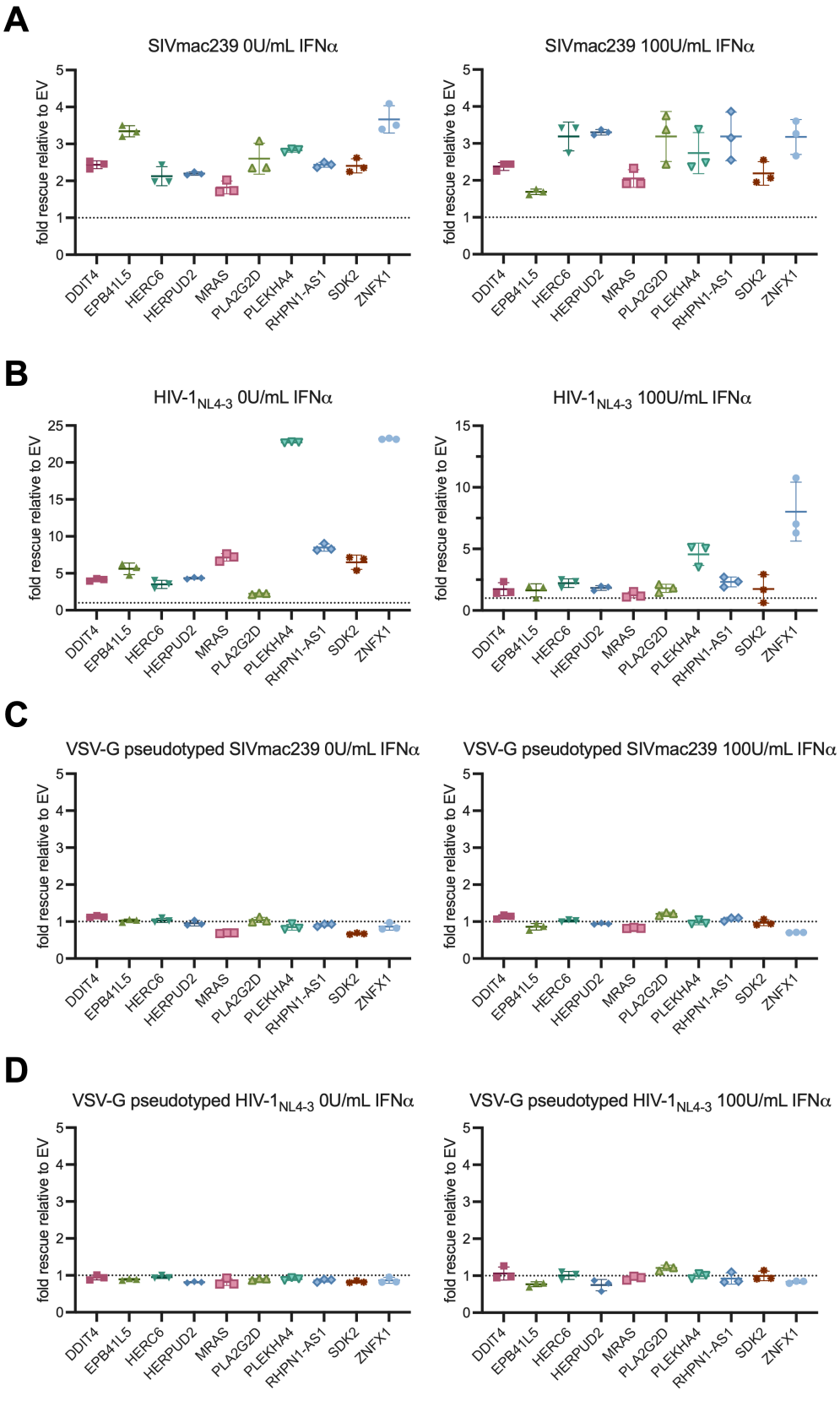
A
SIVmac239 0U/mL IFNα
SIVmac239 100U/mL IFNα
B
HIV-1NL4-3 0U/mL IFNα
HIV-1NL4-3 100U/mL IFNα
C
VSV-G pseudotyped SIVmac239 0U/mL IFNα
VSV-G pseudotyped SIVmac239 100U/mL IFNα
D
VSV-G pseudotyped HIV-1NL4-3 0U/mL IFNα
VSV-G pseudotyped HIV-1NL4-3 100U/mL IFNα
fold rescue relative to EV
DDIT4
EPB41L5
HERC6
HERPUD2
MRAS
PLA2G2D
PLEKHA4
RHPN1-AS1
SDK2
ZNFX1

Figure 4.5: Loss of identified hits rescue SIVmac239 and HIV-1 infection in a route-of-entry dependent manner

Single cycle infection assays in MT4-R5 lacking each of the top 10 hits of the screen in the absence or presence of 100U/mL IFNα for native envelope SIVmac239 (A), native envelope HIV-1_{NL4-3} (B), VSV-G pseudotyped SIVmac239 (C), or VSV-G pseudotyped HIV-1_{NL4-3} (D). Rescue relative to control cells expressing an empty CRISPR construct not expressing a targeting sgRNA cassette (EV). Dashed line at Y=1 (no change). Error bars indicate S.D.

4.7 PLEKHA4 impairs HIV-1 infection in an Env-dependent manner

Due to the striking effect of PLEKHA4 KO on HIV-1_{NL4-3} infection in untreated cells, as well as the lack of any prior evidence of antiviral properties of PLEKHA4, we elected to examine this hit in more detail. To do so, we generated single cell clones (SCCs) of PLEKHA4 KO MT4-R5 cells and performed single-cycle infection assays on the resulting clones. In all SCCs, infectivity of HIV-1_{NL4-3} but not VSV-G pseudotyped HIV-1_{NL4-3} was rescued, confirming our earlier results in bulk KO cells (Figure 4.6A). Additionally, there was no enhancement of HIV-1_{NL-YU2} in any of the SCCs (Figure 4.6A).

To confirm that this phenotype is specifically due to loss of PLEKHA4, we performed reconstitution experiments with sgRNA-resistant PLEKHA4 in EV control cells as well as 3 of the PLEKHA4 KO SCCs. Importantly, reconstitution of PLEKHA4 significantly reduced infectivity in all 3 KO clones, confirming that loss of PLEKHA4 in the KO clones is responsible for the phenotype (Figure 4.6B). Moreover, overexpression of PLEKHA4 in the EV control cells impaired infectivity, providing additional support for the antiviral activity of PLEKHA4. As it has been previously reported that PLEKHA4 is a plasma membrane-localized protein, we also assessed whether this property is required for viral restriction (*161*). To do so, we generated a construct of PLEKHA4 lacking the Pleckstrin homology (PH) domain. In agreement with prior findings, we observed that WT PLEKHA4 bearing a C-terminal mScarlet tag localizes to the

plasma membrane. However, we observed diffuse cytoplasmic staining in HT1080 cells transduced with PLEKHA4$_{\Delta PH}$-mScarlet, similar to that of soluble mScarlet, indicating decreased membrane localization. Importantly, PLEKHA4$_{\Delta PH}$ retained antiviral activity, suggesting that plasma-membrane localization is not necessary for restriction of HIV-1 entry.

The above data indicates that PLEKHA4 restricts retroviral entry in an Env-dependent manner. To determine if these results extend to other HIV-1 Envelopes, we titrated a panel of HIV-1$_{NL4-3}$-based clones expressing various Envs on WT and PLEKHA4 KO cells. Indeed, we observed a diverse, Env-dependent response to PLEKHA4 KO (Figure 4.6C). Some Envs, such as those from the transmitter-founder strain N61 or SF162, displayed responses very similar to NL4-3 (30-fold and 22-fold vs. 31-fold, respectively). Others, such as ADA, G8, or YU2, exhibited minimal (<2-fold) responsiveness to PLEKHA4 KO. We observed an intermediate phenotype for Bal, BG505, and CH505, ranging from 3- to 6-fold enhancement in PLEKHA4 KO cells. Importantly, the magnitude of effect of PLEKHA4 KO on a particular Env correlated with the sensitivity of that Env to IFNα (Figure 4.6D, R^2=0.54). Taken together, these results indicate that PLEKHA4 restricts HIV-1 infection in a manner that depends on Env and route-of-entry.

As further support that PLEKHA4 restricts envelope-mediated HIV-1 entry, we generated recombinant NeonGreen-P (NG-P) tagged VSV viruses bearing a highly PLEKHA4-sensitive (N61) or PLEKHA4-resistant (ADA) HIV-1 envelope in lieu of the VSV-G protein. The resulting chimeric viruses, termed rVSV$_{N61}$ NG-P or rVSV$_{ADA}$ NG-P, thus enter cells via with CD4 and CCR5, but the remainder of infectious process follows the VSV replication cycle. Significantly, while infection with rVSV$_{N61}$ NG-P was facilitated by PLEKHA4 KO and inhibited by PLEKHA4 overexpression, infection of rVSV$_{ADA}$ NG-P was unaffected (Figures

4.6E/F). This provides further evidence that PLEKHA4 specifically restricts HIV-1 entry in an Env-dependent manner.

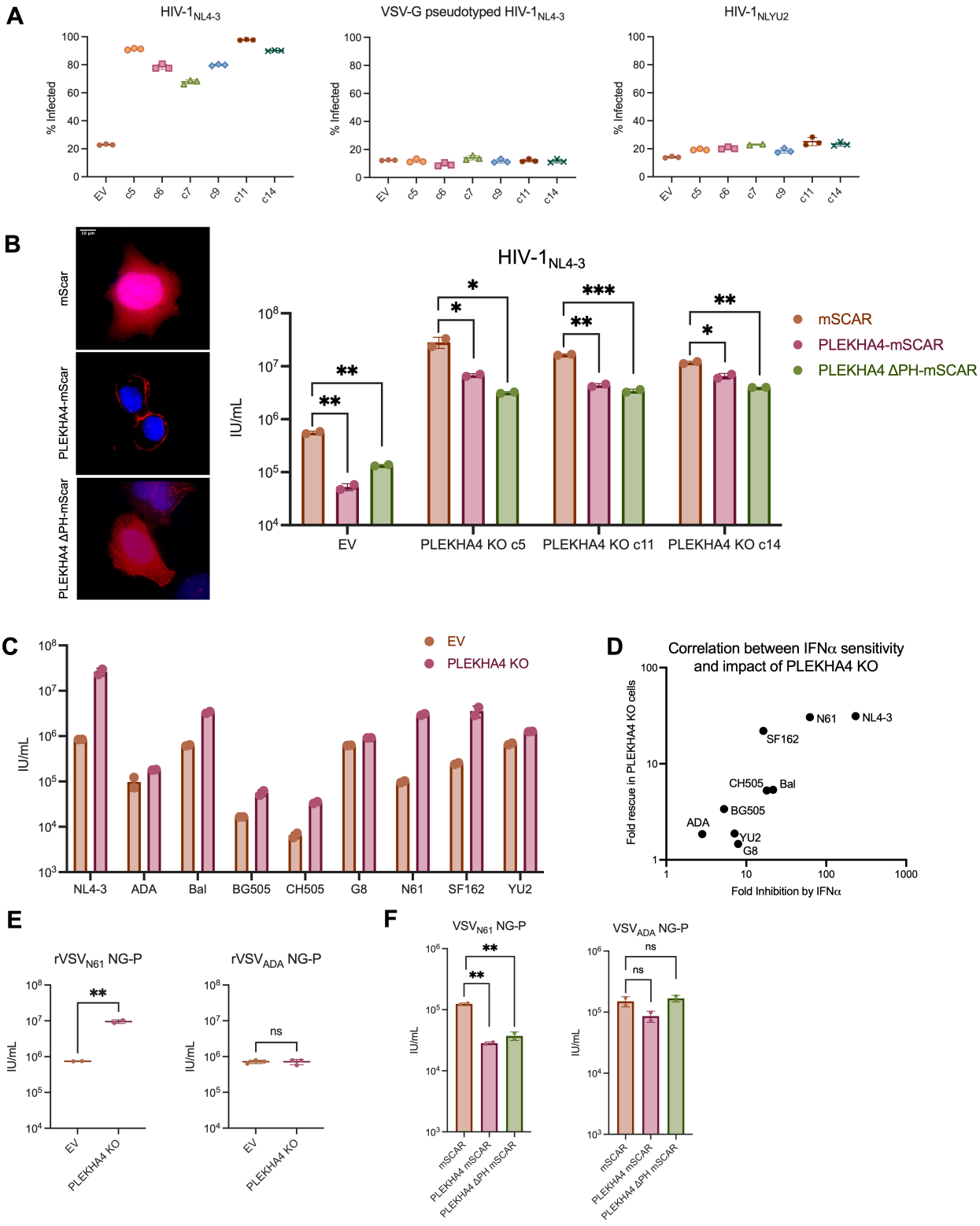

Figure 4.6: PLEKHA4 KO rescues HIV-1 infection in an Env-dependent manner that is independent of PLEKHA4 membrane localization

(A): Single cycle infection assays in 6 independent PLEKHA4 KO single cell clones. (B): Titration of HIV-1_{NL4-3} on EV control or indicated PLEKHA4 KO clones transduced with soluble mScarlet, PLEKHA4-mScarlet, or PLEKHA4$_{\Delta PH}$-mScarlet. (C): Titration of various NL4-3 based proviral clones expressing indicated Env on EV control and PLEKHA4 KO cells. (D): Correlation between IFNα sensitivity and impact of PLEKHA4 KO for various Envs; R^2=0.40. (E): Titration of rVSV$_{N61}$ NG-P or rVSV$_{ADA}$ NG-P on EV control or PLEKHA4 KO cells. (F): Titration of rVSV$_{N61}$ NG-P or rVSV$_{ADA}$ NG-P in EV control cells overexpressing soluble mScarlet, PLEKHA4-mScarlet, or PLEKHA4$_{\Delta PH}$-mScarlet. Error bars indicate S.D.

Importantly, we excluded variations in cell-surface coreceptor expression levels, coreceptor preference, or modulation of SERINC-mediated antagonism as explaining these Env-specific effects (Figure 4.7).

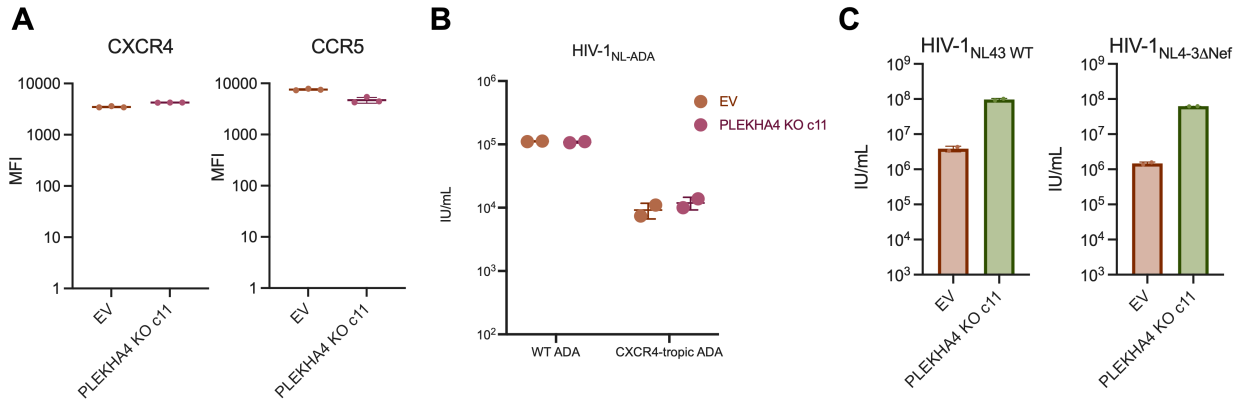

Figure 4.7 The envelope-specific inhibition of HIV-1 entry by PLEKHA4 is not mediated through changes in cell-surface coreceptor expression or SERINC

(A): Mean fluorescence intensity (MFI) of cell-surface stained CXCR4 and CCR5 in EV control or PLEKHA4 KO cells. (B): Titration of WT HIV-1_{NL-ADA} or a previously-described ADA Env mutant that induces a switch from R5 to X4 tropism (*162*). (C): Titration of WT or ΔNef HIV-1_{NL4-3} on EV control and PLEKHA4 KO cells. Error bars indicate S.D.

4.8 PLEKHA4 and IFNα treatment both result in altered expression of extracellular matrix associated genes.

In order to gain more insight into the cellular mechanism(s) whereby PLEKHA4 restricts retroviral entry, we performed bulk RNAsequencing on three independent PLEKHA4 KO single

cell clones (SCCs). Differential expression analysis revealed several differentially upregulated genes in PLEKHA4 KO cells (Figure 4.8A). Surprisingly, pathway analysis of the significantly upregulated genes ($log_2FC > 1$ and padj < 0.05, 101 genes total) revealed that many of these genes function in cellular adhesion. In particularly, multiple different types of collagen are upregulated in PLEKHA4 KO cells (Figure 4.8B). This implies that, physiologically, PLEKHA4 may suppress the expression of a variety of cellular membrane proteins functioning in cellular adhesion, in particular the collagens.

Since IFNα treatment results in a dramatic upregulation of PLEKHA4, we reasoned that additional supporting evidence for a role of PLEKHA4 in suppressing genes involved in cellular adhesion could be obtained if genes such as this were downregulated in IFNα treated cells. Therefore, we performed pathway analysis of the significantly downregulated genes (log2FC < -1, padj <0.05) in our RNAsequencing dataset of IFNα treated cells. Pathway analysis revealed that the most significantly downregulated pathway in IFNα treated cells was cellular adhesion, mirroring the data seen in PLEKHA4 KO cells.

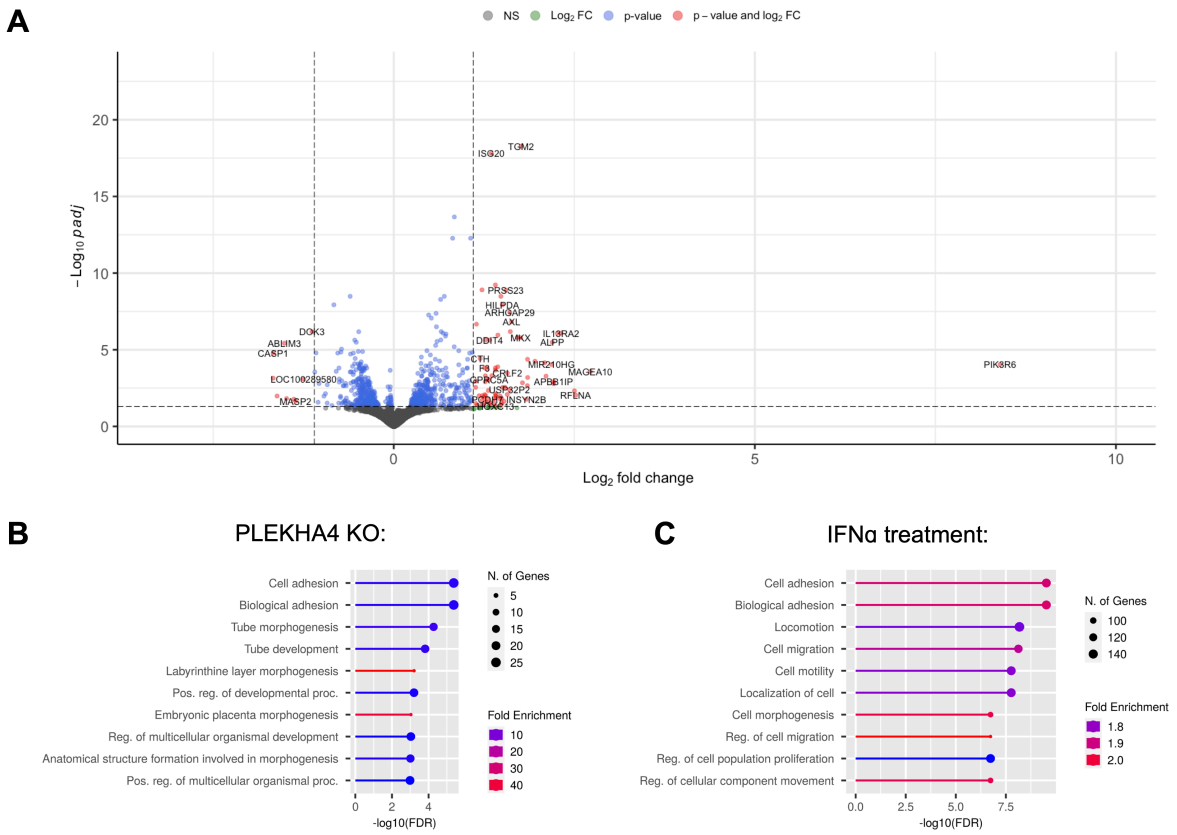

Figure 4.8: PLEKHA4 and IFNα treatment both alter extracellular matrix genes

(A): Volcano plot of differentially expressed genes in PLEKHA4 KO cells vs EV control cells. (B): ShinyGO pathway analysis of differential upregulated genes in the PLEKHA4 KO RNAsequencing dataset, with read counts of selected significantly upregulated genes. (C): ShinyGO pathway analysis of differentially downregulated genes in the IFNα treatment RNAsequencing dataset, with read counts of selected significantly downregulated genes.

4.9 Collagenase treatment of PLEKHA4 KO cells restores infectivity to wildtype levels.

Given the above findings that extracellular matrix genes, in particular the collagens, are altered in both PLEKHA4 KO cells and IFNα-treated cells, we reasoned that, if altered expression of these genes is indeed driving the observed phenotype, then reversal of these modifications should restore infectivity to wildtype levels. To test this, we treated EV control and PLEKHA4 KO cells with collagenase and titrated a panel of HIV-1_{NL4-3}-based clones expressing various Envs. Astonishingly, collagenase treatment of PLEKHA4 KO cells restored infectivity of HIV-1_{NL4-3} to wildtype levels (Figure 4.9A). Additionally, the impact of

collagenase treatment on various other Envs correlates well with how sensitive that Env is to PLEKHA4 KO (Figure 4.9B). For instance, ADA, YU2, and G8, which are all minimally responsive to PLEKHA4 KO, are also minimally affected by collagenase treatment. Other envelopes, such as N61 and SF162, which are relatively more sensitive to PLEKHA4 KO are also relatively more sensitive to collagenase treatment. Altogether, this data implies that it is this modulation of the extracellular matrix by PLEKHA4 that drives this Env-specific impairment of retroviral entry.

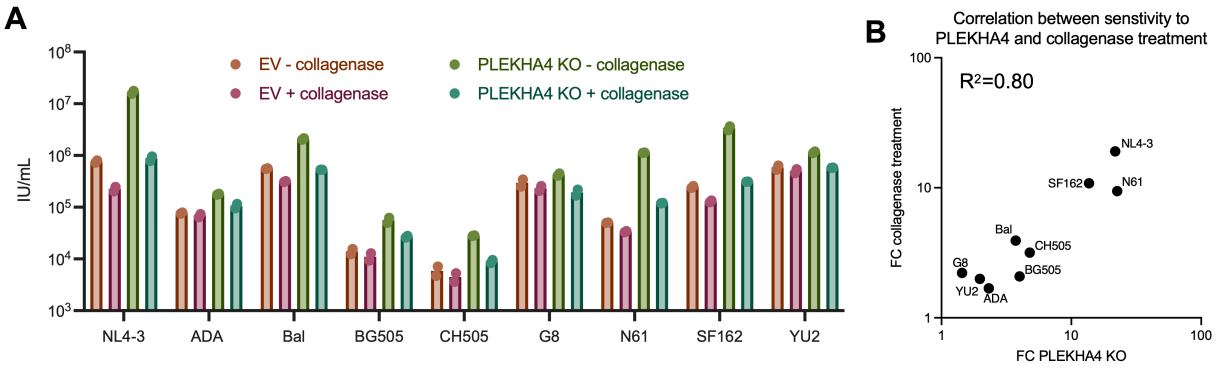

Figure 4.9: Reverting PLEKHA4-mediated changes to the extracellular matrix restores infectivity of PLEKHA4 KO cells to WT levels

(A): Titration of various NL4-3 based proviral clones expressing indicated Env on EV control and PLEKHA4 KO cells in the absence or presence of collagenase. Error bars indicate S.D. (B): Correlation between sensitivity to PLEKHA4 KO and collagenase treatment.

4.10 Restriction of HIV-1 Entry by PLEKHA4 maps to the gp120 subunit of Env, and regions of Env imparting sensitivity to PLEKHA4 also determine sensitivity to collagenase treatment

To gain more insight into the inhibition of retroviral entry by PLEKHA4, we generated viruses bearing recombinant envelopes using the highly PLEKHA4-sensitive NL4-3 Env and the highly PLEKHA4-resistant YU2 Env. Given the above data suggesting restriction by PLEKHA4 is influence by modulation of collagen content in the extracellular matrix, we reasoned that

regions of Env imparting sensitivity to PLEKHA4 would likely map to the surface protein of Env. To directly test this, we generated a chimeric envelopes expressing either NL4-3 gp120 and YU2 gp41 (NY_{gp41}) or YU2 gp120 and NL4-3 gp41 (YN_{gp41}). As indicated in Figure 4.10A, replacing the gp41 subunit of NL4-3 with YU2 did not result in reduced susceptibility to PLEKHA4, and vice versa. This implies that sequences in the gp120 subunit, but not the gp41 subunit, determine sensitivity to PLEKHA4.

Given the above findings that sequences in gp120 determine sensitivity to PLEKHA4, we generated additional chimeric viruses focused in the gp120 subunit (see diagram, Figure 4.10B). We found that replacement of any selection of NL4-3 Env sequences with YU2 sequences rendered chimeras less sensitive to PLEKHA4 KO and less sensitive to collagenase treatment. In a complementary fashion, replacement of YU2 sequences with NL4-3 sequences rendered chimeric viruses more sensitive to PLEKHA4 KO and more sensitive to collagenase treatment. Overall, this implies that the properties of Env determining sensitivity to PLEKHA4 do not map to a singular motif but are more global properties of Env. Furthermore, that direct manipulations resulting in altered sensitivity to PLEKHA4 also altered sensitivity to collagenase is further evidence that the phenotype observed in PLEKHA4 KO results, at least in part, due to modulation of the extracellular matrix by PLEKHA4.

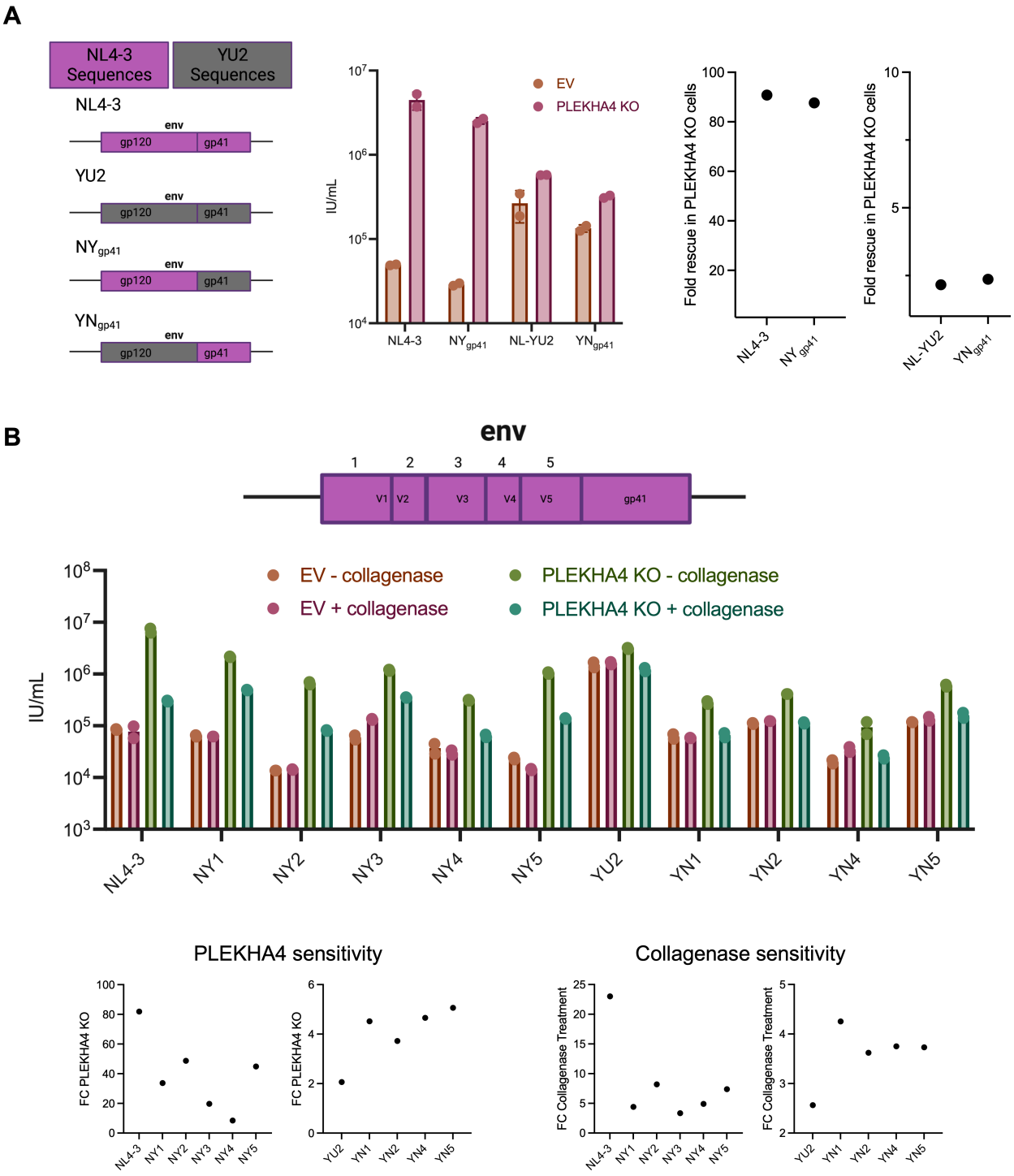

Figure 4.10: Restriction of HIV-1 Entry by PLEKHA4 maps to gp120 subunit of Env, and regions imparting sensitivity to PLEKHA4 also determine sensitivity to collagenase treatment

(A): Titration of NL4-3 based proviral clones expressing: WT NL4-3 Env, WT YU2 Env, a

chimeric virus expressing the NL4-3 ectodomain and the YU2 transmembrane domain/cytoplasmic tail ($NY_{TM/CT}$), or a chimeric virus expressing the YU2 ectodomain and the NL4-3 transmembrane domain/cytoplasmic tail ($YN_{TM/CT}$). Error bars indicate S.D. (B): Titration of NL4-3 based proviral clones expressing: WT NL4-3 Env, WT YU2 Env, or various chimeras expressing primarily NL4-3 Env with indicated YU2 fragments (NYX) or primarily YU2 Env with indicated NL4-3 fragments (YNX) on EV control or PLEKHA4 KO cells in the absence or presence of collagenase. Errors bars indicate S.D.

4.11 Effect of PLEKHA4 on HIV-1 infectivity and the ECM is modulated by PIK3R6

In order to gain more insight into the cellular mechanisms whereby PLEKHA4 exerts its effect on the extracellular matrix and HIV-1 infectivity, we revisited the RNAsequencing dataset of PLEKHA4 KO cells. One gene in particular, PIK3R6, was very strongly upregulated in PLEKHA4 KO cells (log_2FoldChange of 8.4). We thus hypothesize that modulation of these gene by PLEKHA4 may be contributing to the observed phenotype. In order to test this, we performed CRISPR KO studies in EV control and PLEKHA4 KO cells by supplying these cells with an additional CRISPR vector encoding neomycin resistance, either an additional EV control vector or one targeting PIK3R6. We observed that the effect of PLEKHA4 KO was nearly entirely eradicated in PIK3R6 KO cells (Figure 4.11A). Furthermore, since our previous data indicated that the effect of PLEKHA4 could be reverted by treating cells with collagenase, we reasoned that, if PIK3R6 was modulating this phenotype in PLEKHA4 KO cells, then collagenase treatment should have no effect in PLEKHA4/PIK3R6 double KO cells. Indeed, we observed no effect of collagenase treatment on titers of HIV-1_{NL4-3} in PIK3R6 KO cells (Figure 4.11A). As infectivity in PLEKHA4 KO cells can be reverted to wildtype levels following either treatment with collagenase or PIK3R6 KO, and PLEKHA4/PIK3R6 double KO cells were insensitive to collagenase treatment, we hypothesized that PIK3R6 is responsible for modulations to the extracellular matrix resulting in this phenotype. To test this hypothesis, we performed cell-surface staining for collagen in EV control, PIK3R6 KO, PLEKHA4 KO, and

PLEKHA4/PIK3R6 double KO cells. We observed a modest but statistically significant increase in cell-surface staining of collagen in PLEKHA4 KO cells that is reverted to baseline levels following KO of PIK3R6 (Figure 4.11B-C). As a control for antibody specificity, we also stained cells that had been treated with collagenase. There was a reduction in signal in collagenase-treated cells, indicating specificity of this antibody for collagen.

In an orthogonal approach, we also assessed the effect of PIK3R6 overexpression on HIV-1_{NL4-3} titers and cell surface collagen levels. As expected, overexpression of PIK3R6 increased infectivity of HIV-1_{NL4-3} in EV control cells (Figure 4.11D). Importantly, infectivity was not further increased in PLEKHA4 KO cells, implying that this phenotype is already saturated by the PIK3R6 overexpression seen in PLEKHA4 KO cells. Furthermore, the increase in infectivity observed in EV control cells overexpressing PIK3R6 could be reverted by collagenase treatment, providing addition evidence that modulation of PIK3R6 is contributing to the ECM alterations observed in PLEKHA4 KO cells. However, to provide more direct support for this, we also performed cell-surface collagen staining in PIK3R6 overexpressing cells and found that PIK3R6 overexpression increases levels of cell-surface collagen (Figure 4.11E-F). Overall, this data suggests that PIK3R6 is responsible, at least in part, for PLEKHA4-mediated alterations to the extracellular matrix that influence HIV-1 infectivity. The more modest impact of PIK3R6 on the expression levels of cell-surface collagen relative to the dramatic effects of PIK3R6 and collagenase treatment on HIV-1 infectivity likely indicates that PIK3R6 influences multiple aspects of the extracellular matrix. Future work is needed to clarify potential additional impacts of PIK3R6 on the extracellular matrix.

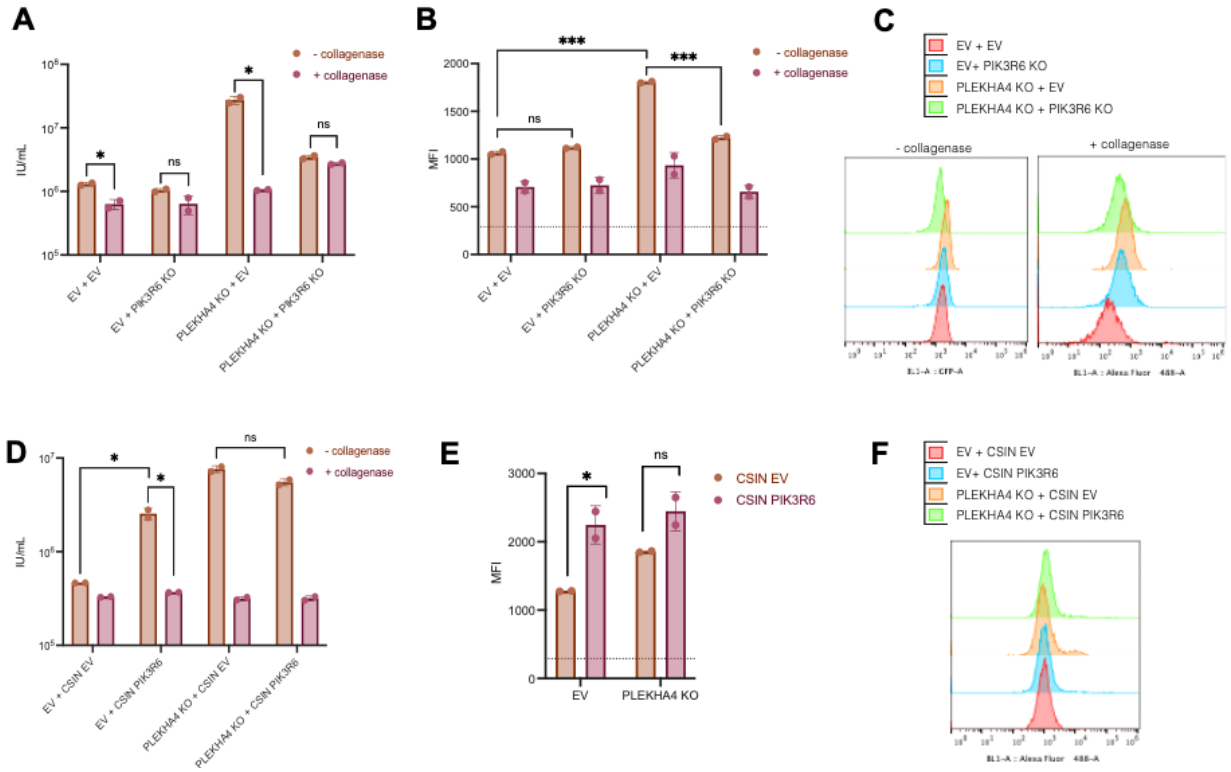

Figure 4.11 Sensitivity to PLEKHA4 and collagenase treatment is modulated by PIK3R6

(A): Titration of HIV-1_{NL4-3} on EV control or PLEKHA4 KO cells bearing either an additional EV control CRISPR vector encoding neomycin resistance or a PIK3R6-targeting guide in the presence or absence of collagenase. (B): MFI quantification of cell-surface staining of collagen in EV control or PLEKHA4 KO cells bearing either an additional EV control CRISPR vector encoding neomycin resistance or a PIK3R6-targeting guide in the presence or absence of collagenase. (C): Representative histogram plots from B. (D): Titration of HIV-1_{NL4-3} on EV control or PLEKHA4 KO cells bearing either an empty CSIN expression vector (EV) or CSIN expressing a PIK3R6 coding sequencing in the presence or absence of collagenase. (E): MFI quantification of cell-surface staining of collagen in EV control or PLEKHA4 KO cells bearing either an empty CSIN expression vector or CSIN expressing a PIK3R6 coding sequence. (F): Representative histogram plots from E. Error bars indicate S.D.

4.12 Implications on the design of next-generation antivirals

Studying the cellular mechanisms responsible for innate inhibition of viral infection in human cells can provide insight into the evolutionary dynamics of host-pathogen interaction, illustrating how hosts counteract viral infection and how viruses adapt to establish infection in new hosts. This has profound implications in human health and disease. That is, a more detailed picture of cellular defenses against viral infection—and how the virus is able to evolve evasion

mechanisms against these defenses—may elucidate exploitable vulnerabilities in this process that could be utilized for the design of new vaccination and therapeutic targets.

In this study, we uncovered a novel role for PLEKHA4 as an inhibitor of retroviral entry. These studies, which demonstrate that specific characteristics of Env determine sensitivity to robust inhibition by cellular antiviral proteins, not only illustrate fundamental processes essential the biology of retroviral entry, but also have potential implications in the design of next-generation antiretroviral therapies. For instance, the Env-dependent differences in response to IFNα and PLEKHA4 KO suggest that particular Env sequences might have evolved to evade host innate responses. Indeed, it has been previously shown that transmitter/founder viruses are relatively less sensitive to Type I Interferon than isolates from chronic infection (*163–165*). Similarly, most of the transmitter/founder strains we tested (with the exception of N61) were much less sensitive to PLEKHA4 KO and IFNα than NL4-3. It is therefore conceivable that small molecules designed to phenocopy the effect of PLEKHA4, while also negating the currently unresolved Env characteristics that result in resistance to PLEKHA4, could be exploited pharmacologically as novel inhibitors of retroviral entry. Future work is needed to determine the utility of such an approach.

CHAPTER 5. Discussion

The burden of viral disease due to emerging and re-emerging viral pathogens is pronounced and expected to continue to increase over time. One potential strategy to mitigate the significant morbidity and mortality of both current and future viral disease is the expansion of clinically available antivirals. Indeed, unlike bacterial illness, where effective antibiotics exist for most pathogenic bacteria, the vast majority of pathogenic human viruses have no targeted antiviral treatment, highlighting an urgent unmet need in antiviral approaches. In my thesis, I used both

targeted and high-throughput approaches to identify and characterize fundamental mechanisms of host-viral interactions. Although far removed from direct clinical implications, this work and the foundational insights gained are important for two major reasons. First, basic virological studies have a long history of illuminating basic mechanisms and expanding our understanding of cell biology. Indeed, although we studied VPS29 in the context of facilitating human coronavirus infection, we identified a novel role for this gene in regulating the pH status of endosomes and, consequently, the activity of endolysosomal proteases. Likewise, although PLEKHA4 was studied through the lens of restricting retroviral infection, through transcriptomics and functional approaches I uncovered key insights into the cellular role of this sparsely studied protein. Second, although the findings in this thesis are not directly translatable to the clinic, furthering the understanding of key parameters in the viral lifecycle can help guide future work aimed at designing novel therapies for viral infection. Perhaps the most famous example of this type of situation is the rapid and successful deployment of vaccines and targeted therapies for SARS-CoV-2. The speed at which vaccines were able to be developed and employed was highly influenced by decades of fundamental work on human and animal coronaviruses, including over a decade of work on the closely related, highly pathogenic human coronavirus SARS-CoV. Indeed, immediately following the release of the SARS-CoV-2 genomic sequence, based on prior studies with coronaviruses it was apparent that the most attractive target for the development of vaccine-induced neutralizing antibodies would be the spike protein. This certainly turned out to be the case, as illustrated by the remarkable efficiency of spike-based vaccines in preventing infection, serious illness, and death. Additionally, remdesivir, a highly effective antiviral that quickly became standard of care for those hospitalized with COVID-19, had previously been shown to be effective against SARS-CoV,

MERS-CoV, bat reservoir CoVs, as well as endemic HCoVs, allowing its rapid re-purposing for use as a therapy for SARS-CoV-2 (*166–169*). Below, I highlight the insights gained from the fundamental studies undertaken in this thesis (loss-of-function/viral mutagenesis studies, genome-scale loss-of-function studies, and targeted high-throughput loss-of-function studies) and discuss potential therapeutic implications of this work.

5.1 Identifying and characterizing Gag amino acid residues that rescue IP_6 deficiency: implications for the development of novel HIV-1 capsid inhibitors

Although nowadays HIV-1 infection can be incredibly well controlled—and even prevented entirely (*170*)—by highly effective antiretroviral treatments, the potential for the virus to develop mutations that render it resistant to the current arsenal of antiretroviral therapies warrants continued exploration for novel antiretroviral treatment strategies. Indeed, there are multiple reports of individuals taking pre-exposure prophylaxis therapy for the prevention of HIV-1 becoming infected with highly drug-resistant strains of HIV-1 despite treatment adherence (*171–173*). Additionally, although rare, there are reports of patients recently diagnosed with HIV-1 infection failing to respond to antiretroviral therapy due to acquiring a highly multi-drug resistant strain and needing to be treated with experimental compounds (*174*). There is thus an urgent need to continue investigating antiretroviral treatment strategies, particularly developing novel drugs with different mechanisms of action.

One potential class of drugs with a different mechanism that could be used to treat HIV-1 infection are capsid inhibitors, compounds that directly bind the HIV-1 capsid and inhibit infection by interfering with vital functions of capsid. One such drug in this class, Lenacapavir (GS-6207), has recently shown promise in Phase 1 clinical studies, resulting in a reduction of HIV-1 viral load in patients with multidrug resistant HIV-1—highlighting the potential promise

of such an approach. (*175*). Thus, when Dick *et al.* reported in 2018 that the interaction between the ubiquitous cellular polyanion IP_6 and specific residues in capsid is required for both HIV-1 assembly and maturation by stabilizing both the immature and mature lattice, there was rightful speculation on the potential utility of inhibiting this interaction as a novel antiretroviral strategy. Indeed, such a strategy could be very powerful, as a single intervention would result in multiple defects on viral infection

Our work on passaging defective viruses containing substitutions in the IP_6 binding residues (R18, K290, and K359) in an attempt to identify second-site revertant mutations thus has critical implications on the prospect of targeting the IP_6-capsid interaction as a potential novel antiviral strategy. For instance, despite several attempts, we were unable to generate revertant mutants for HIV-1_{K290A} and HIV-$1_{R18A.}$ The inability to generate revertant mutants for HIV-1_{R18A} and HIV-1_{K290A} is likely due to more substantial impairment. Indeed, previous groups have shown that HIV-1_{K290A} is impaired to a greater extent than HIV-1_{K359A}, potentially because K290 binds the 5 equatorial phosphates on IP_6 while K359 coordinates the single axial phosphate, suggesting a greater role for K290 in coordinating IP_6 (*117*). The inability to generate a revertant mutant rescuing HIV-1_{R18A} could be explained by functions of this residue in addition to coordinating IP_6, such as recruitment the cellular protein FEZ1 or as service as a conduit for dNTPs into the mature core (*117*, *176–178*). Thus, our work implies that, should novel capsid inhibitors be developed that are based on perturbing the interaction between capsid and IP_6, those that impair the function of the R18 and/or K290 sites should be prioritized, as our data suggests those residues will be less prone to mutations that could render the inhibitor ineffective.

Regarding the K359 residue, we identified a single-site revertant mutation, the stabilizing T371I substitution, that rescued replication competence of the IP_6-binding-deficient mutant HIV-

1_{K359A}. Indeed, HIV-$1_{K359A/T371I}$ was fully infectious despite containing the K359A substitution that renders VLP assembly unresponsive to IP_6 *in vitro* and which substantially impairs IP_6 incorporation into virions (*116*, *120*). We found no significant reduction in yield of HIV-$1_{K359A/T371I}$ from IPMK KO 293T cells, in contrast to WT HIV-1. This finding suggests that HIV-$1_{K359A/T371I}$ is no longer dependent on IP_6 or requires substantially lower concentrations of IP_6 in virus producing cells. An important implication of this finding is that inhibitors of IP_6-capsid interactions may be rendered ineffective in virions that accumulate a T371I substitution.

It is important to note, however, that the T371I substitution itself comes at a fitness cost. Indeed, this capsid-stabilizing substitution reduces infectivity of HIV-1 by ~1 log when introduced into wildtype HIV-1. This data thus implies that the stability of capsid is very tightly regulated for optimal infectivity. Interventions that destabilize capsid, such as abolishing interaction with IP_6 through mutagenesis or ablating the IP_6 synthetic machinery, result in infectivity defects. Likewise, interventions that result in hyper-stabilization of the capsid, such as introduction of the T371I substitution, also impair infectivity. However, stabilizing interventions are able to compensate for destabilizing ones and rescue infectivity. This has important implications for the design of inhibitors that target capsid-IP_6 interactions. For instance, to limit the emergence of resistant mutants, small molecules should result in either a stabilization effect at both sites or a destabilization effect at both sites. For example, based on our data, an inhibitor that results in increased stability at the T371 site should impair infectivity, as should an inhibitor that results in decreased stability at the K290/K359 sites. Yet, in either of those situations, resistance mutants could emerge that negate the effect, such as mutations that result in destabilization at the K290/K359 sites or mutations that result in increased stabilization at the T371 site, respectively. However, an inhibitor that results in a stabilizing effect at the T371 site

as well as a stabilizing effect at the K290/K359 site (or, likewise, a destabilizing effect at the K290/K359 site as well as a destabilizing effect at the T371 site) could result in more substantial impairment that is also more resilient to the development of resistance mutations.

5.2 The broad requirement of VPS29: implications for the development of host-targeted therapies as novel antivirals

In the past few years, there has been widespread adoption of genome-scale CRISPR screening technology to perform unbiased assessments of human genes influencing viral infection. This has resulted in a considerable growth not only of highly detailed knowledge regarding host determinants of viral infection, but also potential novel therapeutic targets. That is, pharmacologically targeting host proteins required for viral infection is a potentially attractive strategy for the development of novel antiviral therapies. Indeed, in the dozens of genome-scale loss-of-function CRISPR screens that have been performed in recent years, many have identified genes for which pharmacological inhibitors already exist. For example, several groups reported genes involved in cholesterol homeostasis as vital for CoV infection. Two groups independently identified genes in the sterol regulatory element-binding protein (SREBP) pathway (*20*, *21*), and Wang *et al.* showed treatment of cells with 25-hydroxycholesterol or PF-429242, both of which impair the SREBP pathway, resulted in dose-dependent decreases in Spike-mediated entry of pseudoviruses. Likewise, several groups identified PIK3C3 as essential for SARS-CoV-2, HCoV-OC43, and HCoV-229E (*20–23*, *91*, *94*), and multiple groups observed that PIK3C3 inhibitors such as Compound-19, PIK-III, autophinib, or SAR405 impaired SARS-CoV-2 infection as well as HCoV-OC43 and HCoV-229E infection (*20*, *94*). Similarly, in a screen for SARS-CoV-2, Israeli *et al.* found that the transcription factor GATA6 stimulates expression of SARS-CoV-2 receptor ACE2, and that the drug Pyrrothiogatain, which inhibits the ability of

GATA6 to bind DNA, decreased ACE2 expression and SARS-CoV-2 viral titers (*95*). Importantly, these types of findings are not unique to screens performed on the coronaviruses. In a screen for influenza A virus, Yi *et al.* identified the guanine nucleotide exchange factor CYTH2 as a novel regulator of IAV endosomal entry and showed that pharmacological inhibition with the antagonist SecinH3 impaired IAV infection *in vitro* and protected mice from IAV infection *in vivo* (*179*). Finally, for Zika virus, Wang *et al,* identified the plasma-membrane localized αvβ5 integrin (ITGB5) as a novel entry factor for ZIKV, and showed through *in vivo* studies showing that treatment of mice with the αvβ5 inhibitor cilengitide resulted in significantly decreased ZIKV RNA detected in whole brains of infected mice (*24*). Although by no means an exhaustive list, that several groups performing screens with diverse viruses identified genes with available inhibitors that protect against viral infection both *in vitro* and *in vivo* demonstrates the power of this technique to identify promising targets for novel antiviral treatments.

We identified the retromer complex subunit protein VPS29 as one such potentially promising target. We showed that VPS29 was broadly required by diverse coronaviruses, including: HCoV-OC43, HCoV-229E, HCoV-NL63, rVSV/SARS-CoV-2, Pangolin-CoV/Gx, Pangolin-CoV/Gd, WIV16, as well as the Omicron variant of SARS-CoV-2. Importantly, multiple other groups also identified components of the retromer complex (VPS26/VPS29/VPS35) in screens utilizing SARS-CoV-2, providing additional support for the robustness of this gene in promoting CoV infection (*20*, *23*, *38*, *94*). Mechanistically, we showed that vesicles in VPS29 KO cells were enlarged, deacidified, and had decreased Cathepsin L activity, which resulted in virions becoming entrapped therein. Thus, one potential strategy to convert these findings into novel therapies is to employ pharmaceuticals that lead to the same net effect on the cell: namely,

endosome deacidification. Importantly, for CoV infection, since fusion between viral and endosomal membranes is prompted by structural rearrangements following exposure to low pH and proteolytic cleavage, and the activity of the endosomal proteases themselves also require exposure to low pH, the effect of endosome acidification on CoV entry is likely multifactorial. This makes perturbing this process as a novel antiviral strategy particularly attractive, as a single intervention could result in multiple, distinct inhibitory effects on the viral lifecycle. However, while inhibitors of the proton pumps in the endosomal membrane that regulate endosome acidification, known as V-ATPases, do exist, their clinical utility is limited by substantial toxicity (*180*). Therefore, a more attractive therapeutic strategy may be specifically perturbing the function of the retromer complex, which could result in viral inhibition without extensive non-specific and toxic effects on the cell. Indeed, although the low potency and specificity of known retromer inhibitors has limited the utility of these compounds as treatments, very recent reports of novel retromer inhibitors with nanomolar affinities and high specificity warrants further exploration of these compounds as potential novel antiviral drugs (*181–185*).

This highlights, of course, perhaps the most significant barrier to the clinical development of host-targeted antiviral drugs: the challenge of balancing impairing viral processes with minimizing adverse effects caused by disruption of fundamental biological processes. One advantage of utilizing loss-of-function CRISPR screening to identify potential host targets is that genes essential to the survival of the cell are effectively removed from consideration, as cells harboring guides targeting these genes will not survive to be placed under selection. Nevertheless, many of the genes and pathways hijacked by viruses to complete their lifecycle are components of essential organismal processes, making it difficult to target these processes without completely altering normal physiology. For instance, as nearly every screen performed

on the human coronaviruses identified genes involved in heparan sulfate proteoglycan biosynthesis, interfering with this process would appear to be a very attractive strategy with unparalleled broad-spectrum antiviral activity. However, cell surface heparan sulfate is vital for normal physiology, in particular the anticoagulant properties of vascular endothelial cell surface heparan sulfate. Thus, the risks associated with indiscriminately perturbing such a vital process very likely outweigh the potential benefits of antiviral activity. A potential strategy to overcome these limitations is rational design of host-directed therapies to maximize impairment of viral processes while minimizing effects on host physiology. For example, Clausen *et al.* showed that non-anticoagulant derivates of heparin (the pharmacological analog of heparan sulfate) impair SARS-CoV-2 infection, potentially illustrating a promising strategy of targeting viral infection without dramatically altering normal physiology (*16*). While additional work is needed to determine the clinical utility of such strategies, I believe this approach deserves consideration as a potentially promising strategy for novel host-directed antiviral approaches.

5.3 PLEKHA4 as a potent inhibitor of HIV-1 entry: implications for the development of HIV-1 entry inhibitors.

As discussed in section 5.1, although highly effective antiretroviral therapy exists for patients living with HIV-1, the emergence of multidrug resistant strains of HIV-1 highlights the urgent need to continue developing novel antiretroviral treatments, particularly those with different mechanisms of action. Furthermore, >1 million people per year acquire HIV-1 infection, highlighting an urgent need for novel prevention strategies (*186*). One universal step of the viral lifecycle that could be targeted pharmacologically for both treatment and prevention is viral entry into target cells. Targeting this step of the viral lifecycle is a particularly attractive candidate for novel antiviral approaches, as entirely preventing viral entry would prevent cellular

changes and immune activation resulting from the cytosolic presence of viral genetic material, which is associated with cytotoxicity and morbidity. There are currently four FDA-approved medications that prevent HIV-1 entry: Enfuviritide (T-20), which inhibits membrane fusion, the CCR5-antagonist Maraviroc, which prevents association of the HIV-1 envelope with the CCR5 coreceptor, the anti-CD4 monoclonal antibody Ibalizumab, which prevents HIV-1 binding with the CD4 receptor, and the Env-binding drug fostemsavir, which prevents the interaction between Env and cell-surface receptors (*49*, *187–189*). Additionally, the HIV-1 envelope glycoprotein has received intense interest as the antigenic target of HIV-1 vaccines.

However, due to intense genetic variation and heavy glycosylation of the HIV-1 envelope, attempts to elicit neutralizing antibodies that protect patients from acquiring HIV-1 have thus far been unsuccessful, and the development of efficacious HIV-1 vaccines remains elusive (*190*). Thus, additional interventions aimed at preventing HIV-1 entry into cells are urgently needed. To gain more insight into potential strategies to inhibit HIV-1 entry, I performed targeted genetic screens in a cell line where HIV-1 entry was dramatically inhibited by IFNα in order to identify gene(s) mediating this effect. I identified one such gene, PLEKHA4, which dramatically inhibits HIV-1 infection in an envelope-dependent manner. Further mechanistic follow-up revealed that PLEKHA4 modifies the property of the extracellular matrix, and different HIV-1 envelopes are differentially sensitive to these modifications. It remains, however, unclear exactly how PLEKHA4 alters the composition of the extracellular matrix, and what exact biophysical properties of the HIV-1 envelope dictate this phenotype. One potential explanation is that PLEKHA4 decreases the expression of cellular adhesions glycoproteins that serve as cofactors for particular HIV-1 envelopes. This would result in a decreased binding and entry efficiency of HIV-1 envelopes utilizing these proteins as cofactors. Another potential explanation is that a

PLEKHA4-mediated decrease in plasma-membrane expression of adhesion proteins alters downstream signaling pathways influencing cytoskeletal dynamics. This could influence the dynamics of receptor-mediated viral entry, which may vary based on envelope. Alternatively, such alterations could impact cell motility or cell-cell interactions, leading to varying effects on viral entry. Future work is needed to resolve which possible effect(s) most influence viral entry.

Studying the basic mechanisms of how antiviral proteins are able to inhibit infection can be informative for the development of novel antiviral approaches. For example, in this case, the cell has already evolved a highly potent mechanism to inhibit HIV-1 entry. Although additional work is needed to precisely clarify the effect of PLEKHA4 on the extracellular matrix and the properties of the HIV-1 envelope that confer sensitivity to this, this information could be very informative in guiding new strategies to inhibit HIV-1 entry. For instance, understanding how these modifications to the extracellular matrix block HIV-1 entry can guide the rational development of small molecule inhibitors that mimic this effect and thus provide a novel pharmacological strategy to prevent HIV-1 entry. Furthermore, additional clarification regarding why some HIV-1 envelopes are sensitive to inhibition by PLEKHA4 and the cellular effects it produces while some envelopes are resistant to these effects could provide additional insight on how to exploit this property therapeutically. For instance, what is it about the biophysical properties of envelopes that are resistant to inhibition by PLEKHA4 that confers this resistance? Perhaps particular amino acid residues within these envelopes—or specific modifications that occur at these residues—allow the virus to circumvent this inhibition. In this case, it is therefore conceivable that molecules aimed at negating this effect while also mimicking the effect of PLEKHA4 could yield a drug with broad-spectrum activity against diverse HIV-1 envelopes. Another possibility is that PLEKHA4-sensitive envelopes utilize a different subset of specific

cofactors on the cell surface than PLEKHA4-resistant envelopes do. Understanding what it is about the HIV-1 envelope that results in this effect could prompt the design of compounds aimed at blocking these interactions as novel antiviral approaches. Regardless of which exact scenario is ultimately responsible for this effect, the knowledge that PLEKHA4 can robustly inhibit several strains of HIV-1 warrants the consideration of attempting to recapitulate this phenotype as a novel antiviral strategy.

5.4 Conclusion

In this thesis, I employed diverse approaches to gain additional mechanistic insight into host-viral interactions using HIV-1 and the human coronaviruses as model systems. These fundamental studies are critical for furthering our understanding of the basic principles of viral infection in human cells, a critical first step in the identification of potential targets for novel antiviral strategies. For each technique I employed, I have reviewed the rationale for each approach, summarized the key findings obtained, and discussed the potential relevance for the development of novel antiviral therapies. I believe the implications of these findings deserve consideration in the field as potentially applicable to the development of additional strategies to reduce the burden of viral disease.

Materials and Methods

Cells and media

HEK-293T (*H. Sapiens;* sex: female), A549 (*H. Sapiens;* sex: male), HT1080 (*H. Sapiens;* sex: male), MDCK (*Canis familiaris*) and Vero cells (*Cercopithecus aethiops*) were obtained from ATCC, and Huh7.5 cells (generously provided by Charles M. Rice) were maintained at 37°C and 5% CO_2 in Dulbecco's Modified Eagle Medium (DMEM, Gibco) supplemented with 10% fetal bovine serum. NHBE cells (*H. Sapiens*) were obtained from ATCC (Cat# ATCC PCS-300-010) and maintained at 37°C and 5% CO_2 in Airway Epithelial Cell Basal Medium (ATCC PCS-300-030) supplemented with Bronchial Epithelial Cell Growth Kit (ATCC PCS-300-040). MT4 cells were maintained in Roswell Park Memorial Institute (RPMI) 1640 Medium (Gibco) supplemented with 10% fetal calf serum and gentamycin. Cells were maintained at 37°C and 5% CO_2. All cells were assessed for Mycoplasma contamination. All transfections with viral plasmids were performed with polyethyleneimine.

HIV-1 and SIVmac239 viral stock production

293T cells were seeded at 6 x 10^6 cells per 10cm dish and transfected the next day using polyethylenimine. 8 hours post transfection, cells were placed in fresh medium. For generation of full-length virus, 293T cells were transfected with 15 μg of proviral plasmid. For generation of imaging constructs, 293T cells were transfected with 6μg of proviral plasmid, 6μg of SYN-GP, and 1.2 μg of VSV-G. At 48 hours post transfection, supernatants were harvest and passed through a .22μM filter. Titer of full-length infectious viruses was determined by serial dilution on MT4 cells. At 48 hours post infection, cells were fixed with 4% PFA and assessed via flow cytometry. Titer of imaging constructs was determined by serial dilution on TZM-bl cells. 48

hours post infection, cells were fixed with 0.5% glutaraldehyde and stained with X-gal to visualize number of infected foci.

Production of HCoV and rVSV stocks

HCoV-OC43 (strain: ATCC VR-759) and HCoV-229E (strain: ATCC VR-740) were obtained from Zeptometrix Corporation, and HCoV-NL63 (strain: Amsterdam I) was obtained from the Biodefense and Emerging Infections Research Resources Repository. Viral stocks were generated by propagation on Huh7.5 cells. The IAV strains A/WSN/33 was propagated in MDCK cells. RSV strain A2-line19F expressing the red fluorescent protein monomeric Katushka 2 (mKate2;(*191*)) was propagated in Vero cells. Adenovirus 5 was purchased from ATCC (VR-1516) and propagated in A549 cells. VSV_{IND}(eGFP) was propagated on 293T cells (*192*). The replication-competent chimeric recombinant vesicular stomatitis virus encoding SARS-CoV-2 S and green fluorescent protein (eGFP), rVSV/SARS-2/GFP_{2E1}, has been described previously (*193*) and was propagated on 293T-ACE2 cells. rVSV/EBOV-GP was obtained from Kartik Chandran (*151*) and was propagated on Vero cells. To generate rVSV/SARS-CoV-2_{NG-P}, the spike CDS was reverse transcribed and PCR amplified from rVSV/SARS-2/GFP_{2E1} using primers: P-NG-2E1-S-MluI_F: MLUAGAGATCGATCTGTTTCCTTGACACGCGTATGTTTGTGTTCCTGGTGCTGCTGCCA and P-NG-2E1-S-NotI_R: AACATGAAGAATCTGTTGTGCAGGGCGGCCGCCTTACAACAGGAGCCACAGGAA. The resulting fragment was ligated into VSV NG-P (*194*) plasmid linearized with MluI and NotI using T4 ligase (NEB). Rescued rVSV/SARS-CoV-2_{NG-P} was propagated on 293T-ACE2 cells.

Genome-wide CRISPR KO screening

The human genome-wide Brunello Library (*131*) in lentiCRISPRv2 was obtained from Addgene (cat# 73179) and amplified according to depositor's instructions. Resulting plasmid DNA was validated via NGS sequencing to confirm appropriate coverage and representation (the resulting library contained 0.0% undetected guides and a skew ratio of the top 10% represented guides to the bottom 10% represented guides was 3.94, well below the recommended cutoff of 10 for an "ideal" library (*153*)(*153*)). To generate lentiviral preparations of the Brunello library, 293T cells (6 x 10^6 cells per 10 cm dish) were transfected with 6µg lentiCRISPRv2-Brunello, 6µg NL-gagpol, and 1.2 µg VSV-G using PEI. 48 hours post transfection, supernatants were pooled and concentrated using Amicon Ultra Centrifugal Filters. Concentrated lentiviral preps were stored at -80°C and titrated on A549 cells based on puromycin resistance. Briefly, 10-fold serial dilutions (from 10^{-1} to 10^{-6}) were used to transduce 40,000 A549 cells in a 24 well plate format. 48 hours post transduction, cells were trypsinized and moved up to 6 well plates in the presence of 1.25 µg/mL puromycin. 9 days post transduction, cells were fixed, stained with Crystal Violet, and stained foci were counted to measure the number of cells surviving selection (i.e. those that were transduced with lentiCRISPRv2 harboring a puromycin resistance cassette). To perform the screen, 1.3 x 10^8 A549 cells were transduced with lentiCRISPRv2-Brunello at an MOI of 0.3 in order to generate a population of single KO cells at high (>500X) coverage. Two days post transduction, cells were placed in selection with 1.25 µg/mL puromycin and passaged for 7 days, until there were no untransduced cells remaining. Thereafter, in triplicates with 8x10^6 cells per flask, A549-Brunello cells were infected or not with HCoV-OC43 at an MOI of 0.1, and passaged for 7 days until >95% infection-induced cell death occurred. Cellular gDNA was isolated using Zymogen Quick-DNA Midiprep Plus Kit (Zymo Research), and sequencing

libraries prepared via amplication of sgRNA loci utilizing F primers containing P5 and Read 1 Sequencing Primer and a R primer containing P7, a barcode, and the multiplexing Index Read Sequencing Primer, as described in Joung *et al,* 2017. Resulting libraries were gel purified, pooled, and sequenced on the Illumina HiSeq at Genewiz using 80 cycles of Read 1 (Forward) and 8 Cycles of Index 1 using standard Illumina sequencing primers.

Generation of SIV-CRISPR ISG screening library

To identify ISGs in MT4-R5 cells, 1×10^6 MT4-R5 cells were treated or not in 3 biological replicates with 1000U/mL. 24 hours after treatment, total RNA was isolated using the Nucleospin RNA isolation kit (Machery Nagel). RNA-seq libraries were prepared from total RNA using poly(A) enrichment and sequenced on Illumina NextSeq High Output flow cell with 1x75 bp read length. Differential gene expression analysis of RNA-seq data was performed using DESeq2 (*195*). An ISG was defined as all genes having a log2FC > 1 and a padj <0.05. We constructed a library of sgRNAs that includes 8 unique sgRNAs per ISG. To do so, we searched and compiled sgRNA sequences from previously published genome-wide KO libraries. We started with the Brunello library, which is based on some of the most recently updated and improved algorithms (*131*). Next, sgRNA sequences were added at random from the GeCKO library, up to 8 unique sgRNAs for each gene (*196*). For genes in which 8 unique sequences could not be obtained from a combination of the Brunello and GeCKO libraries, additional sgRNA sequences were added from the Lander/Sabatini and Moffat libraries (*197–199*). For genes in which 8 unique guides could not be obtained from these libraries—a total of 138 genes—sgRNA sequences were de novo designed using the Broad Institute's GPP sgRNA designer (https://portals.broadinstitute.org/gpp/public/analysis-tools/sgrna-design). Finally, 200 non-targeting controls (NTCs) were added from the GeCKO library. Our resulting library

contained 7,864 unique sgRNA sequences which were synthesized in a bulk pool by Twist Biosciences. To generate a screening vector, we repaired the self-inactivating ΔU3 3' LTR of lentiCRISPRv2 with the full 3' LTR sequence of SIVmac239. Additionally, we replaced the HIV-1 based 5' LTR, packaging signal, and rev-response element with the equivalent sequences from SIVmac239. Finally, we included a truncated SIVmac239 Gag sequence, as previous work in our lab has demonstrated that this increases packaging efficiency of viral RNA in VLPs (data not shown). The bulk oligo pool library was amplified with primers Array_F: TAACTTGAAAGTATTTCGATTTCTTGGCTTTATATATCTTGTGGAAAGGACGAAACACCG and Array_R: ACTTTTTCAAGTTGATAACGGACTAGCCTTATTTTAACTTGCTATTTCTAGCTCTAAAAC and cloned into BsmBI-digested SIV-CRISPR using Gibson assembly. Ligated products were electroporated into ElectroMAX™ Stbl4™ Competent Cells (Invitrogen cat# 11635018) according to manufacturer's instructions and grown overnight on bioassay dishes (Thermo cat# 166508) at 30 degrees Celsius. The next day, colonies were scraped, pooled, and DNA was isolated using the NucleoBond Xtra Midi EF kit (Machery Nagel cat# 740420.50). The resulting SIV-CRISPR ISG library was deep sequenced to confirm adequate representation and contains 7863 of the 7864 desired sgRNA sequences. The percentage of perfectly matching guides was 94.4%, and the skew ratio of the top 10% represented guides to the bottom 10% represented guides was 2.66 (per established protocols, an ideal library has >70% matching guides and a skew ratio of <10) (*153*).

SIV-CRISPR ISG CRISPR screening

A large-scale preparation of the library was created by packaging the SIV-CRISPR ISG Library into VLPs using the SIVmac gag-pol packaging plasmid SIV3+ and the pseudotyping

envelope VSV-G (*200*). VLPs were then titered using Blasticidin resistance on TZM-bl cells. MT4-R5 cells were transduced with SIV-CRISPR ISG Library at adequate coverage (>500x per sgRNA) and a low MOI (0.3) in order to generate a large population of MT4-R5 cells with single SIV-CRISPR integrations. Following selection in Blasticidin to remove untransduced cells, cells were treated or not in triplicate with 100U/mL IFNα. 24 hours after treatment (or lack thereof), cells were infected with SIVmac239 at an MOI of 0.5. Three days post-infection, cells were pelleted and supernatant containing packaged SIV-CRISPR was harvested. From the supernatant, virions were pelleted and viral RNA (vRNA) was extracted from pelleted virions. After reverse transcription into cDNA, sgRNA cassettes from the packaged SIV-CRISPR genomes was amplified with barcoded primers containing Illumina adapters and sequenced using the Illumina NextSeq Platform, as described previously (*153*). The relative enrichment of sgRNA sequences in the vRNA from IFNα treated cells was analyzed using the model-based analysis of genome-wide CRISPR/Cas9 knockout (MAGeCK) statistical package (*132*).

Generation of CRISPR KO cell lines

sgRNA sequences were cloned into lentiCRISPRv2 bearing either a Blasticidin, Hygromycin, Puromycin, or Neomycin resistance cassette digested with BsmBI. lentiCRISPR v2 was a gift from Feng Zhang (Addgene plasmid # 52961; http://n2t.net/addgene:52961; RRID:Addgene_52961). VLPs were generated by transfecting 1×10^6 293Ts/well with 1 µg lentiCRISPRv2, 1 µg of Gag-Pol, and 0.2 µg of VSV-G. Media was changed 8 hours post transfection and at 48 hours post transfection, VLPs were harvested and passed through 0.22 µM filter. Target cells were transduced with lentiCRISPRv2 VLPs bearing sgRNA sequences or an empty control and placed in selection until no untransduced cells remained. Editing was verified by amplifying and sequencing target loci. Single cell clones were obtained by limiting dilution

and assessment of clonality was verified using Synthego ICE, which identifies Indel frequency in Sanger sequencing data (Synthego Performance Analysis, ICE Analysis. 2019. v2.0.). sgRNA sequences:

IPMK g1	5’-ATGTACGGGAAGGACAAAGT-3’
IPMK g2	5’-GGTGGACTCGATCGCCGGTG-3’
IPMK g3	5’-CCGGCCACCTGATGCGAGAG-3’
CCDC22	5’-CCGCAGGGTTGATCACACGC-3’
CCDC93	5’-TAGAATCCAAAGCTGATCCA-3’
COMMD3	5’-CTTGAAACATATCGACCCAG-3’
VPS29	5’-GGACATCAAGTTATTCCATG-3’
WDR81	5’-CGTGGACCCAATCTAGCACG-3’
WDR91	5’-GTAGCTCCAATAATCCCGAA-3’
HERPUD2	5'-TTGCCCATCATTGTTAACTT-3'
ZNFX1	5'-CATGTTGTGGACAAATACCA-3'
EPB41L5	5'-CTAAGTCCATCATCACGTGT-3'
HERC6	5'-AAAATAATACAAGTTTCCTG-3'
PLEKHA4	5'-GACATCAATGCGACTCAACG-3'
PLA2G2D	5'-GGTGTGATTCCAATCCAGGG-3'
DDIT4	5'-TGAGCGCGGCGGCCGATCTG-3'
SDK2	5'-CACCGTTGACAGGATGACAA-3'
MRAS	5'-CAACCTCCCCACATACAAGC-3'
RHPN1-AS1	5'-ATGCTTCCAAAGTTCACACT-3'
ZNFX1	5’-CATGTTGTGGACAAATACCA-3’

PIK3R6	5’- TCTGGTACCACGGGTCTACG-3’

Generation of IP_6 binding-null mutants

All full-length proviral plasmids used in this study were based on the HIV-1 clone NHG, a previously described HIV-1 clone that encodes GFP in place of Nef (Accession number: JQ585717). Mutant viruses were derived from this parental plasmid using primer mutagenesis with fragments assembled into NHG digested with SpeI and SbfI using NEB HiFi DNA Assembly Master Mix according to the manufacturer’s instructions. Primers used for mutagenesis include: K359A F: 5’-CCGGCCATGCTGCAAGAGTTTTG; K359A R: 5’-CAAAACTCTTGCAGCATGGCCGG; T371I F: 5’-GCAATGAGCCAAGTAATAAATCCAGCTACC; T371I R: 5’-GGTAGCTGGATTTATTACTTGGCTCATTGC; P289S F: 5’-CATAAGACAAGGAAGTAAGGAACCCTTTAGAG; P289S R: 5’-CTCTAAAGGGTTCCTTACTTCCTTGTCTTATG; R57G F: 5’-TCAAAGTAGGACAGTATGATC; R57G R: 5’- GATCATACTGTCCTACTTTGA. The imaging construct HIV-1 NG was derived from NL4-3. The region of NL4-3 encoding Pol was deleted from bp 2294-4813 and a unique XbaI was added at bp 2301; Vpu was deleted and Env was truncated by removing bp 6056 – 7250 inserting NheI at 6056. These deletions and restriction sites were created through overlap PCR and cloned into NL4-3 via SphI and NheI (NL4-3 BssHII 5’- GCTGAAGCGCGCACGGCAAGAGGCG 5’-CTGAAGCGCGCACGGCAAGAGGCGAGG and dPol Xba AS 5’-CTACTATTCTTTCCCCTGCACTCTAGACTACTACTTTATTGTGACGAGGGGTCGC; dPol Xba S 5’-

GCGACCCCTCGTCACAATAAAGTAGTAGTCTAGAGTGCAGGGGAAAGAATAGTAG and dVpudEnv NheI AS 5'-CTCCTCGCTAGCGTACTACTTACTGCTTTGATAG). The sequence encoding neon green (NG) was codon optimized to have nucleotide composition and codon usage similar to that of Pol using the Codon Optimization On-Line Tool from Singapore University (http://cool.syncti/org) and was synthesized by GeneArt. Neon Green was fused into the p6* frame of Pol through overlap PCR and inserted via SphI and XbaI (NL4-3 SphI 5' AGTGCATGCAGGGCCTATTGCACC, Pol-NG AS 5'-CATGTTATCCTCCTCGCCCTTGCTCACCATCTTTATTGTGACGAGGGGTCGCTGCCA; Pol-NG S 5'-TGGCAGCGACCCCTCGTCACAATAAAGATGGTGAGCAAGGGCGAGGAGGATAACAT G, NG XbaI 5'-CTCCTCTCTAGACTACTTGTACAGCTCGTCCATGCCCAT).Mutagenesis of this construct was accomplished using the same primers as above.

Single cycle infectivity assays from IPMK-KO 293T cells

WT control or IPMK KO 293T cells were seeded at 2.5 x 10^5 cells/well in a 24 well plate and transfected with 625 ng of HIV-$1_{WT,}$ HIV-1_{K359A}, or HIV-$1_{K359A/T371I}$ proviral plamids. Virions were prepared as above and titrated on MT4 cells. 24 hours post infection, Dextran Sulfate was added (50µg/mL) to limit infection to a single round. 48 hours post infection, cells were fixed with 4% PFA and assessed via flow cytometry.

Spreading replication assays of IP_6-binding null mutants

5 x 10^4 cells per well were seeded in a 96 well plate and infected at an MOI of 0.001. 16 hours post infection, cells were washed three times and placed in 5µM BVM or DMSO control. Supernatants were collected at indicated timepoints, and levels of reverse transcriptase were quantified using the SYBR-PERT assay as previously described (*201*).

Western blot analysis of HIV-1 virions

293Ts were seeded 5 x 10^5 cells/well in a 12 well dish and transfected the next day with 1.25µg proviral plasmid. 48 hours post transfection, cell lysates and virions pelleted through 20% sucrose (14,000xg for 90 minutes at 4°C) were separated on a NuPage 4-12% Bis-Tris Gel (Invitrogen) and subsequently blotted onto a nitrocellulose membrane. Blots were blocked with Intercept Blocking Buffer (Li-Cor) and probed with primary antibody along with a corresponding IRDye 800CW- or IRDye 680-conjugated secondary antibody. Images were acquired using an Odyssey scanner (Li-Cor Biosciences). HIV-1 CA was detected using a human monoclonal anti-p24 (NIH AIDS Reagent Catalog #530).

Imaging of HIV-1 assembly

5x10^4 TZM-bl cells per well were plated in a Lab-Tek Chamber Slide and infected the following day with indicated imaging construct at an MOI of 1. For fixed samples, cells infected in the presence or absence of 5µM BVM were fixed 48 hours post infection and imaged on a DeltaVision OMX SR imaging system using a 60X Widefield oil immersion objective (Olympus) with an exposure time of 50ms, 10% Transmission, A488 nm laser. For live-cell samples, image acquisition began 26 hours post infection, with cells placed in the presence or absence of 5µM BVM at the time of image acquisition. Images were acquired at 37°C, 5% CO_2 at indicated timepoints using a 60X Widefield oil immersion objective with an exposure time of 45ms, 5% Transmission A488 nm laser. For TIR-FM, cells were imaged approximately 28-30 hours post infection in the presence or absence of 5µM BVM at 37°C, 5% CO_2. Images were acquired every 1 min for 90 min using a 60X RING-TIR-FM objective (Olympus Apo N 60X 1.49 Oil) with an exposure time of 100 ms, 10% Transmission A488 nm laser. Representative images were acquired, and all images were analyzed using Fiji (https://fiji.sc/). Briefly, images

were auto thresholded and Gag-NG punctae quantified using the Analyze Particles function in Fiji. Reported is the mean ± SD for displayed images (n=2 per condition).

Pathway analysis of genome-wide KO hits

All 34 candidate genes were searched using the STRING database (https://string-db.org) for functional enrichment of protein-protein interactions using default settings, except the minimum required interaction score was changed from medium confidence (0.400) to high confidence (0.700). Subsequently, genes were annotated with UniProt keywords (https://uniprot.org)

Respiratory virus infectivity assays

A total of $1x10^4$ cells per well were seeded on a 96-well plate in triplicate. The next day, cells were infected with each virus at an MOI of ~0.3. For HCoV-OC43, HCoV-NL63, and HCoV-229E, infected plates were incubated at 34ºC for 24 hours. For rVSV/SARS-CoV-2, infected plates were incubated at 37ºC for 16 hours. Cells were then fixed in 4% PFA. For rVSV/SARS-CoV-2 and RSV, which encode eGFP and mKate2 reporter genes respectively, number of infected cells were measured directly by flow cytometry. Otherwise, cells were immunostained for viral antigens. Briefly, cells were blocked with 5.0% fetal bovine serum in PBS and permeabilized with 0.5% Saponin before a 30 minutes incubation with: HCoV-OC43: Anti-Coronavirus Group Antigen Antibody, nucleoprotein of OC-43 (1:1000, Sigma MAB9013); HCoV-NL63: Anti coronavirus NL63 (1:1000, Eurofins M.30.HCo.B2D4); HCoV-229: Anti coronavirus 229E (1:1000, Eurofins M.30.HCo.B1E7); IAV: Influenza A NP Antibody, FITC (1:50, Invitrogen MA1-7322); Adenovirus: Adenovirus Hexon Antibody, FITC (1:50, Invitrogen MA1-7329). For unconjugated primary antibodies (HCoV-OC43, HCoV-NL63, and HCoV-229E), a secondary antibody conjugate AF-488 Goat anti-Mouse IgG (H+L) (1:1000, Thermo) was used before infected cells were enumerated via flow cytometry.

siRNA screening of VPS29 interactors

A list of well-known VPS29 interactors ((*141*)) was selected and used to construct a targeted siRNA library constructed of a pool of four different gene specific siRNA sequences (ON TARGETplus SMARTpool siRNA, Dharmacon).

siRNA transfection

siRNAs were reverse-transfected with $5x10^3$ HT1080-ACE2 using RNAiMAX (Thermo Scientific) according to the manufacturer's protocol. Two- or three-days post transfection, cells were infected at an MOI of ~0.3 and processed as above.

VPS29 reconstitution experiments

A VPS29 coding sequence containing silent mutations in the sgRNA targeting sequence was purchased from IDT and cloned into CSIN using NEBuilder HiFi DNA Assembly (NEB). The $VPS29_{I91D}$ and $VPS29_{L152E}$ derivates were obtained via PCR mutagenesis using primers I91D F: GGTCACCAAGTAGATCCTTGGGGA, I91D R: TCCCCAAGGATCTACTTGGTGACC, L152E F: CCATCATTTGTGGAGATGGATATCCAGGC, L152E R: GCCTGGATATCCATCTCCACAAATGATGG. Resulting constructs, including an empty vector CSIN used as a control, were used to transduce single cell clones obtained from bulk EV or VPS29 KO HT1080-ACE2 via limiting dilution. Infectivity assays on the resulting cell lines were performed as above.

HIV-1/Nanoluc CoV Pseudotype Assays

To generate HIV/Nanoluc CoV pseudotyped particles, $5x10^6$ 293T cells were plated in 10mL growth medium in a 10-cm dish. The next day, 7.5 µg pHIV-1_{NL4-3} ΔEnv-NanoLuc and 2.5 µg indicated CoV spike plasmid were transfected using PEI. Media was changed after 8 hours of incubation. After 48 hours post transfection, supernatant was harvested, passed through a 0.22-

µm polyvinylidene fluoride syringe filter (Millipore; SLGVR33RS), aliquoted, and stored at -80ºC. To perform nanoluc assays with the resulting HIV/Nanoluc CoV pseudotyped particles, a total of $1x10^4$ HT1080-ACE2 WT or VPS29 KO cells per well were plated in triplicate in a 96-well plate. The next day, ~$1x10^3$ infectious units of HIV/Nanoluc CoV pseudotyped particles were added to cells and incubated at 37ºC for 48 hours. Thereafter, cells were harvested for Nanoluc luciferase assays using the Nano-Glo® Luciferase Assay System (Promega, Cat# N1150).

Generation of 2x-FYVE mSCAR imaging construct

The lentiviral expression vector CSIN was derived from CSIB (*202*) by exchanging the Blasticidin resistance cassette with Neomycin. Briefly, primers Neo_CSIB_F: AAAAACACGATGATAATATGGCCACAACCAATTGAACAAGATGGATTGCACGCAGGTTCT and Neo_CSIB_R: AGCTTGATATCAAGCTTGCATGCCTGCAGGTCAGAAGAACTCGTCAAGAAGGCGATAGAA were used to amplify the Neomycin resistance cassette and assemble into CSIB linearized with and BstXI and SbfI using NEBuilder HiFi DNA Assembly (NEB). The 2xFYVE-mSCAR endosome labeling construct was constructed by adding 2 FYVE domains to the N-terminus of mScarlett. FYVE domains were PCR amplified from the Hrs protein using primers FYVE_1_F: ACAGACTGAGTCGCCCGGGGGGGATCCGGCCGAGAGGGCCGCCACCGAGAGCGATGCCATGTTTGC, FYVE_1_R: GGCAGCAAACATGGCATCGCTCTCGGATCCTCCTCCTCCCTCCGCTTTCCTGTTCAGCTG, FYVE_2_F: CAGCTGAACAGGAAAGCGGAGGGAGGAGGAGGATCCGAGAGCGATGCCATGTTTG

CTGCC, FYVE_2_R:

TCACTGCCTCGCCCTTGCTCACCATGGATCCTCCTCCTCCCTCCGCTTTCCTGTTCAG

CT. mScarlett was PCR amplified using primers mSCAR_F:

AGCTGAACAGGAAAGCGGAGGGAGGAGGAGGATCCATGGTGAGCAAGGGCGAGGC

AGTGA and mSCAR_R:

GGGGGAGGGAGAGGGGCGGATCAGGCCAGAGAGGCCCTACTTGTACAGCTCGTCCA

TGCC. The resulting fragments were assembled into CSIB linearized with SfiI using NEBuilder HiFi DNA Assembly (NEB).

pHrodo Dextran Endocytosis Assay

Cells were plated in a Nunc Lab-Tek II Chamber Slide (Thermo) at $5x10^3$ cells per well. The next day, cells were transduced with 2xFYVE-mSCAR to label endosomes. 48 hours post transduction, cells were treated with pHrodo Green Dextran 10,000 MW (Thermo, cat# P35368) at a concentration of 100 μg/mL for 60 minutes. Alternatively, unlabeled cells were treated with an equal ratio of pHrodo Red Dextran 10,000 MW (Thermo, cat# P10361) and AF-488 Dextran 10,000 MW (Thermo, cat# D22910). Thereafter, cells were washed 3X in PBS and placed in Live Cell Imaging Solution (Thermo Cat# A14291DJ). For 2x-FYVE labeled cells, images were acquired on a DeltaVision OMX SR imaging system using a 60X Widefield oil immersion objective (Olympus) with an exposure time of 50ms, 5.0% Transmission for the AF-488 channel, an exposure time of 50ms, 10% Transmission for the A568 channel, and an exposure time of 150ms, 10% Transmission for the DAPI channel. For co-Dextran-treated cells, images were acquired on a DeltaVision OMX SR imaging system using a 60X Widefield oil immersion objective (Olympus) with an exposure time of 25ms, 10.0% Transmission for the AF-488

channel, an exposure time of 50ms, 10% Transmission for the A568 channel, and an exposure time of 200ms, 10% Transmission for the DAPI channel.

Microscopy of rVSV/SARS-CoV-2 infected cells

Cells were plated in a Nunc Lab-Tek II Chamber Slide (Thermo) at $5x10^3$ cells per well. The next day, cells were transduced with 2xFYVE-mSCAR to label endosomes. For rVSV/SARS-CoV-2_{NG-P} , 48 hours post transduction cells were treated with 5μM E64d (Sigma Aldrich E8640-250UG) for 30 minutes, followed by inoculation with rVSV/SARS-CoV-2_{NG-P} at an MOI of 2. 60 minutes post infection, cells were washed 3x with PBS and fixed in 4% PFA. Alternatively, unlabeled cells were treated with pHrodo Red Dextran and infected with rVSV/SARS-CoV-2_{NG-P} for 60 minutes. 60 minutes post infection, cells were washed 3X with PBS and imaged in Live Cell Imaging Solution. For cells with 2x-FYVE labeled endosomes, images were acquired on a DeltaVision OMX SR imaging system using a 60X Widefield oil immersion objective (Olympus) with an exposure time of 50ms, 10% Transmission for the AF-488 channel, an exposure time of 100ms, 10% Transmission for the A568 channel, and an exposure time of 150ms, 10% Transmission for the DAPI channel. For cells with Dextran Red labeled endosomes, images were acquired on a DeltaVision OMX SR imaging system using a 60X Widefield oil immersion objective (Olympus) with an exposure time of 50ms, 10% Transmission for the AF-488 channel, an exposure time of 50ms, 10% Transmission for the A568 channel, and an exposure time of 200ms, 10% Transmission for the DAPI channel.

Cathepsin L activity assay

Cells were plated $2x10^4$ cells per well in a Nunc Lab-Tek II Chamber Slide (Thermo). The next day, intracellular cathepsin L activity was detected using the Magic Red Cathepsin L Assay Kit (Biorad cat# ICT941). Briefly, cells were incubated in 1X Magic Red and Hoechst 33342

Stain for 30 minutes, then washed 3X with PBS before being placed in Live Cell Imaging Solution (Thermo Cat# A14291DJ). Images were acquired on a DeltaVision OMX SR imaging system using a 60X Widefield oil immersion objective (Olympus) using an exposure time of 50ms, 10% Transmission for the A568 nm channel and an exposure time of 100ms, 10% Transmission for the DAPI channel.

Cathepsin L localization staining

The coding sequence of CTSL was tagged with a 3'V5 and cloned into CSIN using NEBuilder HiFi DNA Assembly (NEB) with primers CTSL_3'_V5_F: ACAGACTGAGTCGCCCGGGGGGGATCCGGCCGAGAGGGCCGCCACCATGAATCCTA CACTCATCCTTGC and CTSL_3'_V5_R: GGGGGAGGGAGAGGGGCGGATCAGGCCAGAGAGGCCTCACGTAGAATCGAGACCG AGGAGAGGGTTAGGGATAGGCTTACCCACAGTGGGGTAGCTGGCT. Cells stably expressing this 3'V5-tagged CTSL were plated in a Nunc Lab-Tek II Chamber Slide (Thermo) at $5x10^3$ cells per well. The next day, cells were transduced with a construct expressing 2xFYVE-mSCAR to label endosomes. 48 hours post transduction, cells were fixed in 4% PFA, permeabilized with 0.1% triton, blocked with FBS and stained for V5 (invitrogen cat# 46-0705, 1:1000) and antibody conjugate AF- 488 Goat anti-Mouse IgG (H+L) (Thermo, 1:1000). Images were acquired on a DeltaVision OMX SR imaging system using a 60X Widefield oil immersion objective (Olympus) with an exposure time of 50ms, 5.0% Transmission for the AF-488 channel, an exposure time of 100ms, 10% Transmission for the A568 channel, and an exposure time of 100ms, 10% Transmission for the DAPI channel.

IFNα treatment spreading replication assays

5×10^4 cells per well were seeded in a 96 well plate and infected at an MOI of 0.001. 16 h post infection, cells were washed three times and placed in the presence or absence of 100U/mL IFNα. Supernatants were collected at indicated timepoints, and levels of reverse transcriptase were quantified using the SYBR-PERT assay as previously described (*201*).

IFNα treatment single cycle infection assays

5×10^4 cells per well were seeded in a 96 well plate and placed in 100U/mL IFNα. 24 hours after IFNα treatment, cells were infected at an MOI of 0.3. 48 hours post infection, cells were fixed with 4% PFA and assessed via flow cytometry.

IFNα treatment release assays

5×10^4 MT4 cells were infected with VSV-G pseudotyped virus at an MOI of 1. 16 hours post infection, cells were washed and placed in the presence or absence of IFNα. 48 hours post infection, supernatants were harvested and either assessed for RT activity or titered on TZM-bl cells.

Chimeric Env generation

For ease of cloning and Gibson assembly, fragments of Env were selected at regions such that both the 5' and the 3' end of the fragment had at least 20 base pairs of 100% homology between the NL4-3 Env and the YU2 Env, allowing the same set of primers to be used to amplify both the NL43 and YU2 fragment. These primer sequences were:

1_F	AACATATCTATGAAACTTACGG
1_R	TGATATTGAAAGAGCAGTTTTTTAT
2_F	ATAAAAAACTGCTCTTTCAATATCA

2_R	TAGAATCGCAAAACCAGCCGGGGCA
3_F	TGCCCCGGCTGGTTTTGCGATTCTA
3_R	TTAAAGATTATTGTTTTATTATT
4_F	AATAATAAAACAATAATCTTTAA
4_R	GGCATACATTGCTTTTCCTACTTCC
5_F	GGAAGTAGGAAAAGCAATGTATGCC
5_R	ATAGTGCTTCCTGCTGCTCCCAAGA
gp41_F	TCTTGGGAGCAGCAGGAAGCACTAT
gp41_R	GTGGTAGCTGAAGAGGCACA

Fragments were either amplified by PCR or purchased pre-assembled from Twist biosciences, and assembled into an NL4-3 backbone digested with EcoRI and BamHI using NEB Builder HiFi DNA Assembly Master Mix.

Collagenase treatment

Cells were treated with 200 µg/mL Collagenase from *Clostridium histolyticum* (Sigma cat# C9697) for four hours, after which cells were pelleted by centrifugation at 300xg for 5 minutes and placed in fresh media. Virions were titrated on the cells and at 48 hours post infection, cells were fixed with 4% PFA and assessed via flow cytometry.

Graphing and statistical analysis

Graphpad prism 9 software was used to generate all graphs and to carry out all statistical analyses.

Bibliography

1. Microbiology by numbers. *Nat. Rev. Micro.* **9**, 628–628 (2011).

2. D. B. McArthur, Emerging Infectious Diseases. *Nurs. Clin. North Am.* **54**, 297–311 (2019).

3. K. E. Jones, N. G. Patel, M. A. Levy, A. Storeygard, D. Balk, J. L. Gittleman, P. Daszak, Global trends in emerging infectious diseases. *Nature*. **451**, 990–993 (2008).

4. D. M. Morens, A. S. Fauci, Emerging Pandemic Diseases: How We Got to COVID-19. *Cell*. **182**, 1077–1092 (2020).

5. C. J. Carlson, G. F. Albery, C. Merow, C. H. Trisos, C. M. Zipfel, E. A. Eskew, K. J. Olival, N. Ross, S. Bansal, Climate change increases cross-species viral transmission risk. *Nature*. **607**, 555–562 (2022).

6. D. R. Tompa, A. Immanuel, S. Srikanth, S. Kadhirvel, Trends and strategies to combat viral infections: A review on FDA approved antiviral drugs. *Int. J. Biol. Macromol.* **172**, 524–541 (2021).

7. R. J. Geraghty, M. T. Aliota, L. F. Bonnac, Broad-Spectrum Antiviral Strategies and Nucleoside Analogues. *Viruses*. **13** (2021), doi:10.3390/v13040667.

8. COVID Live - Coronavirus Statistics - Worldometer, (available at https://www.worldometers.info/coronavirus/).

9. Global HIV & AIDS statistics — Fact sheet | UNAIDS, (available at https://www.unaids.org/en/resources/fact-sheet).

10. W. C. Summers, in *Encyclopedia of Microbiology* (Elsevier, 2009), pp. 546–552.

11. H. R. Gelderblom, in *Medical Microbiology*, S. Baron, Ed. (University of Texas Medical Branch at Galveston, Galveston (TX), ed. 4th, 1996).

12. V. I. Agol, Cytopathic effects: virus-modulated manifestations of innate immunity? *Trends Microbiol.* **20**, 570–576 (2012).

13. W.-S. Ryu, in *Molecular virology of human pathogenic viruses* (Elsevier, 2017), pp. 31–45.

14. S. Rampersad, P. Tennant, in *Viruses* (Elsevier, 2018), pp. 55–82.

15. B. J. Connell, H. Lortat-Jacob, Human immunodeficiency virus and heparan sulfate: from attachment to entry inhibition. *Front. Immunol.* **4**, 385 (2013).

16. T. M. Clausen, D. R. Sandoval, C. B. Spliid, J. Pihl, H. R. Perrett, C. D. Painter, A. Narayanan, S. A. Majowicz, E. M. Kwong, R. N. McVicar, B. E. Thacker, C. A. Glass, Z. Yang, J. L. Torres, G. J. Golden, P. L. Bartels, R. N. Porell, A. F. Garretson, L. Laubach, J. Feldman, X. Yin, Y. Pu, B. M. Hauser, T. M. Caradonna, B. P. Kellman, C. Martino, P. L. S. M. Gordts, S. K. Chanda, A. G. Schmidt, K. Godula, S. L. Leibel, J. Jose, K. D. Corbett, A. B. Ward, A. F. Carlin, J. D. Esko, SARS-CoV-2 Infection Depends on Cellular Heparan Sulfate and ACE2. *Cell*. **183**, 1043-1057.e15 (2020).

17. A. Milewska, M. Zarebski, P. Nowak, K. Stozek, J. Potempa, K. Pyrc, Human coronavirus NL63 utilizes heparan sulfate proteoglycans for attachment to target cells. *J. Virol.* **88**, 13221–13230 (2014).

18. A. Szczepanski, K. Owczarek, M. Bzowska, K. Gula, I. Drebot, M. Ochman, B. Maksym, Z. Rajfur, J. A. Mitchell, K. Pyrc, Canine respiratory coronavirus, bovine coronavirus, and human coronavirus OC43: receptors and attachment factors. *Viruses*. **11** (2019), doi:10.3390/v11040328.

19. F. Baribaud, S. Pöhlmann, R. W. Doms, The role of DC-SIGN and DC-SIGNR in HIV and SIV attachment, infection, and transmission. *Virology*. **286**, 1–6 (2001).

20. R. Wang, C. R. Simoneau, J. Kulsuptrakul, M. Bouhaddou, K. A. Travisano, J. M. Hayashi, J. Carlson-Stevermer, J. R. Zengel, C. M. Richards, P. Fozouni, J. Oki, L. Rodriguez, B. Joehnk, K. Walcott, K. Holden, A. Sil, J. E. Carette, N. J. Krogan, M. Ott, A. S. Puschnik, Genetic Screens Identify Host Factors for SARS-CoV-2 and Common Cold Coronaviruses. *Cell*. **184**, 106-119.e14 (2021).

21. W. M. Schneider, J. M. Luna, H.-H. Hoffmann, F. J. Sánchez-Rivera, A. A. Leal, A. W. Ashbrook, J. Le Pen, I. Ricardo-Lax, E. Michailidis, A. Peace, A. F. Stenzel, S. W. Lowe, M. R. MacDonald, C. M. Rice, J. T. Poirier, Genome-scale identification of SARS-CoV-2 and pan-coronavirus host factor networks. *Cell* (2020), doi:10.1016/j.cell.2020.12.006.

22. D. Poston, Y. Weisblum, A. Hobbs, P. D. Bieniasz, VPS29 exerts opposing effects on endocytic viral entry. *MBio*. **13**, e0300221 (2022).

23. M. Grodzki, A. P. Bluhm, M. Schaefer, A. Tagmount, M. Russo, A. Sobh, R. Rafiee, C. D. Vulpe, S. M. Karst, M. H. Norris, Genome-scale CRISPR screens identify host factors that promote human coronavirus infection. *Genome Med.* **14**, 10 (2022).

24. S. Wang, Q. Zhang, S. K. Tiwari, G. Lichinchi, E. H. Yau, H. Hui, W. Li, F. Furnari, T. M. Rana, Integrin αvβ5 Internalizes Zika Virus during Neural Stem Cells Infection and Provides a Promising Target for Antiviral Therapy. *Cell Rep.* **30**, 969-983.e4 (2020).

25. R. J. Park, T. Wang, D. Koundakjian, J. F. Hultquist, P. Lamothe-Molina, B. Monel, K. Schumann, H. Yu, K. M. Krupzcak, W. Garcia-Beltran, A. Piechocka-Trocha, N. J. Krogan, A. Marson, D. M. Sabatini, E. S. Lander, N. Hacohen, B. D. Walker, A genome-

wide CRISPR screen identifies a restricted set of HIV host dependency factors. *Nat. Genet.* **49**, 193–203 (2017).

26. A. Rebendenne, P. Roy, B. Bonaventure, A. L. Chaves Valadão, L. Desmarets, M. Arnaud-Arnould, Y. Rouillé, M. Tauziet, D. Giovannini, J. Touhami, Y. Lee, P. DeWeirdt, M. Hegde, S. Urbach, K. E. Koulali, F. G. de Gracia, J. McKellar, J. Dubuisson, M. Wencker, S. Belouzard, O. Moncorgé, J. G. Doench, C. Goujon, Bidirectional genome-wide CRISPR screens reveal host factors regulating SARS-CoV-2, MERS-CoV and seasonal HCoVs. *Nat. Genet.* **54**, 1090–1102 (2022).

27. D. S. Dimitrov, Virus entry: molecular mechanisms and biomedical applications. *Nat. Rev. Microbiol.* **2**, 109–122 (2004).

28. E. A. Berger, P. M. Murphy, J. M. Farber, Chemokine receptors as HIV-1 coreceptors: roles in viral entry, tropism, and disease. *Annu. Rev. Immunol.* **17**, 657–700 (1999).

29. N. Herold, M. Anders-Ößwein, B. Glass, M. Eckhardt, B. Müller, H.-G. Kräusslich, HIV-1 entry in SupT1-R5, CEM-ss, and primary CD4+ T cells occurs at the plasma membrane and does not require endocytosis. *J. Virol.* **88**, 13956–13970 (2014).

30. K. Miyauchi, Y. Kim, O. Latinovic, V. Morozov, G. B. Melikyan, HIV enters cells via endocytosis and dynamin-dependent fusion with endosomes. *Cell*. **137**, 433–444 (2009).

31. G. M. Jakobsdottir, M. Iliopoulou, R. Nolan, L. Alvarez, A. A. Compton, S. Padilla-Parra, On the Whereabouts of HIV-1 Cellular Entry and Its Fusion Ports. *Trends Mol. Med.* **23**, 932–944 (2017).

32. C. Schwegmann-Wessels, G. Herrler, Sialic acids as receptor determinants for coronaviruses. *Glycoconj. J.* **23**, 51–58 (2006).

33. H. Hofmann, K. Pyrc, L. van der Hoek, M. Geier, B. Berkhout, S. Pöhlmann, Human coronavirus NL63 employs the severe acute respiratory syndrome coronavirus receptor for cellular entry. *Proc Natl Acad Sci USA*. **102**, 7988–7993 (2005).

34. V. S. Raj, H. Mou, S. L. Smits, D. H. W. Dekkers, M. A. Müller, R. Dijkman, D. Muth, J. A. A. Demmers, A. Zaki, R. A. M. Fouchier, V. Thiel, C. Drosten, P. J. M. Rottier, A. D. M. E. Osterhaus, B. J. Bosch, B. L. Haagmans, Dipeptidyl peptidase 4 is a functional receptor for the emerging human coronavirus-EMC. *Nature*. **495**, 251–254 (2013).

35. C. L. Yeager, R. A. Ashmun, R. K. Williams, C. B. Cardellichio, L. H. Shapiro, A. T. Look, K. V. Holmes, Human aminopeptidase N is a receptor for human coronavirus 229E. *Nature*. **357**, 420–422 (1992).

36. J. K. Millet, G. R. Whittaker, Host cell proteases: Critical determinants of coronavirus tropism and pathogenesis. *Virus Res.* **202**, 120–134 (2015).

37. K. Shirato, M. Kawase, S. Matsuyama, Wild-type human coronaviruses prefer cell-surface TMPRSS2 to endosomal cathepsins for cell entry. *Virology*. **517**, 9–15 (2018).

38. Y. Zhu, F. Feng, G. Hu, Y. Wang, Y. Yu, Y. Zhu, W. Xu, X. Cai, Z. Sun, W. Han, R. Ye, D. Qu, Q. Ding, X. Huang, H. Chen, W. Xu, Y. Xie, Q. Cai, Z. Yuan, R. Zhang, A genome-wide CRISPR screen identifies host factors that regulate SARS-CoV-2 entry. *Nat. Commun.* **12**, 961 (2021).

39. B. Meng, A. Abdullahi, I. A. T. M. Ferreira, N. Goonawardane, A. Saito, I. Kimura, D. Yamasoba, P. P. Gerber, S. Fatihi, S. Rathore, S. K. Zepeda, G. Papa, S. A. Kemp, T. Ikeda, M. Toyoda, T. S. Tan, J. Kuramochi, S. Mitsunaga, T. Ueno, K. Shirakawa, A. Takaori-Kondo, T. Brevini, D. L. Mallery, O. J. Charles, CITIID-NIHR BioResource COVID-19 Collaboration, Genotype to Phenotype Japan (G2P-Japan) Consortium, Ecuador-COVID19 Consortium, J. E. Bowen, A. Joshi, A. C. Walls, L. Jackson, D. Martin, K. G. C. Smith, J. Bradley, J. A. G. Briggs, J. Choi, E. Madissoon, K. B. Meyer, P. Mlcochova, L. Ceron-Gutierrez, R. Doffinger, S. A. Teichmann, A. J. Fisher, M. S. Pizzuto, A. de Marco, D. Corti, M. Hosmillo, J. H. Lee, L. C. James, L. Thukral, D. Veesler, A. Sigal, F. Sampaziotis, I. G. Goodfellow, N. J. Matheson, K. Sato, R. K. Gupta, Altered TMPRSS2 usage by SARS-CoV-2 Omicron impacts infectivity and fusogenicity. *Nature*. **603**, 706–714 (2022).

40. B. J. Willett, J. Grove, O. MacLean, C. Wilkie, N. Logan, G. De Lorenzo, W. Furnon, S. Scott, M. Manali, A. Szemiel, S. Ashraf, E. Vink, W. Harvey, C. Davis, R. Orton, J. Hughes, P. Holland, S. V. Silva, D. Pascall, K. Puxty, A. da Silva Filipe, G. Yebra, S. Shaaban, M. T. G. Holden, R. M. Pinto, R. Gunson, K. Templeton, P. Murcia, A. Patel, The COVID-19 DeplOyed VaccinE (DOVE) Investigators, COVID-19 EVADE Cohort Study, The COVID-19 Genomics UK (COG-UK) Consortium, The G2P-UK National Virology Consortium, J. Haughney, D. L. Robertson, M. Palmarini, S. Ray, E. C. Thomson, The hyper-transmissible SARS-CoV-2 Omicron variant exhibits significant antigenic change, vaccine escape and a switch in cell entry mechanism. *medRxiv* (2022), doi:10.1101/2022.01.03.21268111.

41. T. P. Peacock, J. C. Brown, J. Zhou, N. Thakur, J. Newman, R. Kugathasan, K. Sukhova, M. Kaforou, D. Bailey, W. S. Barclay, The SARS-CoV-2 variant, Omicron, shows rapid replication in human primary nasal epithelial cultures and efficiently uses the endosomal route of entry. *BioRxiv* (2022), doi:10.1101/2021.12.31.474653.

42. M. Voysey, S. A. C. Clemens, S. A. Madhi, L. Y. Weckx, P. M. Folegatti, P. K. Aley, B. Angus, V. L. Baillie, S. L. Barnabas, Q. E. Bhorat, S. Bibi, C. Briner, P. Cicconi, A. M. Collins, R. Colin-Jones, C. L. Cutland, T. C. Darton, K. Dheda, C. J. A. Duncan, K. R. W. Emary, K. J. Ewer, L. Fairlie, S. N. Faust, S. Feng, D. M. Ferreira, A. Finn, A. L. Goodman, C. M. Green, C. A. Green, P. T. Heath, C. Hill, H. Hill, I. Hirsch, S. H. C. Hodgson, A. Izu, S. Jackson, D. Jenkin, C. C. D. Joe, S. Kerridge, A. Koen, G. Kwatra, R. Lazarus, A. M. Lawrie, A. Lelliott, V. Libri, P. J. Lillie, R. Mallory, A. V. A. Mendes, E. P. Milan, A. M. Minassian, A. McGregor, H. Morrison, Y. F. Mujadidi, A. Nana, P. J. O'Reilly, S. D. Padayachee, A. Pittella, E. Plested, K. M. Pollock, M. N. Ramasamy, S.

Rhead, A. V. Schwarzbold, N. Singh, A. Smith, R. Song, M. D. Snape, E. Sprinz, R. K. Sutherland, R. Tarrant, E. C. Thomson, M. E. Török, M. Toshner, D. P. J. Turner, J. Vekemans, T. L. Villafana, M. E. E. Watson, C. J. Williams, A. D. Douglas, A. V. S. Hill, T. Lambe, S. C. Gilbert, A. J. Pollard, Oxford COVID Vaccine Trial Group, Safety and efficacy of the ChAdOx1 nCoV-19 vaccine (AZD1222) against SARS-CoV-2: an interim analysis of four randomised controlled trials in Brazil, South Africa, and the UK. *Lancet*. **397**, 99–111 (2021).

43. J. Sadoff, G. Gray, A. Vandebosch, V. Cárdenas, G. Shukarev, B. Grinsztejn, P. A. Goepfert, C. Truyers, H. Fennema, B. Spiessens, K. Offergeld, G. Scheper, K. L. Taylor, M. L. Robb, J. Treanor, D. H. Barouch, J. Stoddard, M. F. Ryser, M. A. Marovich, K. M. Neuzil, L. Corey, N. Cauwenberghs, T. Tanner, K. Hardt, J. Ruiz-Guiñazú, M. Le Gars, H. Schuitemaker, J. Van Hoof, F. Struyf, M. Douoguih, ENSEMBLE Study Group, Safety and Efficacy of Single-Dose Ad26.COV2.S Vaccine against Covid-19. *N. Engl. J. Med.* **384**, 2187–2201 (2021).

44. F. P. Polack, S. J. Thomas, N. Kitchin, J. Absalon, A. Gurtman, S. Lockhart, J. L. Perez, G. Pérez Marc, E. D. Moreira, C. Zerbini, R. Bailey, K. A. Swanson, S. Roychoudhury, K. Koury, P. Li, W. V. Kalina, D. Cooper, R. W. Frenck, L. L. Hammitt, Ö. Türeci, H. Nell, A. Schaefer, S. Ünal, D. B. Tresnan, S. Mather, P. R. Dormitzer, U. Şahin, K. U. Jansen, W. C. Gruber, C4591001 Clinical Trial Group, Safety and Efficacy of the BNT162b2 mRNA Covid-19 Vaccine. *N. Engl. J. Med.* **383**, 2603–2615 (2020).

45. L. R. Baden, H. M. El Sahly, B. Essink, K. Kotloff, S. Frey, R. Novak, D. Diemert, S. A. Spector, N. Rouphael, C. B. Creech, J. McGettigan, S. Khetan, N. Segall, J. Solis, A. Brosz, C. Fierro, H. Schwartz, K. Neuzil, L. Corey, P. Gilbert, H. Janes, D. Follmann, M. Marovich, J. Mascola, L. Polakowski, J. Ledgerwood, B. S. Graham, H. Bennett, R. Pajon, C. Knightly, B. Leav, W. Deng, H. Zhou, S. Han, M. Ivarsson, J. Miller, T. Zaks, COVE Study Group, Efficacy and safety of the mRNA-1273 SARS-CoV-2 vaccine. *N. Engl. J. Med.* **384**, 403–416 (2021).

46. P. T. Heath, E. P. Galiza, D. N. Baxter, M. Boffito, D. Browne, F. Burns, D. R. Chadwick, R. Clark, C. Cosgrove, J. Galloway, A. L. Goodman, A. Heer, A. Higham, S. Iyengar, A. Jamal, C. Jeanes, P. A. Kalra, C. Kyriakidou, D. F. McAuley, A. Meyrick, A. M. Minassian, J. Minton, P. Moore, I. Munsoor, H. Nicholls, O. Osanlou, J. Packham, C. H. Pretswell, A. San Francisco Ramos, D. Saralaya, R. P. Sheridan, R. Smith, R. L. Soiza, P. A. Swift, E. C. Thomson, J. Turner, M. E. Viljoen, G. Albert, I. Cho, F. Dubovsky, G. Glenn, J. Rivers, A. Robertson, K. Smith, S. Toback, 2019nCoV-302 Study Group, Safety and Efficacy of NVX-CoV2373 Covid-19 Vaccine. *N. Engl. J. Med.* **385**, 1172–1183 (2021).

47. L. M. Walker, D. R. Burton, Passive immunotherapy of viral infections: "super-antibodies" enter the fray. *Nat. Rev. Immunol.* **18**, 297–308 (2018).

48. P. Dorr, M. Westby, S. Dobbs, P. Griffin, B. Irvine, M. Macartney, J. Mori, G. Rickett, C. Smith-Burchnell, C. Napier, R. Webster, D. Armour, D. Price, B. Stammen, A. Wood,

M. Perros, Maraviroc (UK-427,857), a potent, orally bioavailable, and selective small-molecule inhibitor of chemokine receptor CCR5 with broad-spectrum anti-human immunodeficiency virus type 1 activity. *Antimicrob. Agents Chemother.* **49**, 4721–4732 (2005).

49. J. M. Kilby, S. Hopkins, T. M. Venetta, B. DiMassimo, G. A. Cloud, J. Y. Lee, L. Alldredge, E. Hunter, D. Lambert, D. Bolognesi, T. Matthews, M. R. Johnson, M. A. Nowak, G. M. Shaw, M. S. Saag, Potent suppression of HIV-1 replication in humans by T-20, a peptide inhibitor of gp41-mediated virus entry. *Nat. Med.* **4**, 1302–1307 (1998).

50. K. D. Raney, M. Gotte, C. E. Cameron, Eds., *Viral Genome Replication* (Springer US, Boston, MA, 2009).

51. R. Craigie, F. D. Bushman, HIV DNA integration. *Cold Spring Harb. Perspect. Med.* **2**, a006890 (2012).

52. W.-S. Hu, S. H. Hughes, HIV-1 reverse transcription. *Cold Spring Harb. Perspect. Med.* **2** (2012), doi:10.1101/cshperspect.a006882.

53. A. Cheng, W. Zhang, Y. Xie, W. Jiang, E. Arnold, S. G. Sarafianos, J. Ding, Expression, purification, and characterization of SARS coronavirus RNA polymerase. *Virology*. **335**, 165–176 (2005).

54. M. G. Mateu, Assembly, stability and dynamics of virus capsids. *Arch. Biochem. Biophys.* **531**, 65–79 (2013).

55. N. Jouvenet, S. J. D. Neil, C. Bess, M. C. Johnson, C. A. Virgen, S. M. Simon, P. D. Bieniasz, Plasma membrane is the site of productive HIV-1 particle assembly. *PLoS Biol.* **4**, e435 (2006).

56. W. I. Sundquist, H.-G. Kräusslich, HIV-1 assembly, budding, and maturation. *Cold Spring Harb. Perspect. Med.* **2**, a006924 (2012).

57. E. O. Freed, HIV-1 assembly, release and maturation. *Nat. Rev. Microbiol.* **13**, 484–496 (2015).

58. J. Klumperman, J. K. Locker, A. Meijer, M. C. Horzinek, H. J. Geuze, P. J. Rottier, Coronavirus M proteins accumulate in the Golgi complex beyond the site of virion budding. *J. Virol.* **68**, 6523–6534 (1994).

59. H. Vennema, G. J. Godeke, J. W. Rossen, W. F. Voorhout, M. C. Horzinek, D. J. Opstelten, P. J. Rottier, Nucleocapsid-independent assembly of coronavirus-like particles by co-expression of viral envelope protein genes. *EMBO J.* **15**, 2020–2028 (1996).

60. C. L. Ricaña, R. A. Dick, Inositol phosphates and retroviral assembly: A cellular perspective. *Viruses*. **13** (2021), doi:10.3390/v13122516.

61. W. M. McFadden, A. A. Snyder, K. A. Kirby, P. R. Tedbury, M. Raj, Z. Wang, S. G. Sarafianos, Rotten to the core: antivirals targeting the HIV-1 capsid core. *Retrovirology*. **18**, 41 (2021).

62. S. K. Carnes, J. H. Sheehan, C. Aiken, Inhibitors of the HIV-1 capsid, a target of opportunity. *Curr. Opin. HIV AIDS*. **13**, 359–365 (2018).

63. J. O. Link, M. S. Rhee, W. C. Tse, J. Zheng, J. R. Somoza, W. Rowe, R. Begley, A. Chiu, A. Mulato, D. Hansen, E. Singer, L. K. Tsai, R. A. Bam, C.-H. Chou, E. Canales, G. Brizgys, J. R. Zhang, J. Li, M. Graupe, P. Morganelli, Q. Liu, Q. Wu, R. L. Halcomb, R. D. Saito, S. D. Schroeder, S. E. Lazerwith, S. Bondy, D. Jin, M. Hung, N. Novikov, X. Liu, A. G. Villaseñor, C. E. Cannizzaro, E. Y. Hu, R. L. Anderson, T. C. Appleby, B. Lu, J. Mwangi, A. Liclican, A. Niedziela-Majka, G. A. Papalia, M. H. Wong, S. A. Leavitt, Y. Xu, D. Koditek, G. J. Stepan, H. Yu, N. Pagratis, S. Clancy, S. Ahmadyar, T. Z. Cai, S. Sellers, S. A. Wolckenhauer, J. Ling, C. Callebaut, N. Margot, R. R. Ram, Y.-P. Liu, R. Hyland, G. I. Sinclair, P. J. Ruane, G. E. Crofoot, C. K. McDonald, D. M. Brainard, L. Lad, S. Swaminathan, W. I. Sundquist, R. Sakowicz, A. E. Chester, W. E. Lee, E. S. Daar, S. R. Yant, T. Cihlar, Clinical targeting of HIV capsid protein with a long-acting small molecule. *Nature*. **584**, 614–618 (2020).

64. L. Rheinemann, W. I. Sundquist, in *Encyclopedia of Virology* (Elsevier, 2021), pp. 519–528.

65. S. Stertz, M. Reichelt, M. Spiegel, T. Kuri, L. Martínez-Sobrido, A. García-Sastre, F. Weber, G. Kochs, The intracellular sites of early replication and budding of SARS-coronavirus. *Virology*. **361**, 304–315 (2007).

66. J. Tooze, S. A. Tooze, S. D. Fuller, Sorting of progeny coronavirus from condensed secretory proteins at the exit from the trans-Golgi network of AtT20 cells. *J. Cell Biol.* **105**, 1215–1226 (1987).

67. M. Oostra, C. A. M. de Haan, R. J. de Groot, P. J. M. Rottier, Glycosylation of the severe acute respiratory syndrome coronavirus triple-spanning membrane proteins 3a and M. *J. Virol.* **80**, 2326–2336 (2006).

68. C. E. McBride, J. Li, C. E. Machamer, The cytoplasmic tail of the severe acute respiratory syndrome coronavirus spike protein contains a novel endoplasmic reticulum retrieval signal that binds COPI and promotes interaction with membrane protein. *J. Virol.* **81**, 2418–2428 (2007).

69. T. S. Fung, D. X. Liu, Post-translational modifications of coronavirus proteins: roles and function. *Future Virol.* **13**, 405–430 (2018).

70. T. R. Ruch, C. E. Machamer, The coronavirus E protein: assembly and beyond. *Viruses*. **4**, 363–382 (2012).

71. S. Ghosh, T. A. Dellibovi-Ragheb, A. Kerviel, E. Pak, Q. Qiu, M. Fisher, P. M. Takvorian, C. Bleck, V. W. Hsu, A. R. Fehr, S. Perlman, S. R. Achar, M. R. Straus, G. R. Whittaker, C. A. M. de Haan, J. Kehrl, G. Altan-Bonnet, N. Altan-Bonnet, β-Coronaviruses Use Lysosomes for Egress Instead of the Biosynthetic Secretory Pathway. *Cell*. **183**, 1520-1535.e14 (2020).

72. S. J. D. Neil, T. Zang, P. D. Bieniasz, Tetherin inhibits retrovirus release and is antagonized by HIV-1 Vpu. *Nature*. **451**, 425–430 (2008).

73. N. Van Damme, D. Goff, C. Katsura, R. L. Jorgenson, R. Mitchell, M. C. Johnson, E. B. Stephens, J. Guatelli, The interferon-induced protein BST-2 restricts HIV-1 release and is downregulated from the cell surface by the viral Vpu protein. *Cell Host Microbe*. **3**, 245–252 (2008).

74. A. Moscona, Neuraminidase inhibitors for influenza. *N. Engl. J. Med.* **353**, 1363–1373 (2005).

75. A. Engelman, P. Cherepanov, The structural biology of HIV-1: mechanistic and therapeutic insights. *Nat. Rev. Microbiol.* **10**, 279–290 (2012).

76. P. V'kovski, A. Kratzel, S. Steiner, H. Stalder, V. Thiel, Coronavirus biology and replication: implications for SARS-CoV-2. *Nat. Rev. Microbiol.* **19**, 155–170 (2020).

77. Centers for Disease Control (CDC), Mortality attributable to HIV infection/AIDS--United States, 1981-1990. *MMWR Morb Mortal Wkly Rep*. **40**, 41–44 (1991).

78. D. D. Richman, AZT resistance in isolates of HIV. *Immunodefic. Rev.* **2**, 315–318 (1991).

79. R. M. Gulick, J. W. Mellors, D. Havlir, J. J. Eron, C. Gonzalez, D. McMahon, D. D. Richman, F. T. Valentine, L. Jonas, A. Meibohm, E. A. Emini, J. A. Chodakewitz, Treatment with indinavir, zidovudine, and lamivudine in adults with human immunodeficiency virus infection and prior antiretroviral therapy. *N. Engl. J. Med.* **337**, 734–739 (1997).

80. A. C. Collier, R. W. Coombs, D. A. Schoenfeld, R. L. Bassett, J. Timpone, A. Baruch, M. Jones, K. Facey, C. Whitacre, V. J. McAuliffe, H. M. Friedman, T. C. Merigan, R. C. Reichman, C. Hooper, L. Corey, Treatment of human immunodeficiency virus infection with saquinavir, zidovudine, and zalcitabine. AIDS Clinical Trials Group. *N. Engl. J. Med.* **334**, 1011–1017 (1996).

81. S. Vella, HIV therapy advances. Update on a proteinase inhibitor. *AIDS*. **8 Suppl 3**, S25-9 (1994).

82. L. Menéndez-Arias, Mutation rates and intrinsic fidelity of retroviral reverse transcriptases. *Viruses*. **1**, 1137–1165 (2009).

83. M. Kane, T. M. Zang, S. J. Rihn, F. Zhang, T. Kueck, M. Alim, J. Schoggins, C. M. Rice, S. J. Wilson, P. D. Bieniasz, Identification of Interferon-Stimulated Genes with Antiretroviral Activity. *Cell Host Microbe*. **20**, 392–405 (2016).

84. I. Busnadiego, M. Kane, S. J. Rihn, H. F. Preugschas, J. Hughes, D. Blanco-Melo, V. P. Strouvelle, T. M. Zang, B. J. Willett, C. Boutell, P. D. Bieniasz, S. J. Wilson, Host and viral determinants of Mx2 antiretroviral activity. *J. Virol.* **88**, 7738–7752 (2014).

85. K. Lee, Z. Ambrose, T. D. Martin, I. Oztop, A. Mulky, J. G. Julias, N. Vandegraaff, J. G. Baumann, R. Wang, W. Yuen, T. Takemura, K. Shelton, I. Taniuchi, Y. Li, J. Sodroski, D. R. Littman, J. M. Coffin, S. H. Hughes, D. Unutmaz, A. Engelman, V. N. KewalRamani, Flexible use of nuclear import pathways by HIV-1. *Cell Host Microbe*. **7**, 221–233 (2010).

86. A. Cimarelli, S. Sandin, S. Höglund, J. Luban, Rescue of multiple viral functions by a second-site suppressor of a human immunodeficiency virus type 1 nucleocapsid mutation. *J. Virol.* **74**, 4273–4283 (2000).

87. R. Van Duyne, L. S. Kuo, P. Pham, K. Fujii, E. O. Freed, Mutations in the HIV-1 envelope glycoprotein can broadly rescue blocks at multiple steps in the virus replication cycle. *Proc Natl Acad Sci USA*. **116**, 9040–9049 (2019).

88. C. R. King, A. Mehle, The later stages of viral infection: An undiscovered country of host dependency factors. *PLoS Pathog.* **16**, e1008777 (2020).

89. D.-Y. Jin, Special issue: applications of CRISPR technology in virology 2018. *Viruses*. **11** (2019), doi:10.3390/v11090839.

90. V. C. Chitalia, A. H. Munawar, A painful lesson from the COVID-19 pandemic: the need for broad-spectrum, host-directed antivirals. *J. Transl. Med.* **18**, 390 (2020).

91. J. Baggen, L. Persoons, E. Vanstreels, S. Jansen, D. Van Looveren, B. Boeckx, V. Geudens, J. De Man, D. Jochmans, J. Wauters, E. Wauters, B. M. Vanaudenaerde, D. Lambrechts, J. Neyts, K. Dallmeier, H. J. Thibaut, M. Jacquemyn, P. Maes, D. Daelemans, Genome-wide CRISPR screening identifies TMEM106B as a proviral host factor for SARS-CoV-2. *Nat. Genet.* **53**, 435–444 (2021).

92. J. Wei, M. M. Alfajaro, P. C. DeWeirdt, R. E. Hanna, W. J. Lu-Culligan, W. L. Cai, M. S. Strine, S.-M. Zhang, V. R. Graziano, C. O. Schmitz, J. S. Chen, M. C. Mankowski, R. B. Filler, N. G. Ravindra, V. Gasque, F. J. de Miguel, A. Patil, H. Chen, K. Y. Oguntuyo, L. Abriola, Y. V. Surovtseva, R. C. Orchard, B. Lee, B. D. Lindenbach, K. Politi, D. van Dijk, C. Kadoch, M. D. Simon, Q. Yan, J. G. Doench, C. B. Wilen, Genome-wide CRISPR Screens Reveal Host Factors Critical for SARS-CoV-2 Infection. *Cell*. **184**, 76-91.e13 (2021).

93. A. Kratzel, J. N. Kelly, P. V'kovski, J. Portmann, Y. Brüggemann, D. Todt, N. Ebert, N. Shrestha, P. Plattet, C. A. Staab-Weijnitz, A. von Brunn, E. Steinmann, R. Dijkman, G. Zimmer, S. Pfaender, V. Thiel, A genome-wide CRISPR screen identifies interactors of the autophagy pathway as conserved coronavirus targets. *PLoS Biol.* **19**, e3001490 (2021).

94. Z. Daniloski, T. X. Jordan, H.-H. Wessels, D. A. Hoagland, S. Kasela, M. Legut, S. Maniatis, E. P. Mimitou, L. Lu, E. Geller, O. Danziger, B. R. Rosenberg, H. Phatnani, P. Smibert, T. Lappalainen, B. R. tenOever, N. E. Sanjana, Identification of Required Host Factors for SARS-CoV-2 Infection in Human Cells. *Cell*. **184**, 92-105.e16 (2021).

95. M. Israeli, Y. Finkel, Y. Yahalom-Ronen, N. Paran, T. Chitlaru, O. Israeli, I. Cohen-Gihon, M. Aftalion, R. Falach, S. Rotem, U. Elia, I. Nemet, L. Kliker, M. Mandelboim, A. Beth-Din, T. Israely, O. Cohen, N. Stern-Ginossar, A. Bercovich-Kinori, Genome-wide CRISPR screens identify GATA6 as a proviral host factor for SARS-CoV-2 via modulation of ACE2. *Nat. Commun.* **13**, 2237 (2022).

96. S. Zhu, Y. Liu, Z. Zhou, Z. Zhang, X. Xiao, Z. Liu, A. Chen, X. Dong, F. Tian, S. Chen, Y. Xu, C. Wang, Q. Li, X. Niu, Q. Pan, S. Du, J. Xiao, J. Wang, W. Wei, Genome-wide CRISPR activation screen identifies candidate receptors for SARS-CoV-2 entry. *Sci. China Life Sci.* **65**, 701–717 (2022).

97. A. J. Sadler, B. R. G. Williams, Interferon-inducible antiviral effectors. *Nat. Rev. Immunol.* **8**, 559–568 (2008).

98. D. Blanco-Melo, S. Venkatesh, P. D. Bieniasz, Intrinsic cellular defenses agains HIV. *Immunity*. **37**, 399–411 (2012).

99. M. Stremlau, C. M. Owens, M. J. Perron, M. Kiessling, P. Autissier, J. Sodroski, The cytoplasmic body component TRIM5alpha restricts HIV-1 infection in Old World monkeys. *Nature*. **427**, 848–853 (2004).

100. K. Hrecka, C. Hao, M. Gierszewska, S. K. Swanson, M. Kesik-Brodacka, S. Srivastava, L. Florens, M. P. Washburn, J. Skowronski, Vpx relieves inhibition of HIV-1 infection of macrophages mediated by the SAMHD1 protein. *Nature*. **474**, 658–661 (2011).

101. H. Lahouassa, W. Daddacha, H. Hofmann, D. Ayinde, E. C. Logue, L. Dragin, N. Bloch, C. Maudet, M. Bertrand, T. Gramberg, G. Pancino, S. Priet, B. Canard, N. Laguette, M. Benkirane, C. Transy, N. R. Landau, B. Kim, F. Margottin-Goguet, SAMHD1 restricts the replication of human immunodeficiency virus type 1 by depleting the intracellular pool of deoxynucleoside triphosphates. *Nat. Immunol.* **13**, 223–228 (2012).

102. B. Jia, R. Serra-Moreno, W. Neidermyer, A. Rahmberg, J. Mackey, I. B. Fofana, W. E. Johnson, S. Westmoreland, D. T. Evans, Species-specific activity of SIV Nef and HIV-1 Vpu in overcoming restriction by tetherin/BST2. *PLoS Pathog.* **5**, e1000429 (2009).

103. F. Zhang, S. J. Wilson, W. C. Landford, B. Virgen, D. Gregory, M. C. Johnson, J. Munch, F. Kirchhoff, P. D. Bieniasz, T. Hatziioannou, Nef proteins from simian immunodeficiency viruses are tetherin antagonists. *Cell Host Microbe*. **6**, 54–67 (2009).

104. A. Le Tortorec, S. J. D. Neil, Antagonism to and intracellular sequestration of human tetherin by the human immunodeficiency virus type 2 envelope glycoprotein. *J. Virol.* **83**, 11966–11978 (2009).

105. M. A. Takata, D. Gonçalves-Carneiro, T. M. Zang, S. J. Soll, A. York, D. Blanco-Melo, P. D. Bieniasz, CG dinucleotide suppression enables antiviral defence targeting non-self RNA. *Nature*. **550**, 124–127 (2017).

106. Z. Kratovac, C. A. Virgen, F. Bibollet-Ruche, B. H. Hahn, P. D. Bieniasz, T. Hatziioannou, Primate lentivirus capsid sensitivity to TRIM5 proteins. *J. Virol.* **82**, 6772–6777 (2008).

107. J. Bitzegeio, M. Sampias, P. D. Bieniasz, T. Hatziioannou, Adaptation to the interferon-induced antiviral state by human and simian immunodeficiency viruses. *J. Virol.* **87**, 3549–3560 (2013).

108. N. E. Sanjana, O. Shalem, F. Zhang, Improved vectors and genome-wide libraries for CRISPR screening. *Nat. Methods*. **11**, 783–784 (2014).

109. R. Zufferey, T. Dull, R. J. Mandel, A. Bukovsky, D. Quiroz, L. Naldini, D. Trono, Self-inactivating lentivirus vector for safe and efficient in vivo gene delivery. *J. Virol.* **72**, 9873–9880 (1998).

110. M. OhAinle, L. Helms, J. Vermeire, F. Roesch, D. Humes, R. Basom, J. J. Delrow, J. Overbaugh, M. Emerman, A virus-packageable CRISPR screen identifies host factors mediating interferon inhibition of HIV. *eLife*. **7** (2018), doi:10.7554/eLife.39823.

111. T. Dorfman, A. Bukovsky, A. Ohagen, S. Höglund, H. G. Göttlinger, Functional domains of the capsid protein of human immunodeficiency virus type 1. *J. Virol.* **68**, 8180–8187 (1994).

112. A. Borsetti, A. Ohagen, H. G. Göttlinger, The C-terminal half of the human immunodeficiency virus type 1 Gag precursor is sufficient for efficient particle assembly. *J. Virol.* **72**, 9313–9317 (1998).

113. M. V. Nermut, D. J. Hockley, J. B. Jowett, I. M. Jones, M. Garreau, D. Thomas, Fullerene-like organization of HIV gag-protein shell in virus-like particles produced by recombinant baculovirus. *Virology*. **198**, 288–296 (1994).

114. J. M. Coffin, S. H. Hughes, H. E. Varmus, Maturation of Viral Particles (1997).

115. S. Campbell, R. J. Fisher, E. M. Towler, S. Fox, H. J. Issaq, T. Wolfe, L. R. Phillips, A. Rein, Modulation of HIV-like particle assembly in vitro by inositol phosphates. *Proc Natl Acad Sci USA*. **98**, 10875–10879 (2001).

116. R. A. Dick, K. K. Zadrozny, C. Xu, F. K. M. Schur, T. D. Lyddon, C. L. Ricana, J. M. Wagner, J. R. Perilla, B. K. Ganser-Pornillos, M. C. Johnson, O. Pornillos, V. M. Vogt, Inositol phosphates are assembly co-factors for HIV-1. *Nature*. **560**, 509–512 (2018).

117. D. L. Mallery, C. L. Márquez, W. A. McEwan, C. F. Dickson, D. A. Jacques, M. Anandapadamanaban, K. Bichel, G. J. Towers, A. Saiardi, T. Böcking, L. C. James, IP6 is an HIV pocket factor that prevents capsid collapse and promotes DNA synthesis. *eLife*. **7** (2018), doi:10.7554/eLife.35335.

118. C. Xu, D. K. Fischer, S. Rankovic, W. Li, R. Dick, B. Runge, R. Zadorozhnyi, J. Ahn, C. Aiken, T. Polenova, A. N. Engelman, Z. Ambrose, I. Rousso, J. R. Perilla, Permeability of the HIV-1 capsid to metabolites modulates viral DNA synthesis. *BioRxiv* (2020), doi:10.1101/2020.04.30.071217.

119. A. Yu, E. M. Y. Lee, J. Jin, G. A. Voth, Atomic-scale characterization of mature HIV-1 capsid stabilization by inositol hexakisphosphate (IP6). *Sci. Adv.* **6** (2020), doi:10.1126/sciadv.abc6465.

120. D. L. Mallery, K. M. R. Faysal, A. Kleinpeter, M. S. C. Wilson, M. Vaysburd, A. J. Fletcher, M. Novikova, T. Böcking, E. O. Freed, A. Saiardi, L. C. James, Cellular IP6 Levels Limit HIV Production while Viruses that Cannot Efficiently Package IP6 Are Attenuated for Infection and Replication. *Cell Rep.* **29**, 3983-3996.e4 (2019).

121. C. L. Ricana, T. D. Lyddon, R. A. Dick, M. C. Johnson, Primate lentiviruses require Inositol hexakisphosphate (IP6) or inositol pentakisphosphate (IP5) for the production of viral particles. *PLoS Pathog.* **16**, e1008646 (2020).

122. G. A. Sowd, C. Aiken, Inositol phosphates promote HIV-1 assembly and maturation to facilitate viral spread in human CD4+ T cells. *PLoS Pathog.* **17**, e1009190 (2021).

123. R. A. Dick, C. Xu, D. R. Morado, V. Kravchuk, C. L. Ricana, T. D. Lyddon, A. M. Broad, J. R. Feathers, M. C. Johnson, V. M. Vogt, J. R. Perilla, J. A. G. Briggs, F. K. M. Schur, Structures of immature EIAV Gag lattices reveal a conserved role for IP6 in lentivirus assembly. *PLoS Pathog.* **16**, e1008277 (2020).

124. J. Fontana, P. W. Keller, E. Urano, S. D. Ablan, A. C. Steven, E. O. Freed, Identification of an HIV-1 Mutation in Spacer Peptide 1 That Stabilizes the Immature CA-SP1 Lattice. *J. Virol.* **90**, 972–978 (2016).

125. K. Waki, S. R. Durell, F. Soheilian, K. Nagashima, S. L. Butler, E. O. Freed, Structural and functional insights into the HIV-1 maturation inhibitor binding pocket. *PLoS Pathog.* **8**, e1002997 (2012).

126. P. W. Keller, C. S. Adamson, J. B. Heymann, E. O. Freed, A. C. Steven, HIV-1 maturation inhibitor bevirimat stabilizes the immature Gag lattice. *J. Virol.* **85**, 1420–1428 (2011).

127. A. T. Nguyen, C. L. Feasley, K. W. Jackson, T. J. Nitz, K. Salzwedel, G. M. Air, M. Sakalian, The prototype HIV-1 maturation inhibitor, bevirimat, binds to the CA-SP1 cleavage site in immature Gag particles. *Retrovirology*. **8**, 101 (2011).

128. Coronaviridae Study Group of the International Committee on Taxonomy of Viruses, The species Severe acute respiratory syndrome-related coronavirus: classifying 2019-nCoV and naming it SARS-CoV-2. *Nat. Microbiol.* **5**, 536–544 (2020).

129. M. E. Killerby, H. M. Biggs, A. Haynes, R. M. Dahl, D. Mustaquim, S. I. Gerber, J. T. Watson, Human coronavirus circulation in the United States 2014-2017. *J. Clin. Virol.* **101**, 52–56 (2018).

130. K. R. Sanson, R. E. Hanna, M. Hegde, K. F. Donovan, C. Strand, M. E. Sullender, E. W. Vaimberg, A. Goodale, D. E. Root, F. Piccioni, J. G. Doench, Optimized libraries for CRISPR-Cas9 genetic screens with multiple modalities. *Nat. Commun.* **9**, 5416 (2018).

131. J. G. Doench, N. Fusi, M. Sullender, M. Hegde, E. W. Vaimberg, K. F. Donovan, I. Smith, Z. Tothova, C. Wilen, R. Orchard, H. W. Virgin, J. Listgarten, D. E. Root, Optimized sgRNA design to maximize activity and minimize off-target effects of CRISPR-Cas9. *Nat. Biotechnol.* **34**, 184–191 (2016).

132. W. Li, H. Xu, T. Xiao, L. Cong, M. I. Love, F. Zhang, R. A. Irizarry, J. S. Liu, M. Brown, X. S. Liu, MAGeCK enables robust identification of essential genes from genome-scale CRISPR/Cas9 knockout screens. *Genome Biol.* **15**, 554 (2014).

133. R. D. Luteijn, F. van Diemen, V. A. Blomen, I. G. J. Boer, S. Manikam Sadasivam, T. H. van Kuppevelt, I. Drexler, T. R. Brummelkamp, R. J. Lebbink, E. J. Wiertz, A Genome-Wide Haploid Genetic Screen Identifies Heparan Sulfate-Associated Genes and the Macropinocytosis Modulator TMED10 as Factors Supporting Vaccinia Virus Infection. *J. Virol.* **93** (2019), doi:10.1128/JVI.02160-18.

134. H. Gao, Y. Lin, J. He, S. Zhou, M. Liang, C. Huang, X. Li, C. Liu, P. Zhang, Role of heparan sulfate in the Zika virus entry, replication, and cell death. *Virology*. **529**, 91–100 (2019).

135. D. Szklarczyk, A. L. Gable, D. Lyon, A. Junge, S. Wyder, J. Huerta-Cepas, M. Simonovic, N. T. Doncheva, J. H. Morris, P. Bork, L. J. Jensen, C. von Mering, STRING v11: protein-protein association networks with increased coverage, supporting functional discovery in genome-wide experimental datasets. *Nucleic Acids Res.* **47**, D607–D613 (2019).

136. UniProt Consortium, UniProt: a worldwide hub of protein knowledge. *Nucleic Acids Res.* **47**, D506–D515 (2019).

137. P. Burda, S. M. Padilla, S. Sarkar, S. D. Emr, Retromer function in endosome-to-Golgi retrograde transport is regulated by the yeast Vps34 PtdIns 3-kinase. *J. Cell Sci.* **115**, 3889–3900 (2002).

138. O. Meier, U. F. Greber, Adenovirus endocytosis. *J. Gene Med.* **6 Suppl 1**, S152-63 (2004).

139. M. A. Krzyzaniak, M. T. Zumstein, J. A. Gerez, P. Picotti, A. Helenius, Host cell entry of respiratory syncytial virus involves macropinocytosis followed by proteolytic activation of the F protein. *PLoS Pathog.* **9**, e1003309 (2013).

140. M. Lakadamyali, M. J. Rust, X. Zhuang, Endocytosis of influenza viruses. *Microbes Infect.* **6**, 929–936 (2004).

141. S. Baños-Mateos, A. L. Rojas, A. Hierro, VPS29, a tweak tool of endosomal recycling. *Curr. Opin. Cell Biol.* **59**, 81–87 (2019).

142. R. Rojas, T. van Vlijmen, G. A. Mardones, Y. Prabhu, A. L. Rojas, S. Mohammed, A. J. R. Heck, G. Raposo, P. van der Sluijs, J. S. Bonifacino, Regulation of retromer recruitment to endosomes by sequential action of Rab5 and Rab7. *J. Cell Biol.* **183**, 513–526 (2008).

143. K. E. McNally, R. Faulkner, F. Steinberg, M. Gallon, R. Ghai, D. Pim, P. Langton, N. Pearson, C. M. Danson, H. Nägele, L. L. Morris, A. Singla, B. L. Overlee, K. J. Heesom, R. Sessions, L. Banks, B. M. Collins, I. Berger, D. D. Billadeau, E. Burstein, P. J. Cullen, Retriever is a multiprotein complex for retromer-independent endosomal cargo recycling. *Nat. Cell Biol.* **19**, 1214–1225 (2017).

144. B. M. Collins, C. F. Skinner, P. J. Watson, M. N. J. Seaman, D. J. Owen, Vps29 has a phosphoesterase fold that acts as a protein interaction scaffold for retromer assembly. *Nat. Struct. Mol. Biol.* **12**, 594–602 (2005).

145. M. E. Harbour, S. Y. A. Breusegem, R. Antrobus, C. Freeman, E. Reid, M. N. J. Seaman, The cargo-selective retromer complex is a recruiting hub for protein complexes that regulate endosomal tubule dynamics. *J. Cell Sci.* **123**, 3703–3717 (2010).

146. D. Jia, J.-S. Zhang, F. Li, J. Wang, Z. Deng, M. A. White, D. G. Osborne, C. Phillips-Krawczak, T. S. Gomez, H. Li, A. Singla, E. Burstein, D. D. Billadeau, M. K. Rosen, Structural and mechanistic insights into regulation of the retromer coat by TBC1d5. *Nat. Commun.* **7**, 13305 (2016).

147. D. J. Gillooly, I. C. Morrow, M. Lindsay, R. Gould, N. J. Bryant, J. M. Gaullier, R. G. Parton, H. Stenmark, Localization of phosphatidylinositol 3-phosphate in yeast and mammalian cells. *EMBO J.* **19**, 4577–4588 (2000).

148. D. H. Schott, D. K. Cureton, S. P. Whelan, C. P. Hunter, An antiviral role for the RNA interference machinery in Caenorhabditis elegans. *Proc Natl Acad Sci USA*. **102**, 18420–18424 (2005).

149. B. Coutard, C. Valle, X. de Lamballerie, B. Canard, N. G. Seidah, E. Decroly, The spike glycoprotein of the new coronavirus 2019-nCoV contains a furin-like cleavage site absent in CoV of the same clade. *Antiviral Res.* **176**, 104742 (2020).

150. K. Schornberg, S. Matsuyama, K. Kabsch, S. Delos, A. Bouton, J. White, Role of endosomal cathepsins in entry mediated by the Ebola virus glycoprotein. *J. Virol.* **80**, 4174–4178 (2006).

151. N. Mulherkar, M. Raaben, J. C. de la Torre, S. P. Whelan, K. Chandran, The Ebola virus glycoprotein mediates entry via a non-classical dynamin-dependent macropinocytic pathway. *Virology*. **419**, 72–83 (2011).

152. B. Malleret, B. Manéglier, I. Karlsson, P. Lebon, M. Nascimbeni, L. Perié, P. Brochard, B. Delache, J. Calvo, T. Andrieu, O. Spreux-Varoquaux, A. Hosmalin, R. Le Grand, B. Vaslin, Primary infection with simian immunodeficiency virus: plasmacytoid dendritic cell homing to lymph nodes, type I interferon, and immune suppression. *Blood*. **112**, 4598–4608 (2008).

153. J. Joung, S. Konermann, J. S. Gootenberg, O. O. Abudayyeh, R. J. Platt, M. D. Brigham, N. E. Sanjana, F. Zhang, Genome-scale CRISPR-Cas9 knockout and transcriptional activation screening. *Nat. Protoc.* **12**, 828–863 (2017).

154. D. Oudshoorn, S. van Boheemen, M. T. Sánchez-Aparicio, R. Rajsbaum, A. García-Sastre, G. A. Versteeg, HERC6 is the main E3 ligase for global ISG15 conjugation in mouse cells. *PLoS ONE*. **7**, e29870 (2012).

155. Y. Wang, S. Yuan, X. Jia, Y. Ge, T. Ling, M. Nie, X. Lan, S. Chen, A. Xu, Mitochondria-localised ZNFX1 functions as a dsRNA sensor to initiate antiviral responses through MAVS. *Nat. Cell Biol.* **21**, 1346–1356 (2019).

156. S. Cui, C. Li, RHPN1-AS1 promotes ovarian carcinogenesis by sponging miR-485-5p and releasing TPX2 mRNA. *Oncol. Rep.* **45** (2021), doi:10.3892/or.2021.8062.

157. P. Kota, E. M. Terrell, D. A. Ritt, C. Insinna, C. J. Westlake, D. K. Morrison, M-Ras/Shoc2 signaling modulates E-cadherin turnover and cell-cell adhesion during collective cell migration. *Proc Natl Acad Sci USA*. **116**, 3536–3545 (2019).

158. K. M. Goodman, M. Yamagata, X. Jin, S. Mannepalli, P. S. Katsamba, G. Ahlsén, A. P. Sergeeva, B. Honig, J. R. Sanes, L. Shapiro, Molecular basis of sidekick-mediated cell-cell adhesion and specificity. *eLife*. **5** (2016), doi:10.7554/eLife.19058.

159. C. Schell, M. Rogg, M. Suhm, M. Helmstädter, D. Sellung, M. Yasuda-Yamahara, O. Kretz, V. Küttner, H. Suleiman, L. Kollipara, R. P. Zahedi, A. Sickmann, S. Eimer, A. S. Shaw, A. Kramer-Zucker, M. Hirano-Kobayashi, T. Abe, S. Aizawa, F. Grahammer, B. Hartleben, J. Dengjel, T. B. Huber, The FERM protein EPB41L5 regulates actomyosin contractility and focal adhesion formation to maintain the kidney filtration barrier. *Proc Natl Acad Sci USA*. **114**, E4621–E4630 (2017).

160. C. Aiken, Pseudotyping human immunodeficiency virus type 1 (HIV-1) by the glycoprotein of vesicular stomatitis virus targets HIV-1 entry to an endocytic pathway and suppresses both the requirement for Nef and the sensitivity to cyclosporin A. *J. Virol.* **71**, 5871–5877 (1997).

161. A. Shami Shah, A. G. Batrouni, D. Kim, A. Punyala, W. Cao, C. Han, M. L. Goldberg, M. B. Smolka, J. M. Baskin, Plekha4/kramer attenuates dishevelled ubiquitination to modulate wnt and planar cell polarity signaling. *Cell Rep.* **27**, 2157-2170.e8 (2019).

162. T. Hatziioannou, G. Q. Del Prete, B. F. Keele, J. D. Estes, M. W. McNatt, J. Bitzegeio, A. Raymond, A. Rodriguez, F. Schmidt, C. Mac Trubey, J. Smedley, M. Piatak, V. N. KewalRamani, J. D. Lifson, P. D. Bieniasz, HIV-1-induced AIDS in monkeys. *Science*. **344**, 1401–1405 (2014).

163. S. S. Iyer, F. Bibollet-Ruche, S. Sherrill-Mix, G. H. Learn, L. Plenderleith, A. G. Smith, H. J. Barbian, R. M. Russell, M. V. P. Gondim, C. Y. Bahari, C. M. Shaw, Y. Li, T. Decker, B. F. Haynes, G. M. Shaw, P. M. Sharp, P. Borrow, B. H. Hahn, Resistance to type 1 interferons is a major determinant of HIV-1 transmission fitness. *Proc Natl Acad Sci USA*. **114**, E590–E599 (2017).

164. A. E. Fenton-May, O. Dibben, T. Emmerich, H. Ding, K. Pfafferott, M. M. Aasa-Chapman, P. Pellegrino, I. Williams, M. S. Cohen, F. Gao, G. M. Shaw, B. H. Hahn, C. Ochsenbauer, J. C. Kappes, P. Borrow, Relative resistance of HIV-1 founder viruses to control by interferon-alpha. *Retrovirology*. **10**, 146 (2013).

165. T. L. Foster, H. Wilson, S. S. Iyer, K. Coss, K. Doores, S. Smith, P. Kellam, A. Finzi, P. Borrow, B. H. Hahn, S. J. D. Neil, Resistance of Transmitted Founder HIV-1 to IFITM-Mediated Restriction. *Cell Host Microbe*. **20**, 429–442 (2016).

166. T. P. Sheahan, A. C. Sims, R. L. Graham, V. D. Menachery, L. E. Gralinski, J. B. Case, S. R. Leist, K. Pyrc, J. Y. Feng, I. Trantcheva, R. Bannister, Y. Park, D. Babusis, M. O. Clarke, R. L. Mackman, J. E. Spahn, C. A. Palmiotti, D. Siegel, A. S. Ray, T. Cihlar, R. Jordan, M. R. Denison, R. S. Baric, Broad-spectrum antiviral GS-5734 inhibits both epidemic and zoonotic coronaviruses. *Sci. Transl. Med.* **9**, eaal3653 (2017).

167. T. P. Sheahan, A. C. Sims, S. R. Leist, A. Schäfer, J. Won, A. J. Brown, S. A. Montgomery, A. Hogg, D. Babusis, M. O. Clarke, J. E. Spahn, L. Bauer, S. Sellers, D. Porter, J. Y. Feng, T. Cihlar, R. Jordan, M. R. Denison, R. S. Baric, Comparative therapeutic efficacy of remdesivir and combination lopinavir, ritonavir, and interferon beta against MERS-CoV. *Nat. Commun.* **11**, 222 (2020).

168. R. L. Gottlieb, C. E. Vaca, R. Paredes, J. Mera, B. J. Webb, G. Perez, G. Oguchi, P. Ryan, B. U. Nielsen, M. Brown, A. Hidalgo, Y. Sachdeva, S. Mittal, O. Osiyemi, J. Skarbinski, K. Juneja, R. H. Hyland, A. Osinusi, S. Chen, G. Camus, M. Abdelghany, S. Davies, N. Behenna-Renton, F. Duff, F. M. Marty, M. J. Katz, A. A. Ginde, S. M. Brown, J. T. Schiffer, J. A. Hill, GS-US-540-9012 (PINETREE) Investigators, Early Remdesivir to Prevent Progression to Severe Covid-19 in Outpatients. *N. Engl. J. Med.* **386**, 305–315 (2022).

169. J. H. Beigel, K. M. Tomashek, L. E. Dodd, A. K. Mehta, B. S. Zingman, A. C. Kalil, E. Hohmann, H. Y. Chu, A. Luetkemeyer, S. Kline, D. Lopez de Castilla, R. W. Finberg, K. Dierberg, V. Tapson, L. Hsieh, T. F. Patterson, R. Paredes, D. A. Sweeney, W. R. Short, G. Touloumi, D. C. Lye, N. Ohmagari, M.-D. Oh, G. M. Ruiz-Palacios, T. Benfield, G. Fätkenheuer, M. G. Kortepeter, R. L. Atmar, C. B. Creech, J. Lundgren, A. G. Babiker, S. Pett, J. D. Neaton, T. H. Burgess, T. Bonnett, M. Green, M. Makowski, A. Osinusi, S. Nayak, H. C. Lane, ACTT-1 Study Group Members, Remdesivir for the Treatment of Covid-19 - Final Report. *N. Engl. J. Med.* **383**, 1813–1826 (2020).

170. R. M. Grant, J. R. Lama, P. L. Anderson, V. McMahan, A. Y. Liu, L. Vargas, P. Goicochea, M. Casapía, J. V. Guanira-Carranza, M. E. Ramirez-Cardich, O. Montoya-Herrera, T. Fernández, V. G. Veloso, S. P. Buchbinder, S. Chariyalertsak, M. Schechter, L.-G. Bekker, K. H. Mayer, E. G. Kallás, K. R. Amico, K. Mulligan, L. R. Bushman, R. J. Hance, C. Ganoza, P. Defechereux, B. Postle, F. Wang, J. J. McConnell, J.-H. Zheng, J. Lee, J. F. Rooney, H. S. Jaffe, A. I. Martinez, D. N. Burns, D. V. Glidden, iPrEx Study Team, Preexposure chemoprophylaxis for HIV prevention in men who have sex with men. *N. Engl. J. Med.* **363**, 2587–2599 (2010).

171. D. J. Colby, E. Kroon, C. Sacdalan, M. Gandhi, R. M. Grant, P. Phanuphak, J. Ananworanich, M. L. Robb, N. Phanuphak, Acquisition of Multidrug-Resistant Human Immunodeficiency Virus Type 1 Infection in a Patient Taking Preexposure Prophylaxis. *Clin. Infect. Dis.* **67**, 962–964 (2018).

172. M. Markowitz, H. Grossman, P. L. Anderson, R. Grant, M. Gandhi, H. Horng, H. Mohri, Newly Acquired Infection With Multidrug-Resistant HIV-1 in a Patient Adherent to Preexposure Prophylaxis. *J. Acquir. Immune Defic. Syndr.* **76**, e104–e106 (2017).

173. D. C. Knox, P. L. Anderson, P. R. Harrigan, D. H. S. Tan, Multidrug-Resistant HIV-1 Infection despite Preexposure Prophylaxis. *N. Engl. J. Med.* **376**, 501–502 (2017).

174. M. C. Puertas, G. Ploumidis, M. Ploumidis, E. Fumero, B. Clotet, C. M. Walworth, C. J. Petropoulos, J. Martinez-Picado, Pan-resistant HIV-1 emergence in the era of integrase strand-transfer inhibitors: a case report. *The Lancet Microbe*. **1**, e130–e135 (2020).

175. S. Segal-Maurer, E. DeJesus, H.-J. Stellbrink, A. Castagna, G. J. Richmond, G. I. Sinclair, K. Siripassorn, P. J. Ruane, M. Berhe, H. Wang, N. A. Margot, H. Dvory-Sobol, R. H. Hyland, D. M. Brainard, M. S. Rhee, J. M. Baeten, J.-M. Molina, CAPELLA Study Investigators, Capsid Inhibition with Lenacapavir in Multidrug-Resistant HIV-1 Infection. *N. Engl. J. Med.* **386**, 1793–1803 (2022).

176. C. Xu, D. K. Fischer, S. Rankovic, W. Li, R. A. Dick, B. Runge, R. Zadorozhnyi, J. Ahn, C. Aiken, T. Polenova, A. N. Engelman, Z. Ambrose, I. Rousso, J. R. Perilla, Permeability of the HIV-1 capsid to metabolites modulates viral DNA synthesis. *PLoS Biol.* **18**, e3001015 (2020).

177. D. A. Jacques, W. A. McEwan, L. Hilditch, A. J. Price, G. J. Towers, L. C. James, HIV-1 uses dynamic capsid pores to import nucleotides and fuel encapsidated DNA synthesis. *Nature*. **536**, 349–353 (2016).

178. P.-T. Huang, B. J. Summers, C. Xu, J. R. Perilla, V. Malikov, M. H. Naghavi, Y. Xiong, FEZ1 Is Recruited to a Conserved Cofactor Site on Capsid to Promote HIV-1 Trafficking. *Cell Rep.* **28**, 2373-2385.e7 (2019).

179. C. Yi, C. Cai, Z. Cheng, Y. Zhao, X. Yang, Y. Wu, X. Wang, Z. Jin, Y. Xiang, M. Jin, L. Han, A. Zhang, Genome-wide CRISPR-Cas9 screening identifies the CYTH2 host gene as a potential therapeutic target of influenza viral infection. *Cell Rep.* **38**, 110559 (2022).

180. Z. Li, L. Du, W. Zhang, X. Zhang, Y. Jiang, K. Liu, P. Men, H. Xu, J. L. Fortman, D. H. Sherman, B. Yu, S. Gao, S. Li, Complete elucidation of the late steps of bafilomycin biosynthesis in Streptomyces lohii. *J. Biol. Chem.* **292**, 7095–7104 (2017).

181. L. Muzio, R. Sirtori, D. Gornati, S. Eleuteri, A. Fossaghi, D. Brancaccio, L. Manzoni, L. Ottoboni, L. D. Feo, A. Quattrini, E. Mastrangelo, L. Sorrentino, E. Scalone, G. Comi, L. Marinelli, N. Riva, M. Milani, P. Seneci, G. Martino, Retromer stabilization results in neuroprotection in a model of Amyotrophic Lateral Sclerosis. *Nat. Commun.* **11**, 3848 (2020).

182. V. J. Mecozzi, D. E. Berman, S. Simoes, C. Vetanovetz, M. R. Awal, V. M. Patel, R. T. Schneider, G. A. Petsko, D. Ringe, S. A. Small, Pharmacological chaperones stabilize retromer to limit APP processing. *Nat. Chem. Biol.* **10**, 443–449 (2014).

183. B. Boland, W. H. Yu, O. Corti, B. Mollereau, A. Henriques, E. Bezard, G. M. Pastores, D. C. Rubinsztein, R. A. Nixon, M. R. Duchen, G. R. Mallucci, G. Kroemer, B. Levine, E.-L. Eskelinen, F. Mochel, M. Spedding, C. Louis, O. R. Martin, M. J. Millan, Promoting the clearance of neurotoxic proteins in neurodegenerative disorders of ageing. *Nat. Rev. Drug Discov.* **17**, 660–688 (2018).

184. P. Zhang, G. Monteiro da Silva, C. Deatherage, C. Burd, D. DiMaio, Cell-Penetrating Peptide Mediates Intracellular Membrane Passage of Human Papillomavirus L2 Protein to Trigger Retrograde Trafficking. *Cell*. **174**, 1465-1476.e13 (2018).

185. K.-E. Chen, Q. Guo, T. A. Hill, Y. Cui, A. K. Kendall, Z. Yang, R. J. Hall, M. D. Healy, J. Sacharz, S. J. Norwood, S. Fonseka, B. Xie, R. C. Reid, N. Leneva, R. G. Parton, R. Ghai, D. A. Stroud, D. P. Fairlie, H. Suga, L. P. Jackson, R. D. Teasdale, T. Passioura, B. M. Collins, De novo macrocyclic peptides for inhibiting, stabilizing, and probing the function of the retromer endosomal trafficking complex. *Sci. Adv.* **7**, eabg4007 (2021).

186. UNAIDS, UNAIDS Global Factsheet (2018).

187. R. M. Gulick, J. Lalezari, J. Goodrich, N. Clumeck, E. DeJesus, A. Horban, J. Nadler, B. Clotet, A. Karlsson, M. Wohlfeiler, J. B. Montana, M. McHale, J. Sullivan, C. Ridgway, S. Felstead, M. W. Dunne, E. van der Ryst, H. Mayer, MOTIVATE Study Teams, Maraviroc for previously treated patients with R5 HIV-1 infection. *N. Engl. J. Med.* **359**, 1429–1441 (2008).

188. B. Emu, J. Fessel, S. Schrader, P. Kumar, G. Richmond, S. Win, S. Weinheimer, C. Marsolais, S. Lewis, Phase 3 Study of Ibalizumab for Multidrug-Resistant HIV-1. *N. Engl. J. Med.* **379**, 645–654 (2018).

189. M. Kozal, J. Aberg, G. Pialoux, P. Cahn, M. Thompson, J.-M. Molina, B. Grinsztejn, R. Diaz, A. Castagna, P. Kumar, G. Latiff, E. DeJesus, M. Gummel, M. Gartland, A. Pierce, P. Ackerman, C. Llamoso, M. Lataillade, BRIGHTE Trial Team, Fostemsavir in Adults with Multidrug-Resistant HIV-1 Infection. *N. Engl. J. Med.* **382**, 1232–1243 (2020).

190. B. F. Haynes, K. Wiehe, P. Borrrow, K. O. Saunders, B. Korber, K. Wagh, A. J. McMichael, G. Kelsoe, B. H. Hahn, F. Alt, G. M. Shaw, Strategies for HIV-1 vaccines that induce broadly neutralizing antibodies. *Nat. Rev. Immunol.* (2022), doi:10.1038/s41577-022-00753-w.

191. A. L. Hotard, F. Y. Shaikh, S. Lee, D. Yan, M. N. Teng, R. K. Plemper, J. E. Crowe, M. L. Moore, A stabilized respiratory syncytial virus reverse genetics system amenable to recombination-mediated mutagenesis. *Virology*. **434**, 129–136 (2012).

192. S. P. Whelan, J. N. Barr, G. W. Wertz, Identification of a minimal size requirement for termination of vesicular stomatitis virus mRNA: implications for the mechanism of transcription. *J. Virol.* **74**, 8268–8276 (2000).

193. F. Schmidt, Y. Weisblum, F. Muecksch, H.-H. Hoffmann, E. Michailidis, J. C. C. Lorenzi, P. Mendoza, M. Rutkowska, E. Bednarski, C. Gaebler, M. Agudelo, A. Cho, Z. Wang, A. Gazumyan, M. Cipolla, M. Caskey, D. F. Robbiani, M. C. Nussenzweig, C. M. Rice, T. Hatziioannou, P. D. Bieniasz, Measuring SARS-CoV-2 neutralizing antibody activity using pseudotyped and chimeric viruses. *J. Exp. Med.* **217** (2020), doi:10.1084/jem.20201181.

194. M. Jia, R. A. Liberatore, Y. Guo, K.-W. Chan, R. Pan, H. Lu, E. Waltari, E. Mittler, K. Chandran, A. Finzi, D. E. Kaufmann, M. S. Seaman, D. D. Ho, L. Shapiro, Z. Sheng, X.-P. Kong, P. D. Bieniasz, X. Wu, VSV-Displayed HIV-1 Envelope Identifies Broadly Neutralizing Antibodies Class-Switched to IgG and IgA. *Cell Host Microbe*. **27**, 963-975.e5 (2020).

195. M. I. Love, W. Huber, S. Anders, Moderated estimation of fold change and dispersion for RNA-seq data with DESeq2. *Genome Biol.* **15**, 550 (2014).

196. O. Shalem, N. E. Sanjana, E. Hartenian, X. Shi, D. A. Scott, T. Mikkelson, D. Heckl, B. L. Ebert, D. E. Root, J. G. Doench, F. Zhang, Genome-scale CRISPR-Cas9 knockout screening in human cells. *Science*. **343**, 84–87 (2014).

197. T. Hart, M. Chandrashekhar, M. Aregger, Z. Steinhart, K. R. Brown, G. MacLeod, M. Mis, M. Zimmermann, A. Fradet-Turcotte, S. Sun, P. Mero, P. Dirks, S. Sidhu, F. P. Roth, O. S. Rissland, D. Durocher, S. Angers, J. Moffat, High-Resolution CRISPR Screens Reveal Fitness Genes and Genotype-Specific Cancer Liabilities. *Cell*. **163**, 1515–1526 (2015).

198. T. Wang, K. Birsoy, N. W. Hughes, K. M. Krupczak, Y. Post, J. J. Wei, E. S. Lander, D. M. Sabatini, Identification and characterization of essential genes in the human genome. *Science*. **350**, 1096–1101 (2015).

199. T. Wang, J. J. Wei, D. M. Sabatini, E. S. Lander, Genetic screens in human cells using the CRISPR-Cas9 system. *Science*. **343**, 80–84 (2014).

200. D. Nègre, P. E. Mangeot, G. Duisit, S. Blanchard, P. O. Vidalain, P. Leissner, A. J. Winter, C. Rabourdin-Combe, M. Mehtali, P. Moullier, J. L. Darlix, F. L. Cosset, Characterization of novel safe lentiviral vectors derived from simian immunodeficiency virus (SIVmac251) that efficiently transduce mature human dendritic cells. *Gene Ther.* **7**, 1613–1623 (2000).

201. M. Pizzato, O. Erlwein, D. Bonsall, S. Kaye, D. Muir, M. O. McClure, A one-step SYBR Green I-based product-enhanced reverse transcriptase assay for the quantitation of retroviruses in cell culture supernatants. *J. Virol. Methods*. **156**, 1–7 (2009).

202. M. Kane, S. S. Yadav, J. Bitzegeio, S. B. Kutluay, T. Zang, S. J. Wilson, J. W. Schoggins, C. M. Rice, M. Yamashita, T. Hatziioannou, P. D. Bieniasz, MX2 is an interferon-induced inhibitor of HIV-1 infection. *Nature*. **502**, 563–566 (2013).